Doping & Decoration of Carbon based Nanoparticles: Applications in Flame Retardancy and Catalysis

By

Marjan Entezar Shabestari

A dissertation submitted by in partial fulfillment of the requirements for the degree of Doctor of Philosophy in

Materials Science and Engineering

Universidad Carlos III de Madrid

Advisors

Dr. Olga Martín Cádiz

Dr. Juan Baselga Llido

Tutor

Dr. Juan Baselga Llido

July 2019

Seek Knowledge from cradle to grave

"Mohammad"

The Prophet of peace

Acknowledgement

First and foremost, I would like to thank God Almighty for giving me the strength, knowledge, and ability to do work. Without his blessings, this achievement would not have been possible.

I would like to thank my family, my beloved parents, my sisters and my brother for their continuous support, love and pray for me, throughout the years. I love you so much!

This thesis would never have been completed without my nice advisors' Pro. Dr. Juan Baselga Llido and Dr. Olga Martin Cadiz helps and supports.

I am deeply grateful to Pro. Dr. Juan Baselga Llido for the continuous support, for his patience, motivation, enthusiasm, immense knowledge in all the time of research and especially in writing of the thesis. Thank you Juan for giving me the opportunity to be your student, I am forever grateful to you!

I owe my deepest gratitude to Dr. Olga Martin Cadiz for her generous supports, advices and comments. Dear Olga, many thanks for trusting me!

I gratefully acknowledge Dr. Viviana Gonzales for tutoring my learning of synthesizing, processing and characterization techniques in the beginning of my work.

I would like to thank all the members (past and present) of Material Science & Engineering department especially GPC group's members for creating a very pleasant working environment for me during these years. I received generous support from you as my extended family. You made my graduate life at Carlos III University very colorful and a memorable experience. Many thanks to all of you!

My deepest appreciation goes to my best friend, lovely husband, Ehsan for his encouraging, constant supports and scientific help that kept me going in difficult moments. My dearest Ehsan, this work was not possible without your support. Finally I have done it !!!

Finally, a huge thank-you to everyone who has been a part of my life directly or indirectly supported and prayed for me along the way.

Published and submitted content

1) **Effect of Nitrogen and Oxygen Doped Carbon Nanotubes on Flammability of Epoxy Nanocomposites**

Marjan E. Shabestari, Ehsan N. Kalali, Viviana Jehová González, De-Yi Wang, Juan P. Fernández-Blázquez, Juan Baselga and Olga Martin, *Carbon* 121 (2017) 193-200 (Published)

2) **Microwave- assisted rapid decoration of Graphene Oxide with Copper hydroxy nitrate $Cu_2(OH)_3NO_3$, Cuprous oxide (Cu_2O) and Copper oxide (CuO) and application in photocatalytic degradation**

Marjan E. Shabestari, Juan Baselga, Olga Martin (In progress)

3) **Facile and Rapid decoration of Graphene Oxide with Copper hydroxy nitrate, Copper (I,II) Oxide and Copper nanoparticles: Preliminary Study of the Catalytic Versatility in Oxidation and Coupling reactions**

Marjan E. Shabestari, Santiago Gómez-Ruiz, Diana Díaz-García, Viviana Jehová González, Juan Baselga, Olga Martín (In progress)

Preface

This dissertation is submitted for the degree of Doctor of Philosophy in the Carlos III University of Madrid. The research described in this thesis was carried out at Material Science and Engineering and Chemical Engineering department during the period November 2014 to September 2018 under the supervision of Dr. Juan Baselga Llido and Dr. Olga Martin Cadiz, professors at the Carlos III University of Madrid.

A part of the results obtained during the course of this thesis have been published in scientific journals.

To the best of my knowledge, the work described in this dissertation is original, except where due reference has been made to the work of others, and nothing is included which is the outcome of work done in collaboration, unless otherwise stated. No part of this dissertation, or any similar to it, has been, or is currently being, submitted for any degree or other qualification at any other university.

Marjan Entezar Shabestari

Madrid

May 2019

Abstract

The present work involves two main parts that will be explained after introduction. A brief introduction about history, properties, synthesis and characterization of carbon nanotubes, graphene and their nanocomposites and nanohybrides will be presented.

The first part of the thesis is focused on the synthesis of different types of nanotubes: pristine carbon nanotubes (CNT), oxygen doped carbon nanotubes (CO_x), and nitrogen doped carbon nanotubes (CN_x) by CVD method. The structure of the nanotubes were confirmed by XRD, XPS, SEM, TEM, TGA and Raman spectroscopy (Chapter 2). The most important difference between the synthesized nanotubes was their aspect ratio which is calculated from 1500-3000 for CN_x to CO_x. Pristine CNT shows the aspect ratio about < 2000.

Subsequently, the epoxy nanocomposites at 2 wt.% constant loading of carbon nanotubes (CNT, CO_x and CN_x) and Diglycidyl ether bisphenol-A (DGEBA) as a good example of thermosetting polymer were have been prepared by three roll milling and cured by 4,4′- Diamio diphenyl sulfone (DDS) as a hardener. The thermal degradation of epoxy nanocomposites as well as glass transition temperatures and elastic moduli were measured by TGA, DSC and DMTA.

The flammability of epoxy nanocomposites was studied by microscale combustion calorimetry (MCC) and limiting oxygen index (LOI) determination. Results showed that the fire retardant properties of nanocomposites improved significantly specially for CO_x, which presented a very high LOI (35%) and a homogeneous and uniform surface after burning. This effect was attributed to the very high aspect ratio of CO_x

tubes. The results showed that introduction of the nanofillers at 2 wt.% loading caused the earlier initial decomposition of the nanocomposites, an increased char yield, and a reduction of the degradation rate of in comparison with pure epoxy.

The influence of addition of nanofillers on the relaxational and mechanical behavior of nanocomposites was evaluated by DSC and DMTA. No significant variations in Tg, storage modulus or loss tangent width were detected, indicating that the addition of nanofillers does not negatively affect the relaxational and mechanical response of the nanocomposites (Chapter4).

In the second part of our work, different copper nanocomponents were synthesized and decorated on graphene oxide by our microwave-assisted method. Copper hydroxyl nitrate double salt (DS) ($Cu_2(OH)_3(NO_3)$) and cuprous oxide (Cu_2O) by changing the solvent in a very simple procedure were obtained from copper nitrate.

Copper nitrate (CuO) and metallic copper can prepared from heating and reduction by ascorbic acid of DS, respectively.

The four copper salts have been decorated on graphene oxide GO following the same microwave-assisted method. (Chapter 3)

The performance of copper salts/GO nanohybrids as photocatalyst in degradation of one common dyes (Rhodamine B) has been studied. As we expected, incorporation of copper oxides (copper with different oxidation number) onto GO via our method resulted in enhancing the properties of initial metal oxides and it was comparable with the CuO and Cu_2O/GO hybrids produced of conventional methods

Photocatalytic activity of DS alone and decorated on GO has been reported for the first time in this work.

In the last part of the thesis, we have checked the performance of decorated copper salts as catalyst in some common organic reactions like: C-C , C-N, and C-S coupling and oxidation of aldehyde (Chapter 6). The catalytic application of DS is introduced for the first time here. The results open up the possibility of a more thorough study of the catalytic performance of the supported copper double salt in other conditions which may be applied in the future for different catalytic and consecutive processes of organic synthesis.

Resumen

El presente trabajo incluye dos bloques principales que se explicarán después de la introducción. Empezaremos con una breve introducción sobre la historia, propiedades, síntesis y caracterización de los nanotubos de carbono, el grafeno y sus nanocompuestos y nanohíbridos.

La primera parte de la tesis se centra en la síntesis de diferentes tipos de nanotubos: nanotubos de carbono prístinos (CNT), nanotubos de carbono dopados con oxígeno (CO_x) y nanotubos de carbono dopados con nitrógeno (CN_x) por el método CVD. La estructura de los nanotubos se confirmó mediante espectroscopía XRD, XPS, SEM, TEM, TGA y Raman (Capítulo 2). La diferencia más importante entre los nanotubos sintetizados fue su relación de aspecto que se calcula de 1500-3000 para CN_x y COx. Los CNT prístinos muestra una relación de aspecto de <2000.

Posteriormente como un buen ejemplo de polímero termoestable se prepararon los nanocompuestos epoxídicos de diglicidil éter de bisfenol-A (DGEBA) a una carga constante del 2% en peso de nanotubos de carbono (CNT, CO_x y CN_x). Se dispersaron por calandrado y se curaron con 4 , 4′- diamio difenil sulfona (DDS). Se midieron la degradación térmica de los nanocompuestos epoxi, las temperaturas de transición vítrea y los módulos elásticos mediante las técnicas de TGA, DSC y DMTA.

La inflamabilidad de los nanocompuestos epoxi se estudió mediante calorimetría de combustión a micro escala (MCC) e índice limitante de oxígeno (LOI). Los resultados mostraron que las propiedades ignífugas de los nanocompuestos mejoraron significativamente especialmente para CO_x, que presentó una LOI muy alta (35%) y

una superficie homogénea y uniforme después de la quema. Este efecto se atribuyó a la muy alta relación de aspecto de los tubos CO_x. Los resultados mostraron que la introducción de nanofillers a una carga del 2% en peso causó la descomposición inicial más temprana de los nanocompuestos, un mayor rendimiento de producción de ceniza y una reducción de la tasa de degradación en comparación con el epoxi puro.

La influencia de la adición de nanofillers en las propiedades de relajación y mecánicas de los nanocompuestos fue evaluada por DSC y DMTA. No se detectaron variaciones significativas en la T_g, el módulo de almacenamiento o el ancho de la tangente de pérdida, lo que indica que la adición de nanofillers no afecta negativamente a la respuesta de relajación y mecánica de los nanocompuestos (Capítulo 4).

En la segunda parte de nuestro trabajo, diferentes nanoderivados de cobre se sintetizaron y anclaron a óxido de grafeno mediante un método propio asistido por microondas. Mediante un procedimiento muy simple partiendo de nitrato de cobre y modificando el disolvente de reacción se obtuvieron preferentemente la sal doble de nitrato-hidróxido de cobre (DS) ($Cu_2(OH)_3(NO_3)$) ó el óxido cuproso (Cu_2O).

El nitrato de cobre (CuO) y el cobre metálico pueden prepararse a partir del calentamiento y la reducción por ácido ascórbico de DS, respectivamente.

Las cuatro sales de cobre se han depositado sobre óxido de grafeno GO siguiendo el mismo método asistido por microondas. (Capítulo 3)

Se ha testado el rendimiento de las sales de cobre / nanohíbridos GO como fotocatalizadores en la degradación de un colorante común (rodamina B). Como esperábamos, la incorporación de óxidos de cobre (cobre con diferente número de oxidación) en GO a través de nuestro método derivó en la mejora de las propiedades

de los óxidos metálicos iniciales y fue comparable con los híbridos CuO y Cu_2O / GO producidos por métodos convencionales.

La actividad fotocatalítica de la DS sola y soportadas en GO ha sido obtenida por primera vez en este trabajo.

En la última parte de la tesis, hemos comprobado la eficacia de las sales de cobre soportadas en GO como catalizadores de algunas reacciones orgánicas comunes : acoplamiento de C-C, C-N y C-S y oxidación del aldehído (Capítulo 6). La aplicación catalítica de DS se estudia en este trabajo por primera vez . Los resultados obtenidos abren la posibilidad a nuevos estudios, más exhaustivo, del rendimiento catalítico de la doble sal de cobre soportada en otras reacciones de química orgánica que pueden plantearse en el futuro.

Table of contents

Chapter 2

Synthesis & Characterization of Oxygen and Nitrogen doped Carbon Nanotubes

Chapter 3

Microwave-assisted Decoration of Graphene Oxide (GO) by Copper hydroxy nitrate $Cu_2(OH)_3NO_3$ (DS), Cuprous oxide (Cu_2O), Copper oxide (CuO), and Metallic copper

List of Figures

List of Schemes

List of Tables

List of Abbreviations

°C: Centigrade degree

λ_{max} : Wavelength of maximum absorbance

AFM: Atomic force microscopy

ASTM: American Society for Testing and Materials

CNT: Carbon nanotube

CO_x: Oxygen doped carbon nanotube

CN_x: Nitrogen doped carbon nanotube

CuO: Copper oxide

Cu^0: Metallic copper

Cu_2O: Cuprous oxide

CVD: Chemical vapor deposition

DDS: 4,4′- Diamino diphenyl sulfone

DGEBA: Diglycidyl ether of bisphenol A

DMTA: Dynamic mechanical thermal analysis

DRS: Diffuse reflectance spectroscopy

DS: Copper hydroxy nitrate double salt

DSC: Differential scanning calorimetry

EDX: Energy-dispersive X-ray spectroscopy

E_g: Bandgap energy or forbidden energy

EP: Epoxy resin

FESEM: Field Emission Scanning Electron Microscopy

FTIR: Fourier transform infrared spectroscopy

FWHM: Full width at half maximum

GO: Graphene oxide

GC: Gas Chromatography

HRR: Heat release rate

LOI: Limiting oxygen index

MCC: Microscale combustion calorimetry

MONPs: Metal oxides nanoparticles

mw: Microwave irradiation

MWNT: Multi-walled carbon nanotubes

pHRR: Peak of heat release rate

rGO: Reduced graphene oxide

RhB: Rhodamine B

SEM: Scanning electron microscopy

SWNT: Single-walled carbon nanotubes

$T_{5\%}$: The temperature at which the mass loss is 5%

$T_{max\%}$: The temperature at which the mass loss is maximum

TEM: Transmission electron microscopy

Tg: Glass transition temperature

TGA: Thermogravimetric analysis

THR: Total heat release

TON: Turnover number

T_{max}: The temperature at which the maximum mass loss rate occurs

UV-Vis: Ultraviolet-Visible

wt.%: Weight percent

XRD: X-ray diffraction

XPS: X-ray photoelectron spectroscopy

Chapter 1
Introduction

1.1 Carbon nanomaterials

Carbon is one of the universal material that has been ever found. Single carbon atom has six electrons with $1s^2$, $2s^2$ $2p^2$ atomic orbital configuration. Even pure carbon can have quite a few allotropes. This is because the four valence electrons can make different types of bonds with other atoms. The special electronic configuration of carbon leads to sp (e.g. Acetylene) that are separated by an angle of 180°, sp^2 (e.g., fullerenes C_{60}, carbon nanotubes, graphite, graphene) that are coplanar separated by 120°, or sp^3 (e.g., diamond) hybridization forms that are separated by 109.5°. Fig. 1.1 shows different allotropes of carbon.

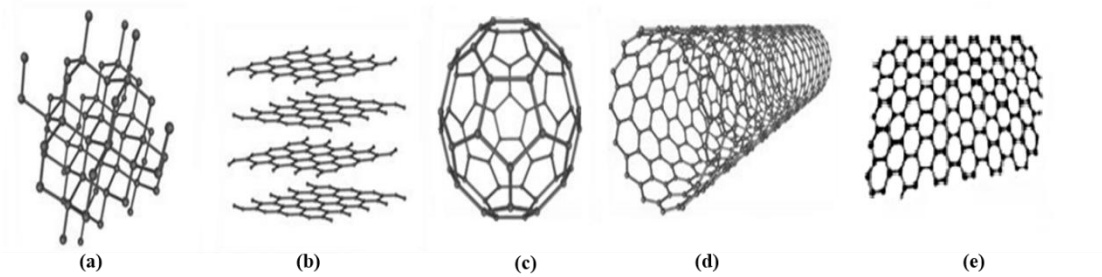

Fig. 1.1 Allotropes of carbon (a) diamond, (b) graphite, (c) fullerenes C_{60}, (d) carbon nanotubes, (e) graphene

Carbon nanotubes and graphene have received significant attention from both the academia and the industry due to their exceptional properties.

1.2 Carbon nanotubes (CNTs)

Since the accidental discovery by Sumio Iijima of the NEC Corporation in the soot of the arc-discharge method [1] in 1991, carbon nanotubes (CNTs) have generated a great deal of research in most areas of science and engineering due to their attractive physico-

chemical properties: stronger than steel, harder than diamond and electrical conductivity higher than copper [2].

A single crystalline carbon nanotube is a hollow tube made from pure carbon in a hexagonal arrangement. In this hexagonal order, each carbon shares a sp^2 covalent bond with its three neighboring atoms. The bond distance is approximately 1.5 Å. CNTs have a typical diameter of 1-5nm, about 100,000 times thinner than an average human hair and they can be several hundred microns long.

Carbon nanotubes (CNTs) exhibit a remarkable set of electrical, mechanical, optical and thermal properties that offer opportunities for materials design in many research areas and commercial products[3,4].

1.3 Classifications of CNTs

Nanotubes are considered as nearly one-dimensional structures according to their high length to diameter ratio. There are two types of CNTs, called single walled CNTs (SWCNT) and multi walled CNTs (MWCNT) as shown in Fig. 1.2 The first-discovered carbon nanotube (Iijima, 1991) was in a multi walled form and single walled tubes were found two years later [5]. A SWCNT with their well-defined atomic structure, high length to diameter ratio, and high chemical stability constitute one-dimension molecules that can be considered as a hollow cylindrical structure of pure carbon with a diameter ranges from 0.5 nm to about 10 nm and a length from a few microns to centimeters. Multi-walled carbon nanotubes (MWCNTs) are formed by multiple concentric cylindrical walls with spacing between walls equivalent to the interlayer spacing of graphene sheets (~3 Å) and are typically larger than SWCNT (Fig. 1.2). The

length and diameter of these structures differ a lot from those of SWNTs and, of course, their properties are very different.

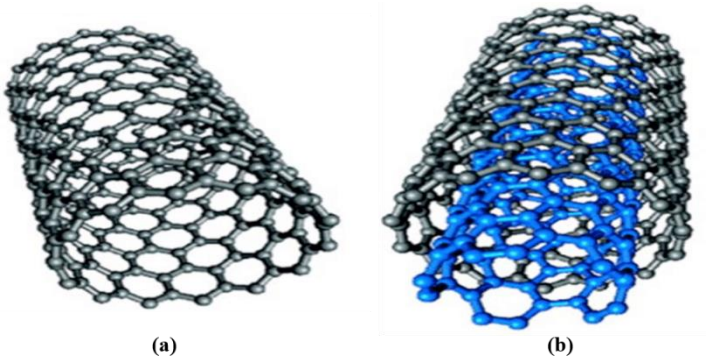

Fig. 1.2 (a) Single walled carbon nanotube (SWCNT),

(b) Multi walled carbon nanotube (MWCNT)

Graphene is a poly-aromatic monoatomic hexagonally arranged layer of carbon atoms with hybridization of sp^2. SWCNT consists of rolling graphene sheets into cylinders with fullerene cap in suitable diameter at their ends [6]. Depending on the rolling-up the graphene sheets and how the hexagons are orientated along the axis of the tube, different designs of SWCNT could exist (Fig. 1.3).

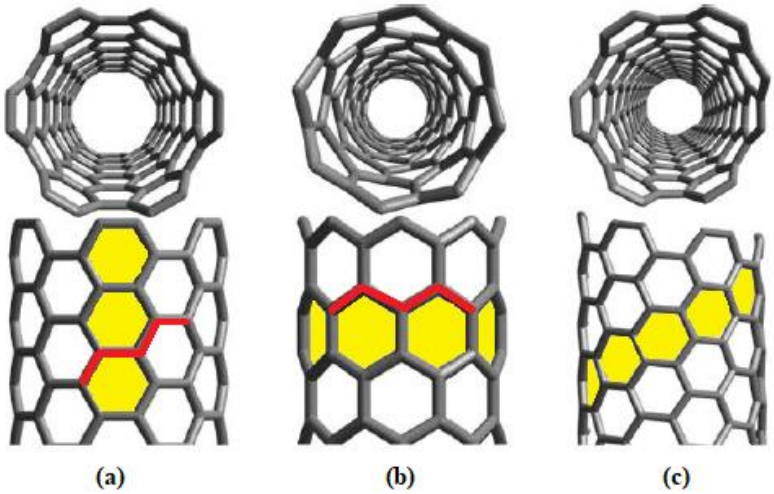

Fig. 1.3 Illustration of three different SWCNT designs (a) armchair (b) zig-zag, and

(c) a helical (chiral) type carbon nanotubes

Three different categories are known as armchair, zigzag and chiral form, which show different electronic properties. An armchair form with conductivity better than copper is the most commonly occurring SWNT [6]. The chiral and zigzag forms of nanotubes are similar to semiconductors in sharing electrical properties.

1.4 Synthesis of carbon nanotubes

Nowadays, CNTs can be synthesized in large quantities by three principal methods: arc discharge, laser ablation and chemical vapor deposition (CVD).

All these methods have some advantages and disadvantages. Depending on desired carbon nanotubes in structure and purification, different method would be required.

CVD is a simple and economic technique to synthesize a large quantity of CNTs [7] in a single step process at low temperature and ambient pressure in compare to two other methods [8]. This method does not need to prior preparation of substrates and further purification of products from carbonaceous side products does not either.

It also offers better control over growth parameters, which is important advantage of apply CVD in our work. Control over the diameter and simultaneously the growth rate of the nanotube can also be maintained.

Common hydrocarbon sources are methane, ethylene, carbon monoxide and acetylene.

The synthesis (Scheme 1.1) is achieved by taking a hydrocarbon sources in the gas phase and using an energy source such as plasma, piezoelectric, or a resistively heated coil, to impart energy to a gaseous carbon molecule.

The energy source is used to crack the molecule into a reactive radical species. These reactive species then diffuse down to the substrate, which is heated and coated on the

catalyst surface (catalysts are usually a first row transition metal such as Ni, Fe, or, Co). Changing initial gas composition leads to change the combination of synthesized CNTs and prepare doped CNTs with elements other than carbon such as nitrogen or oxygen. Reported temperatures for the synthesis of nanotubes by CVD vary somewhat, but are generally within the 650-800 °C range.

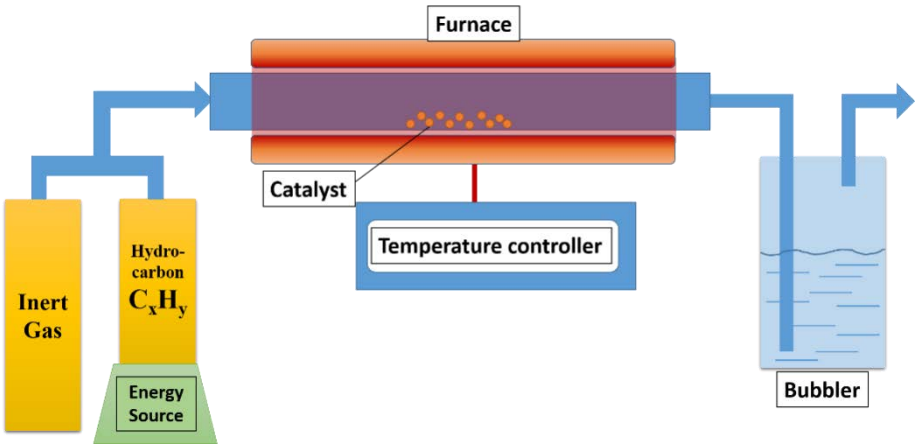

Scheme 1.1 Diagram of a CVD process for CNTs synthesis

In the case of using a liquid hydrocarbon (benzene, alcohol, toluene, etc.), the mixture containing the catalyst (usually transition metal compounds such as ferrocene or other Co or Ni compounds [40]) is heated in a flask using ultrasounds to gasify it and an inert gas that drags the hydrocarbon already converted into steam into the tubular quartz furnace where the synthesis is carried out.

Briefly, CNTs formed as a result of decomposition of hydrocarbon gas, deposit and grow on metal catalyst (substrate). The catalysts particle can stay at the bottom or top of growing carbon nanotube. After cooling the system to room temperature, the resulting nanotubes were collected by scraping the walls of the tube.

1.5 Graphene

Graphene is a two-dimensional, single-layer sheet of sp^2 hybridized carbon atoms. It has attracted enormous attention and research motives for its significant properties. In sp^2 hybridized bond, the in-plane C–C bond is one of the strongest bonds in materials and the out-of-plane is π bond, which imparts a delocalized network or array of electrons resulting electron conduction by providing weak interaction among graphene layers or between graphene and substrate. Graphene is a material with a large theoretical specific surface area (2630 m^2g^{-1}), high intrinsic mobility (200,000 $cm^2v^{-1}s^{-1}$), [9] high Young's modulus (~1.0 TPa) [10] high thermal conductivity (~5000 $Wm^{-1}K^{-1}$) [11], and good electrical conductivity including its ability to stand current density of 10^8 A/cm^2 [12]. Graphene is a very special material because of its unique properties, high hopes have been placed on it for technological applications in many areas [13].

One graphitic layer is well known as single-layer or monoatomic graphene. A two or three graphitic layers is identified as bilayer and tri-layer graphene, respectively. More than 5 up to 10 layer graphene is generally called few layer graphene, and 20–30 layer graphene is referred to as multilayer graphene, thick graphene, or nanocrystalline thin graphite [14] (Fig 1.4).

Graphene unique properties and applications in different areas might be limited by its dispersibility especially when mixed with polar polymer matrices due to its hydrophobicity in nature. Hence, graphene oxide and reduced graphene oxide (rGO) are known as suitable alternative for various applications.

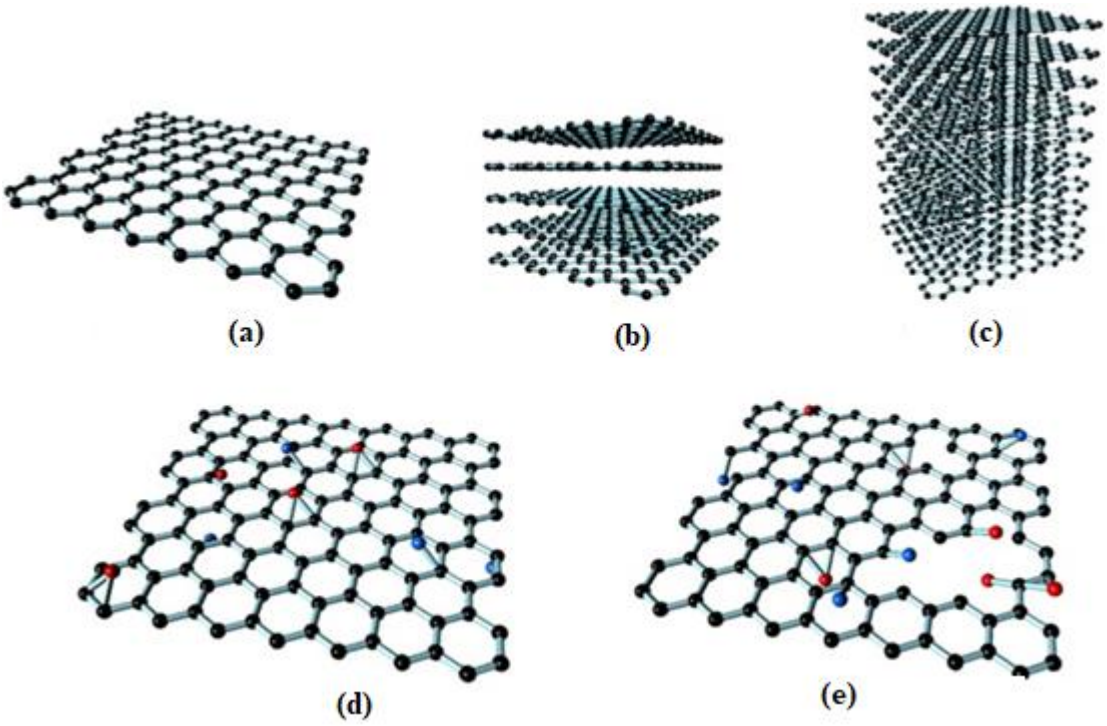

Fig. 1.4 Structural difference between (a) Graphene, (b) Few Layer Graphene (FLG), (c) Graphite, (d) Reduced Graphene Oxide (rGO), and (e) Graphene Oxide (GO)

1.5.1 Graphene oxide (GO)

During the measurement of the atomic weight of carbon, Benjamin Brodie (1859) achieved some of the primary experiments on the chemical properties of graphite [15]. He claimed that significant oxidation of graphite by exposing it to a mixture of fuming HNO_3 and $KClO_3$ solution for several days, could take place. Finally, at the end of his experiment, he called a light yellow color product, as “graphic acid” which today we call it graphite oxide (GO). After about a century later, Hummers and Offeman (1958) found a significantly safer synthesis of graphite oxide using a mixture of graphite with $NaNO_3$, and $KMnO_4$ in concentrated H_2SO_4 [16]. GO is a layer of graphene with oxygen atoms, OH and COOH groups attached to it (see Fig 1.4).

GO as the same as graphene has been explored in a wide range of applications, such as

electronic and photonic devices, drug delivery, energy generation/storage, optical devices, chemical/bio sensors, etc. [17,18].

1.5.2 Reduction of graphene oxide (rGO)

The reduced GO (rGO) sheets are usually considered as one kind of chemically derived graphene (Fig 1.4). Different reduction methods such as thermal reduction, photo catalyst reduction, solvothermal/hydrothermal reduction, microwave and photo reduction have been reported in order to provide reduced graphene oxide (rGO) [19]. Chemical reduction of GO is a suitable method to synthesized reduced graphene oxide (rGO) and graphene in large quantities.

1.6 Synthesis of graphene

After discovery of graphene in 2004, different methods were developed to generate thin graphitic films and few layer graphene, depending on the desired size, purity and crystallinity of the final product [20]. A summary of common synthesis methods is shown in Scheme 1.2. There are two main approaches; 'Top- down' and 'Bottom- up'. The first one involves the production of graphene or modified graphene sheets by separation/ exfoliation of bulk graphite or graphite derivatives such as graphite oxide (GO) and graphite fluoride. Whereas in "bottom- up" methods graphene is grown on different substrates, which are subsequently removed latterly [21]. This means starting at atomic scale and building up atom by atom to the desired final size of the material. The top-down approach is widely used for graphene synthesis in large quantity and the resulting graphene nanosheets can be conveniently complexed with other functional

components to fabricate novel materials [22].

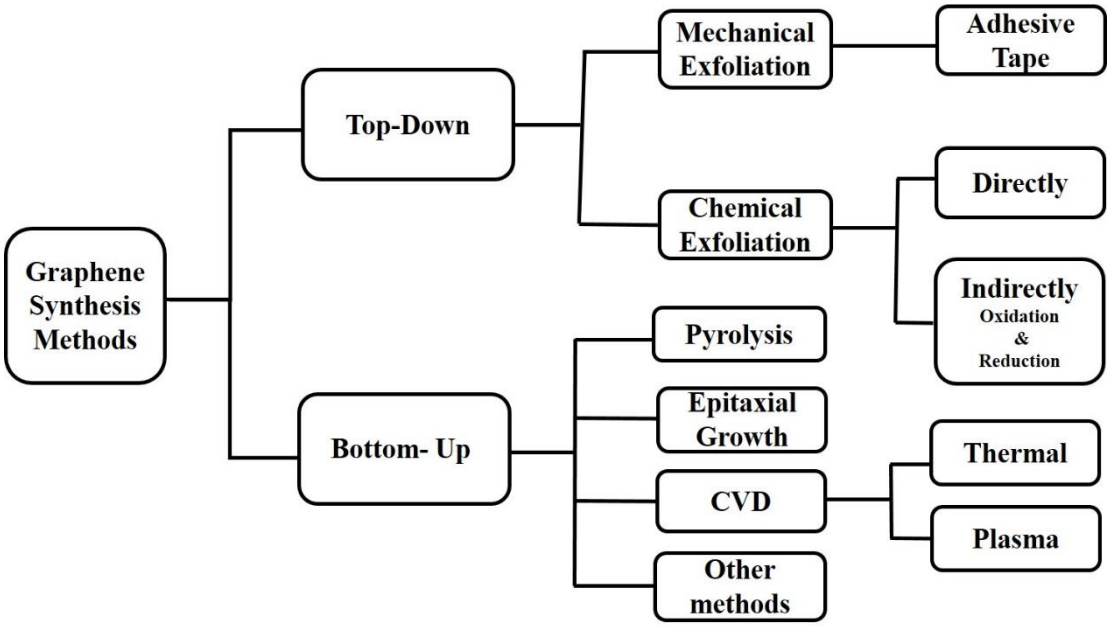

Scheme 1.2 Graphene synthesis methods

1.6.1 Exfoliation

Graphite is formed of mono-atomic graphene layer bundling through overlapping of partially filled *p* orbital perpendicular to the plane of the sheet together by weak van der Waals forces. The inter layer band energy and distance between layers is 2 eV/nm^2 and 3.34 Å, respectively.

Mechanical cleavage or exfoliation with the large lattice spacing via weak bonding in the perpendicular direction is the reverse of stacking with the small lattice spacing and stronger bonding in the hexagonal plane. An external stress about 300 nN/μm^2 is required to separate one mono-atomic layer from graphite via mechanical cleavage [23]. Mechanical exfoliation using a simple “scotch tape” is the most famous method that belongs to this group which was first reported for the production of graphene by Novoselov and Gaim in 2004 [24].

Although, the quality of the prepared graphene by these methods is high with almost no defects, this process has major disadvantages to obtain larger amounts of graphene [25].

Directly chemical graphite exfoliation in the liquid phase as another Top-down method to produce graphene has been already reported by some research groups [26]. In this strategy, choosing the most suitable solvent or surfactants to exfoliate and disperse graphene is very important. The low yield efficiency (typically <0.01 mg mL^{-1}) [27] and longtime procedure (400h) are the most disadvantages of these approaches [28].

Indirectly graphite exfoliation with preliminary oxidation is another chemical method. This method is a two-step procedure. First step includes decrease the interlayer van der Waals forces by phenyl hydrazine, hydroxylamine, glucose, ascorbic acid, hydroquinone, pyrrole, oxidation of layers, or inserting large alkaline ions between the graphite layers [29]. In this step, graphene intercalated compounds are formed (GICs). The second step is the exfoliation of GICs to obtain few layers by reduction, rapid heating, sonication or ultracentrifugation [30,31].

Different reduction methods such as photocatalytic, thermal, solvothermal, hydrothermal, microwave [32], sonochemical [33], and photo reduction have been reported in order to provide reduced graphene oxide (rGO) [34].

Elemental analysis (atomic C/O ratio) of the rGO revealed the existence of a significant amount of oxygen, indicating that reduced graphene oxide is not the same as pristine graphene (Fig. 1.4). Normally maximum reduction cannot be achieved and some parts of oxidized group will remain [35].

The common ways for oxidation of graphite are Brodie and Hummers' methods. (see

also section 1.5.1). Hummers' oxidation method is still the favored method because of the following reasons [36]:

i) Replacement of $KClO_3$ by $KMnO_4$ as the oxidation agent, which resulted in elimination of toxic gas byproducts and improving the reaction safety

ii) The shorter oxidation time is needed in this method

iii) It is easy to disperse the resulted GO in water

iv) A larger restoration of the pristine graphite 2D structure is achieved [37].

In this work, we have prepared oxidized graphite flake according to the Hummers' method.

1.7 Carbon based nanocomposites

Carbon nanotubes or graphene can be utilized in two main different ways: as a nanofiller additive to prepare nanocomposites with special properties or as a supporting medium to be functionalized or decorated.

Many of the noticeable properties of carbon nanoparticles can be best obtained by incorporating them into some form of matrix to make different composites. Carbon based nanocomposites are made up of a polymer matrix and carbon nanotubes (CNTs), graphene, graphene oxide (GO) or reduced graphene oxide (rGO) as the fillers.

The incredible potential based on these nanofillers are very important for many structural materials, particularly in modifying the electrical, thermal, mechanical, optical, photoelectrical properties of carbon based nanocomposites [38,39].

Because of the nanometer size, high aspect ratio, and Van der Waals attraction between each set of tubes in CNT and layers in graphene, they have high surface energy and a

significant tendency for agglomeration and bundling.

Furthermore, nanocarbon materials with special characteristics like highly hydrophobic surface area, week binding capability and low solubility in organic solvent are almost nonreactive in chemical reactions.

To employ these carbon nanoparticles as effective reinforcement in polymer nanocomposites, proper dispersion and appropriate interfacial adhesion between the carbon nanoparticles and polymer matrix have to be guaranteed.

1.7.1 Distribution vs. Dispersion of carbon nanoparticles

Dispersion refers to the allocation of the nanoparticles within the matrix, whereas the distribution indicates the breaking of the aggregates into small sizes. A sufficient distribution does not inevitably implies a good dispersion, and vice versa. Scheme 1.3 (a) illustrates a case of poor distribution and poor dispersion, (b) good dispersion but poor distribution, (c) good distribution but poor dispersion and (d) good distribution and good dispersion [40].

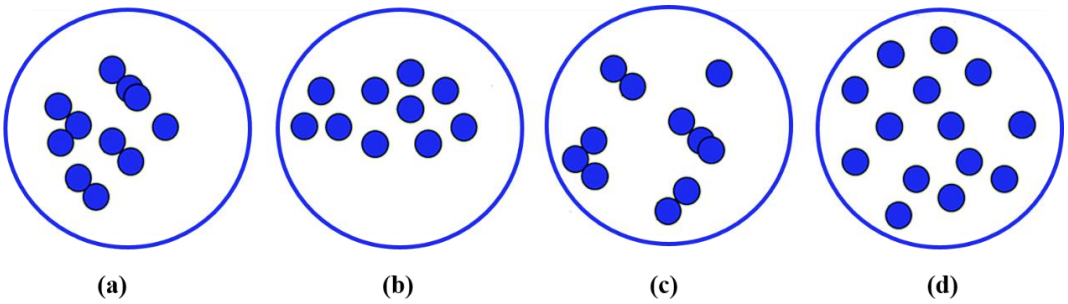

Scheme 1.3 illustration of (a) poor distribution and poor dispersion, (b) poor distribution but good dispersion, (c) good distribution but poor dispersion and (d) good distribution and good dispersion

Usually, it is difficult to achieve a good dispersion of CNTs and graphene due to their large surface area; however, there are techniques available to break up these agglomerations.

1.8 Methods to improve carbon nanomaterials dispersion

All techniques to disperse the carbon nanoparticle aggregates into finer structures to enhance the desired properties of the composites belong to two main categories: physical and chemical techniques.

The most convenient physical approaches for dispersing are ball milling, calendaring, high shear mixing and ultrasonication. Physical or mechanical methods can only break up agglomerates into smaller parts or single-agglomerates so the dispersion quality is often inadequate [41].

1.8.1 Non-covalent functionalization of CNTs

The non-covalent functionalization of CNTs could be achieved by π–π stacking interactions between conjugated molecules and the graphitic sidewall of nanotubes [42]. The non-covalent modifications of CNTs can preserve their desired remarkable properties and improving their solubility, simultaneously. Interaction between CNTs and some polymers (wrapping with polymers) such as polyphenyl ethers (PPE) [43], polyethylene glycol (PEG) [44], and polyvinylpyrrolidone (PVP) [45] are good examples to affect dispersion and stability of nanotubes in polymer matrix.

The non-covalent interaction methods of CNTs do not destroy the intrinsic sp^2-hybridized conjugated system of the nanotubes walls, so the properties of the final

structure of the material can be preserved. This method has another important feature that makes it even more interesting, which is the reversibility. Actually, it is possible to recover the bare CNTs from the CNT-coated both in aqueous or organic solvents [46].

1.8.2 Covalent functionalization of CNTs

In this group, functionalization is based on the covalent chemical bonding between carbon atom of CNTs surface and functional groups. This method in comparison to the non-covalent strategy is more effective, and can be better controlled.

Because of the extra strain in the cap region of CNTs, the carbon atoms in this areas are highly reactive than atoms on the sidewall [47]. Therefore, according to the location of functional groups, covalent modification can be classified into two groups including to the sidewalls and ends (caps) defect of the CNTs.

A change in hybridization from sp^2 to sp^3 and simultaneously a loss of π-conjugation system on graphene layer resulted from sidewall functionalization.

Oxidative damaging of CNTs is one of the most common and effective example of the caps functionalization series. Oxidant can open the ends and convert the capped CNTs into open fullerene pipes. The oxidative processes involving sp^2 hybridized carbon atoms start with the creation of an alcohol group, followed by a ketone group, and finally yielding a carboxylic group [48].

Typical functionalization could be occurred by exposing CNTs framework to a strong acid, mixture of acids like HNO_3-H_2SO_4, strong oxidants such as $KMnO_4$, Ozone, hydrogen peroxide, etc. [49]. In the presence of strong oxidizing agents, the graphitic structure of CNTs is also attacked, thus creating a large number of unwanted defect

sites is inevitable.

Finding the most effective oxidant with less amount of damage in nanotubes structure is always favorable. In the next paragraph we will explain more about it.

Oxidation of CNTs with H_2O_2

Using hydrogen peroxide alone or in combination with acid or ultraviolet light (UV) as a powerful oxidant for oxidation of CNTs has been already reported [50,51]. Coupling UV with a mild oxidant like H_2O_2 appears to be efficient with no apparent structural damage on the tubes [52]. In this method hydroxide radicals (OH^*) which are stronger oxidants are generated from hydrogen peroxide by UV illumination according to the following reaction:

$$H_2O_2 + hv \rightarrow 2OH^*$$

In our work we used oxidation of CNTs with UV/H_2O_2 as an effective solution to purify synthesized carbon nanotubes and to improve the epoxy dispersability, simultaneously.

1.9 Doping

According to the definition, doping is the phenomena of introducing either non-carbon atoms or molecules and compounds (impurities) into the layered sp^2 carbon nanosystems in different manners at small concentrations (from parts per million to small weight percentages) [53]. There are three main categories of doping: exohedral (or intercalation), endohedral (encapsulation or filling) and in-plane (or substitutional) doping [54] (Scheme 1.4).

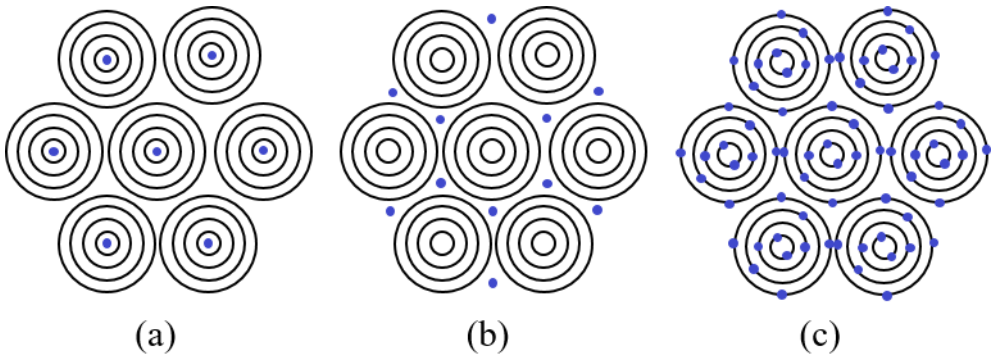

Scheme 1.4 Molecular model of (a) endohedral; (b) exohedral, and (c) in-plane doping in MWCNT bundles

Doping is one of the effective approaches that allows the intrinsic modification of CNTs' chemical properties [55]. The first doping reactions by K and Rb were performed on MWCNTs prepared by the electrical arc-discharge method [56].

There are currently several methods of doping CNT with various substances: nanotubes doping during their growth (i.e. in-situ methods) with gas or liquid phase encapsulation in the cavity of preliminary formed CNT and chemical modification of CNT's surface (i.e. ex-situ methods). In-situ approaches include CNT modification during synthesis by arc-discharge or CVD methods.

Iodination or bromination are good examples to specifically affected CNT, since such doping can produce p-type semiconductors [57].

Nitrogen doped CNTs with bamboo-type structure in a low nitrogen concentrations as another example were generated via pyrolysis of pyridine and methylpyrimidine for the first time [58]. Up to now, numerous applications of nitrogen doped carbon nanotubes have been reported: field emission devices [59], sensors [60], catalysts [61], electrocatalysts for oxygen reduction reaction [62], and batteries [63].

Oxygen doped carbon nanotubes has also been prepared and studied [64].Interesting applications as catalysts for electrophoresis have been reported [65].

CVD was the strategy utilized in this work to synthesize Nitrogen and Oxygen doped carbon nanotubes which we call them CN_x and CO_x respectively. We have followed the nomenclature approach used by Terrones group [64] to highlight that the number of doped sites is unknown.

1.10 Graphene-based nanohybrides

Graphene with significant conductivity, excellent electron mobility and high specific surface area is a good substrate to produce graphene-based compounds via functionalization. Graphene with remarkable properties is a “magic bullet” for the composite world [66].

Graphite and its derivatives like graphene, graphene oxide (GO), and reduced graphene oxide (rGO) have been recognized as attractive catalyst supports because of their extremely high surface area (~2600 m^2/g), high thermal/electrical conductivity, and chemical stability [67].

In recent years, decoration of graphene sheets with metal oxides nanoparticles (MONPs) to prepare graphene metal oxide hybrids has attracted considerable attention for their potential applications in photovoltaic devices, energy harvesting, catalysis, and photocatalysis areas. The synergetic effect between graphene and MONPs resulted in outstanding properties of graphene combination [68].

Anchoring transitional metal oxides such as TiO_2, ZnO, SnO_2, MnO_2, Co_3O_4, Fe_3O_4, Fe_2O_3, NiO, and Cu_2O on graphene are good examples to obtain enhanced efficiency in various applications of these combinations.

Among the aforementioned transitional metal oxide nanoparticles (MONPs), low cost copper based metal oxides are materials with potential and diversified heterogeneous catalytic applications including electrochemical catalysis [69], photocatalysis [70], chemical catalysis in organic synthesis [71].

To date, different strategies to synthesize and support MONPs have been proposed. The most effective methods to MONPs decoration on graphene includes solution mixing method, sol–gel method, hydrothermal/solvothermal method, self-assembly and microwave irradiation [72].

A unique characteristic of microwave processing is rapid, sectional and localized heating, because materials are heated directly through the interaction with microwave energy which is opposite to the slow heating in a conventional furnace [73].

Therefore, due to their excellent properties, preparation of graphene-copper oxide nanohybrides have attracted our interest.

Our focus in the present thesis was to design a convenient and cost effective method using domestic microwave oven to prepare and decorate copper salts on GO.

1.11 Characterization of carbon-based nanoparticles and related nanocomposites

Carbon nanotubes and graphene due to their specific atomic structure have special physical and chemical features. The size, structure, morphology and composition of

synthesized pristine and doped carbon-based nanoparticles and their nanocomposites are characterized and analyzed by different methods such as electron microscopy observations, which includes Scanning Electron Microscopy (SEM), Transmission Electron Microscopy (TEM), and Atomic Force Microscopy (AFM). The spectroscopic analysis like X-Ray Diffraction (XRD), Raman and Infrared (IR) spectroscopies are also useful to characterize the morphology and structure of these nanoparticles. Normally, thermal analysis such as Thermogravimetry Analysis (TGA), Differential Scanning Calorimetry (DSC) and Dynamic Mechanical Thermal Analysis (DMTA) are very helpful to analyze the combination of nanocomposites based on carbon nanoparticles.

1.11.1 Electron microscopy observations

Electron microscopy is one of the essential tools for characterizing any nanomaterial according to the direct shape, size, and structure observation. The local structure and surface of the carbon nanoparticles and their composites can be analyzed at the nanometer level by these techniques. Boehm et al in 1962 observed the single layers and multilayers of colloidal graphite oxide by electron microscopy [74].

Scanning Electron Microscopy (SEM), Transmission Electron Microscopy (TEM), and Atomic Force Microscopy (AFM) are useful tools to check the exfoliation of bundles and the purity of the CNTs. However, TEM and SEM produce damages on the sample due to the use of the electron beam.

SEM method gives information mainly about outer surface morphology of the sample and about chemical composition of CNT and graphene compounds. The only

measurable parameters are a size of carbon particles and a diameter and length of bundles. In this method, information about diameter of one nanotube is impossible to find.

Decorated metallic particles on carbon nanomaterials (i.e. CNT and GO) can be well-defined displayed using SEM.

However, SEM examination provides an overview of nanostructures; a more accurate examination would be done by TEM. It is possible to determine directly the diameter of one nanotube and bundle diameter from TEM images.

AFM is used to study the sample in three dimensions and facilitates forming 3D images of a sample surface with high lateral spatial resolution (0.1 - 1.0 nm), as well as atomic scale vertical resolution (0.01 nm). This method gives us information only about the length of nanotubes and approximate valuation of the bundles diameter [75].Any special sample preparation is required for AFM so it can be used in aqueous solution or vacuum ambient [76].

SEM was performed using a FEI equipment, with a voltage of 10 kV and a secondary electron detector. Dimensions (length and diameter) of synthesized carbon nanotubes were determined over 500 nanotubes for each sample.

TEM analyses of the samples were carried out using a Zeiss EM-10C with a field emission gun operating at 60–100 kV.

The atomic force microscope used for this work was an AFM, JEOL equipped with a JSPM 5200, the measurements being made at room temperature in intermittent contact mode using Si tips.

1.11.2 X-ray Diffraction (XRD)

This technique is based on measuring the intensity and the angle of scattered X-rays from electrons bound to atoms (sample material) as a function of atomic position. Depending on the geometry of the crystal lattice, initial waves scattered by atoms at different positions and angles. The simplest and most frequently used application of scattering theory is the Bragg law. By considering crystals as reflection layers for X-rays, W.H. Bragg derived the following equation:

$$2d\sin\theta = n\lambda$$

where λ is the wavelength of the X-rays, 2θ is the scattering angle, n is an integral number and d represents the distance between successive identical planes of atoms in the crystal.

According to the Bragg's law represented in Fig.1.5, it is possible to perfectly measure the CNTs' crystallinity and the layer distance or interlayer spacing between graphene oxides by XRD.

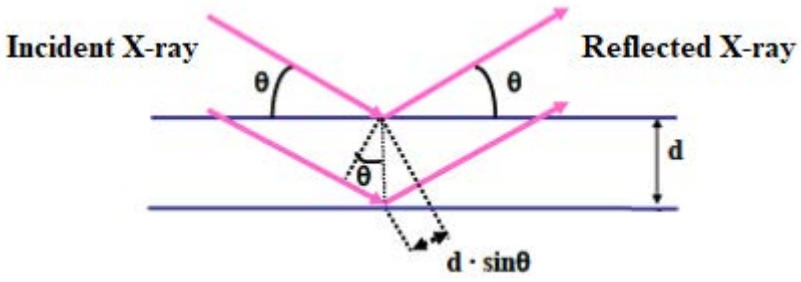

Fig. 1.5 of Bragg's law

In this work XRD patterns were collected in an automatic X'Pert Philips diffractometer using a Cu K_α radiation (λ = 1.54187 Å). Data were collected in the 2θ range from 5° to 80° in step-scanning mode with a step size of 0.01° and a counting time of 0.5 s per step.

1.11.3 X-ray Photoelectron Spectroscopy (XPS)

X-ray photoelectron spectroscopy (XPS) also known as Electron Spectroscopy for Chemical Analysis (ESCA) is one of the best tools which can give a lot of information about the chemical structure of CNTs and GO due to the chemical interaction with organic compounds or gases adsorption [77].

This surface analysis technique using Al Kα provides both elemental and chemical state information by irradiating X-rays on the sample surface, and measuring the kinetic energy of the photoelectrons emitted from the top 1-10 nm of the sample.

The chemical state of an atom alters the binding energy (BE) of a photoelectron which related to the measured photoelectron kinetic energy (KE) by the simple equation:

$$BE = h\nu - KE$$

where hv is the photon (x-ray) energy.

Peaks appear in the spectrum from atoms emitting electrons of a particular characteristic energy. The elemental identity, chemical state, and quantity of all detected surface elements can be derived from these chemical shifts (except hydrogen). The distribution and bonding of heteroatom dopants in carbon nanomaterials (CNTs, GO) can be particularly shown by appears new peaks in XPS according to the bonds formed between carbon atoms and compounds added [78].

XPS in the current work was performed with an Ultra-axis (Kratos) and the chemical surface analysis was performed by adsorption measurements with N_2 at 77K with a max BELSORP (Bel Japan Inc). The recorded spectra were analyzed using CASAXPS software, and RSF database by peak fitting after Shirley background correction.

1.11.4 Raman spectroscopy

Raman spectroscopy is another spectroscopic technique based on inelastic scattering of monochromatic light, usually from a laser source. Photons of the laser source light are absorbed by the sample and then reemitted. Frequency of the reemitted photons is shifted up or down in comparison with original monochromatic frequency, which is called the Raman effect.

All carbon's allotropes forms are Raman active [79]. Raman spectroscopy provides a powerful, fast and non-destructive spectroscopic characterization tool for carbon-based nanomaterials, showing different characteristic spectral features for sp^3, sp^2, and sp carbons. Each band in the Raman spectrum corresponds to a specific vibrational frequency of a bond within the molecule. Raman spectra in the range of 1000 to 2500 cm^{-1} appears for carbon nanotubes and graphene [80]. Fig. 1.6 shows a general Raman spectra of carbon base nanoparticles.

The Raman spectrum of SWCNT consists of four dominant Raman-allowed bands [81]:

(i) A high- frequency bunch called G-band (~1600 cm^{-1}) corresponding to a splitting of the C-C band stretching mode of graphitic carbon atoms in nanotubes (Carbon sp^2)

(ii) Disorder line (D-band) is derived from defects (impurities or disorders) in the carbon network appears at ~1300 cm^{-1}

(iii) A bunch of peaks for poly-disperse samples when resonating conditions are met called as radial breathing mode (RBM) (< 200 cm^{-1})

(iv) G′ (or 2D) band is overtone of D band depends on the diameter of CNTs.

MWCNT have similar Raman spectra to those of SWCNT. The basic differences are

the lack of RBM band (the outer tubes restrict the breathing mode) and a more obvious D-band (the multilayer configuration indicates more disorder in the structure) in Raman spectra of MWCNT [82].

The quality (crystallinity) of CNTs can be measured by comparing the D to G band intensity. If the relative intensity of G and D bands is greater than 9:1, the spectra indicate highly crystalline CNTs.

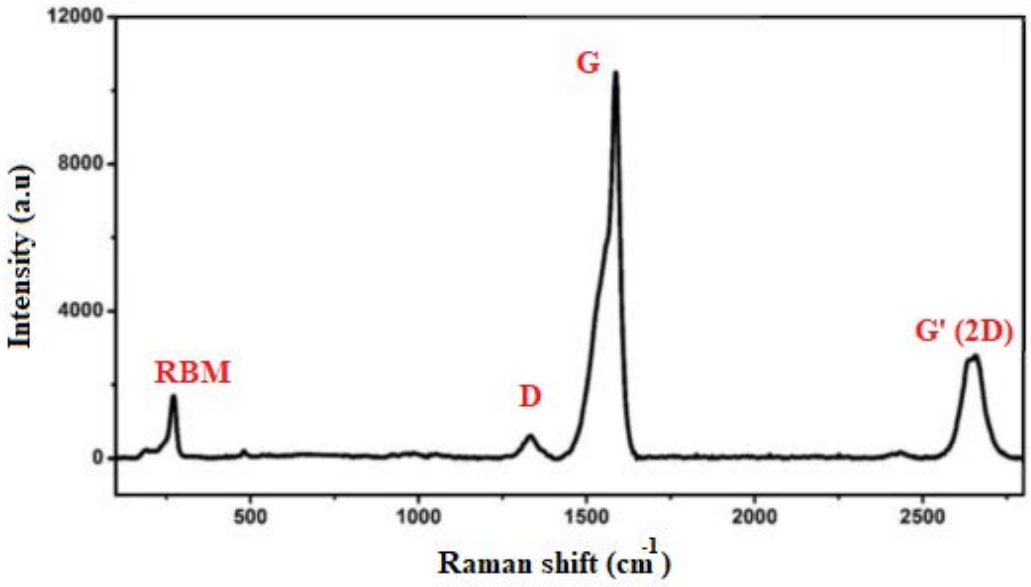

Fig. 1.6 General Raman spectra of carbon based nanoparticles

Raman spectroscopy is also carried out to characterize graphene. It is the fastest and most precise method of identifying the thickness of graphene flakes and estimating its crystalline quality. This is because graphene exhibits characteristic Raman spectra based on number of layers present [83].Observing the ratio between the G (1600 cm^{-1}) and G′ (2700 cm^{-1}) bands in a Raman spectrum helps to determine the number of layers [84].

Raman measurements in our study were carried out via Renishaw confocal microscope

using the 514.5 nm laser excitation.

1.11.5 Thermogravimetric analysis (TGA)

Thermogravimetric analysis (TGA) is an experimental technique that measures the weight changes which occur during the heating the sample. This method can be used to determine the thermal stability of a material as well as the presence of volatile components in a sample. TGA can be also used to measure the purity of carbon nanomaterials as these materials undergo complete loss at elevated temperatures.

In addition, many studies have been observed the importance of studying the thermal properties particularly with TGA of nanocomposites containing CNTs and graphene oxide since a significant enhancement in thermal stability of the polymeric matrices filled with the carbon nanomaterial, compared to unfilled ones [85].

TGA of our samples in this work was performed in a TGA Q50 (TA Instruments) system heating from room temperature to 800 $^{\circ}$C. Approximately 5 mg of samples was heated in an open Pt crucible at a rate of 10 $^{\circ}$C min^{-1} under N_2 (90 mL min^{-1}).

1.11.6 Differential Scanning Calorimetry (DSC)

Differential scanning calorimetry (DSC) is the most broadly used of the thermal analysis techniques in different research areas, development, and quality inspection and testing. By performing DSC over a large temperature range, thermal transitions and relaxations can be quickly identified. The relevant temperatures and the characteristic enthalpic values can be determined using substance quantities of only a few mg. The measured properties by DSC during a thermal scan of nanofillers (CNTs or graphene)

include heat capacities, heats of transitions, kinetic data, sample purity, the degrees of crystallinity, and temperatures of glass transitions (T_g) [85].

Differential scanning calorimetry (DSC) was used to determine the glass transition temperature (Tg) of the nanocomposites using a Mettler Toledo DSC 822 with a liquid nitrogen reservoir. Samples of about 5 mg were scanned from 25 °C to 250 °C at 10 °C.min^{-1}. In order to minimize the effects of previous thermal history, data from a second scan were used for analysis.

1.11.7 Dynamic Mechanical Thermal Analysis (DMTA)

DMTA is frequently used in nanocomposites characterization since it allows the measurement of the dynamic storage modulus (E′), dynamic loss modulus (E″), mechanical loss angle tangent (tan δ= E″/E′). The tan δ illustrates the macromolecules mobility as well as the relaxations in the polymers. Furthermore, DMTA is one of the most used techniques for measuring the glass transition temperature of carbon based polymeric materials (T_g), since it is fast and suitable for quality control applications [86].

DMTA data of our samples were collected using a DMTA Q800 Dynamic Mechanical Analyzer (TA Instruments), with amplitude of 30 μm at 1 Hz. Nanocomposite specimens with nominal dimensions of 60×10×2 mm^3 were mechanically tested in single cantilever mode. The samples were heated from room temperature to 250 °C at a linear rate of 3 °C.min^{-1}.

1.12 Outline of the thesis

In this dissertation, we will present the synthesis of oxygen doped carbon nanotubes and graphene-based nanomaterials and we will study their behavior in different fields: as flame retardants, as photocatalysts and as catalyst for organic synthesis.

The dissertation is divided into six core chapters. Chapter 2 is concerned with the synthesis and characterization of pristine carbon nanotubes (CNT), oxygen doped carbon nanotubes (CO_x) and nitrogen doped carbon nanotubes (CN_x) via CVD method. Chapter 3 will present the microwave assisted versatile copper compound decoration of graphene oxide in different solvents as well as its characterization.

In chapter 4, preparation method and characterization of epoxy nanocomposites based on synthesized carbon nanotubes (CNT, CO_x, CN_x) will be shown and comparative study about the effect of synthesized carbon nanotubes on flame retardancy epoxy nanocomposites will be discussed.

Consequently, study about the performance of copper salts decorated graphene oxide in photodegradation application will be explained, in the chapter 5. In chapter 6, comparative study of organic chemistry catalysis activity of copper salts /GO will be presented. The references which have been used to write the dissertation will be listed at the end.

Chapter 2
Synthesis & Characterization of Oxygen and Nitrogen Doped Carbon Nanotubes

2.1 Introduction

In this chapter, CVD method is described to grow doped CNT with Oxygen and Nitrogen. By changing the combination of the precursor, different CNTs powders in characterization have been produced. Based on the characterization methods, (XRD, XPS, SEM, TEM, Raman spectroscopy, and TGA), pristine carbon nanotube, oxygen and nitrogen doped carbon nanotubes that are abbreviated to CNT, CO_x and CN_x, respectively were well defined.

2.2 Synthesis of carbon nanotubes by CVD

All materials and the solvents were purchased from Aldrich chemical company and used as received. A single furnace equipped with the CVD technique were used to synthesize three different carbon nanotubes. We have followed the method proposed and used in the PhD Thesis of Dr. V.J. González [87]

2.2.1 Synthesis of CNT

CNT synthesized via CVD method by starting from a solution consisting of 95% Toluene and 5% Ferrocene. The precursor was initially sonicated for 20 minutes. Argon gas with a flow of 2.5 $L.min^{-1}$ for 30 minutes at 850 $^{\circ}C$ was used in our single furnace CVD system.

Total obtained weight was in the range 0.9-1.7 g in each synthesis.

2.2.2 Synthesis of CO_x

In the case of CO_x, a different solution containing 94% Toluene, 1% Ethanol and 5%

Ferrocene was used for 30 minutes. The time and temperature in CVD system was the same as CNT processing. Finally, 0.8-0.95g total weight was obtained in each synthesis.

2.2.3 Synthesis of CN_x

The procedure to obtain CN_x was the same as previous ones but using an initial solution containing 5 wt.% of ferrocene ($FeCp_2$) in benzylamine (C_7H_9N). Benzylamine used as a nitrogen defect source. An approximate total weight of 1.2 g was obtained per each synthesis

2.2.4 Oxidation by H_2O_2-UV

All of these synthesized nanotubes, CO_x, CN_x and CNT were purified and improved their epoxy dispersibility by H_2O_2 –UV method described in the previous work of our group [87]. According to that method, the nonotubes were dispersed in H_2O_2 and the solution exposed to UV light meanwhile was stirred for 15 minutes. After the illumination, the nanotubes were filtered and washed with water several times, and then dried at 80ºC under vacuum for 24 hours.

2.3 Characterization of nanotubes

2.3.1 X-Ray Diffraction (XRD) and Raman spectroscopy

XRD was collected in an automatic X'Pert Philips diffractometer using a Cu source. By testing different step size and counting time, we decided to collect the data in the 2θ range from 10° to 90° in step-scanning mode with a step size of 0.02° and a counting time of 2 s per step.

For each sample, various spectra were recorded at different sample positions in order to verify the homogeneity of the sample.

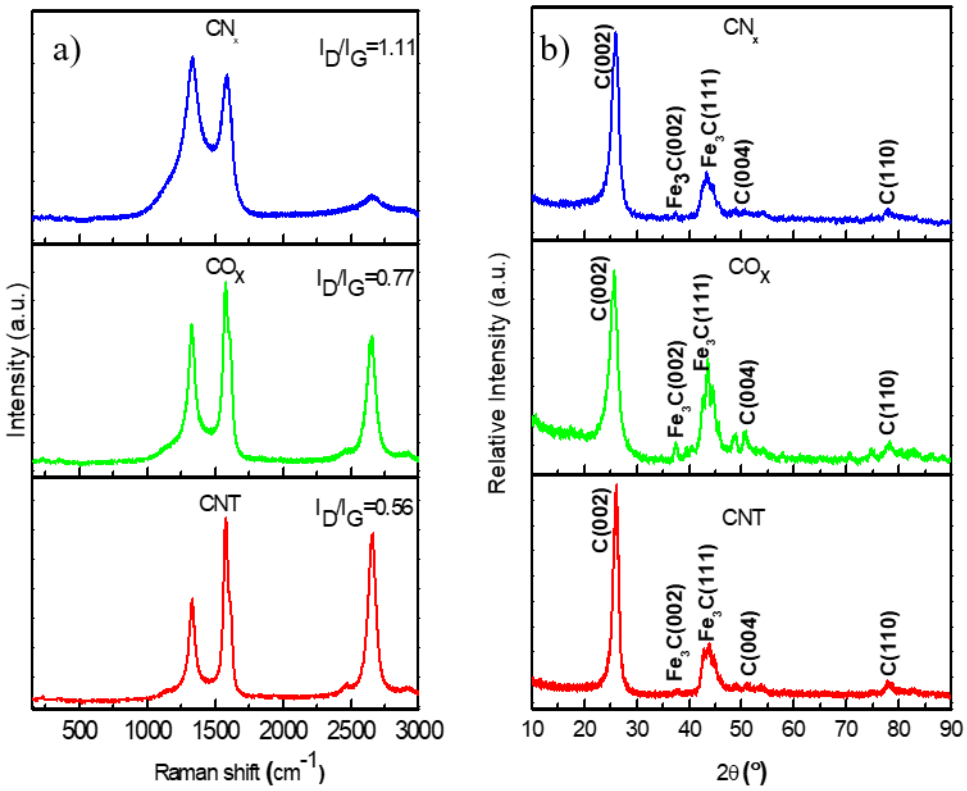

Fig. 2.1 (a) Raman spectroscopy and (b) XRD of CNT, CO_x and CN_x

Raman characterization and XRD analysis (Fig. 2.1 (a) and (b) were used to know the quality of crystallinity and defect of synthesized carbon nanotubes. According to the amount of I_D/I_G for each nanotubes, CNTs have a higher degree of crystallinity in comparison with CO_x and CN_x which is in agreement with TGA results (section 2.4.4).

2.3.2 X-ray Photoelectron Spectroscopy (XPS)

XPS result is shown in Table 2.1 extracted from Fig. 2.2.

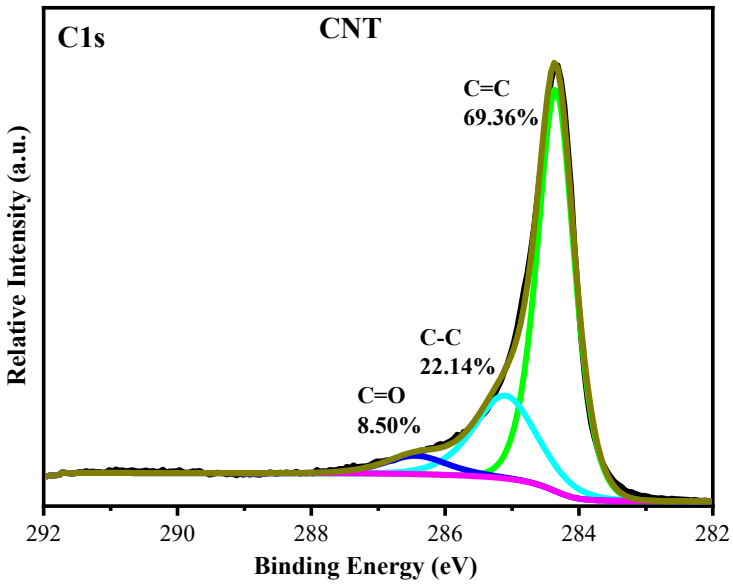

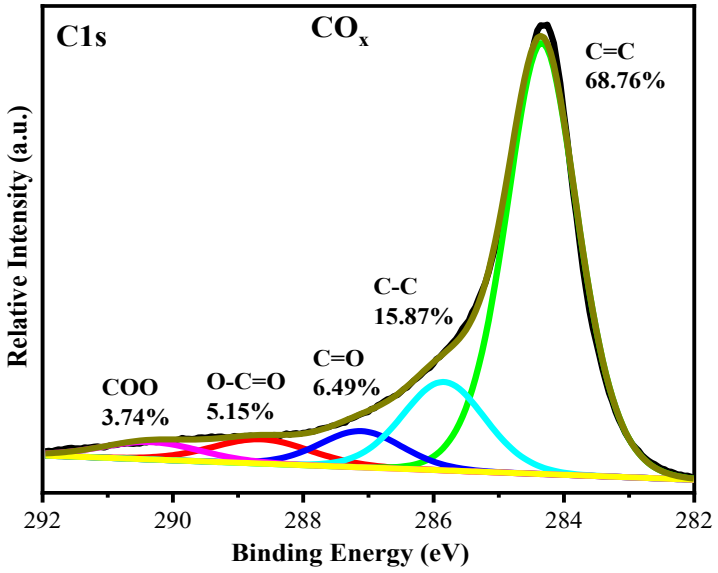

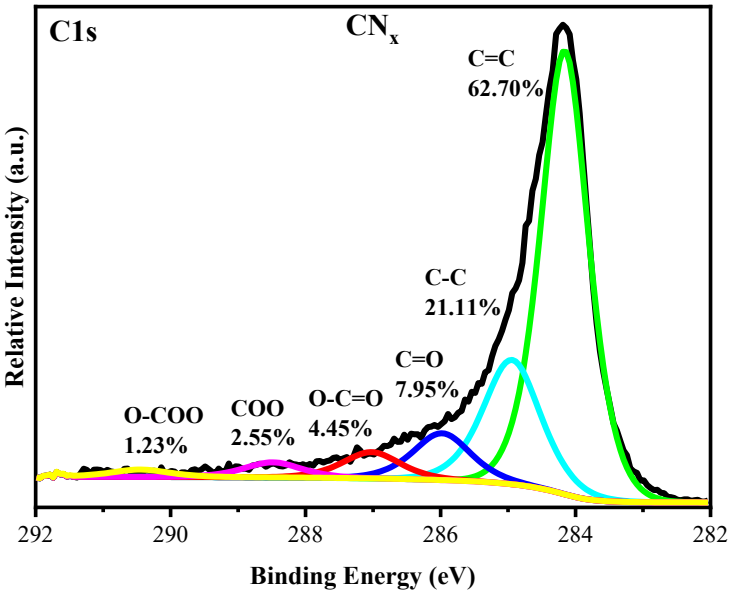

Fig. 2.2 XPS of: CNT, CO_x and CN_x

Based on the results, 99% of carbon atoms of CNT are either aromatic or aliphatic and present the highest percentage of C=C bonding compared to doped nanotubes.

For CO_x and CN_x the fraction of oxidized carbon atoms is about 15% being the amount of N atoms in the structure of CN_x of 1.9%.

Table 2.1. XPS analysis of CNT, CO_x and CN_x

Sample	**C=C**	**C-C**	**C=O**	**O-C=O**	**COO**	**O-COO**	**N**
CNTs	77.57	21.65	0.02	0.71	0.04	0	0
CO_x	68.76	15.87	6.49	5.15	3.74	0	0
CN_x	62.70	21.11	7.95	4.45	2.55	1.23	1.93

These data clearly shows that the amount of carbon atoms involved in oxygen containing functional groups is in the range of 15% for CO_x and CN_x nanotubes, and it seems that there is not too much difference in the nature of the oxygenated functional groups.

All these doping provide great reactivity and solubility, which play an important role in the preparation of polymer nanocomposites and to achieve enhanced interfacial interaction between nanotubes and polymers (chapter 4).

2.3.3 SEM and TEM

Fig. 2.3 represents SEM images of different types of CNTs with their typical tubular structure. Dimensions (length and diameter) were determined over 500 nanotubes for each sample; histograms of lengths and diameters are presented in Figs. 2.4 and 2.5, respectively. The averages are summarized in Table 2.2. The lengths of the nanotubes

were ≥136 μm, the diameters ranged between 60 and 90 nm and CO_x nanotubes presented the highest aspect ratio near 3000.

It can be observed the tendency of nanotubes to present a notably higher length to diameter ratio. This is not surprising since it has already been reported that oxygen in the gas feed (ethanol) helps to keep the Fe catalyst clean from carbon agglomeration and active for longer periods, thus resulting in longer nanotubes [64].

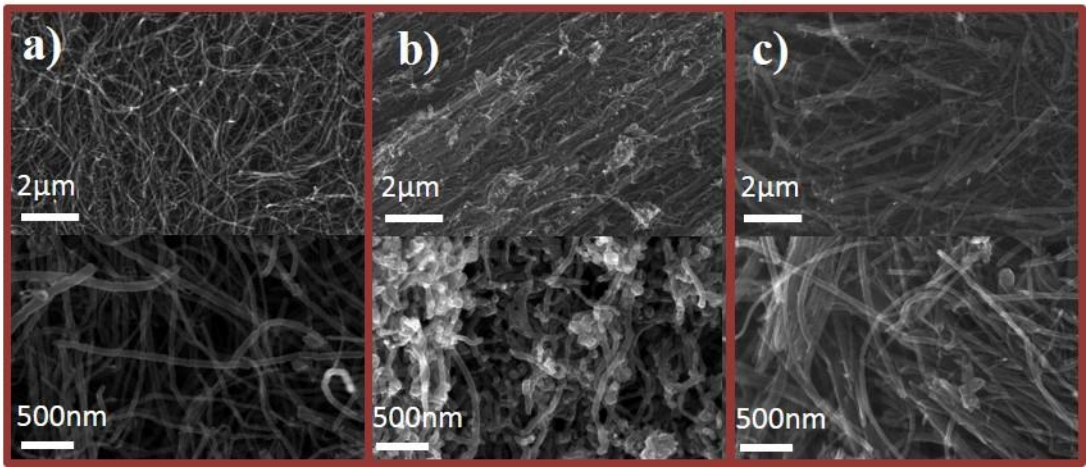

Fig. 2.3 SEM image of: a) CNT, b) CO_x and c) CN_x at two different magnifications

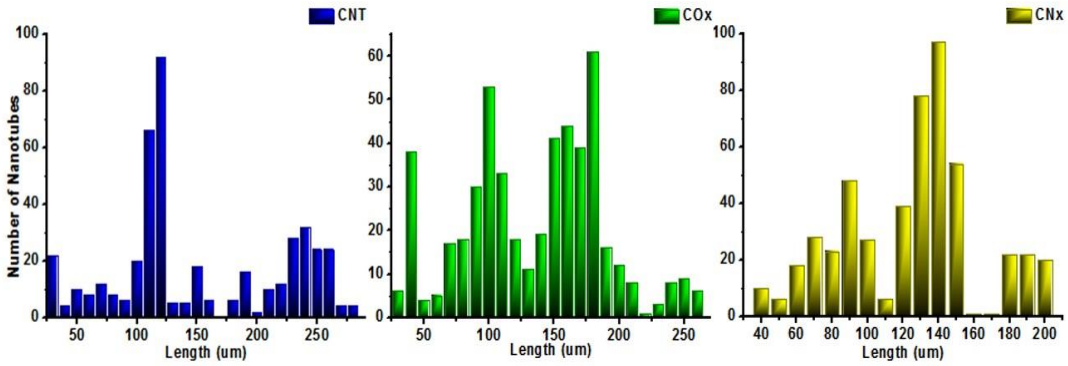

Fig. 2.4 Histograms of lengths of: a) CNT, b) CO_x and, c) CN_x

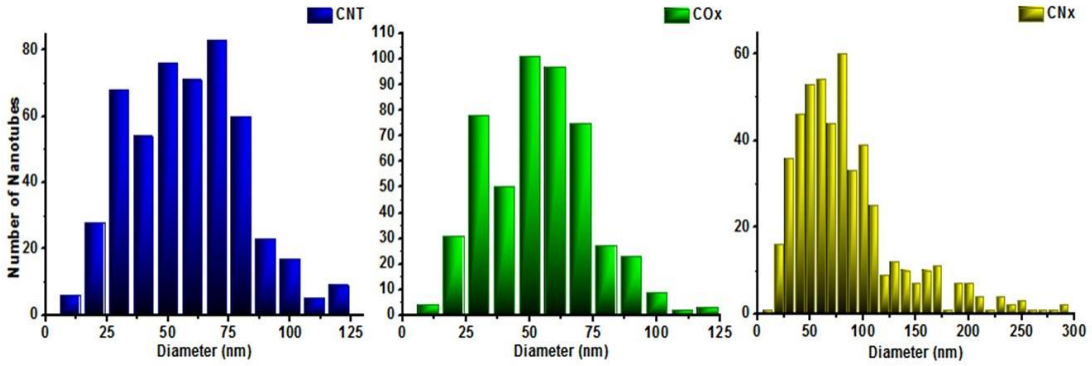

Fig. 2.5 Histograms of diameters of: a) CNT, b) CO_x and, c) CN_x

Table 2.2 Dimensions of CNT, CO_x and CN_x

Sample	Length (µm)	Diameter (nm)	Length/Diameter Ratio
CNT	142 ± 32	75 ± 20	1893
CO_x	182 ± 40	61 ± 16	2983
CN_x	136 ± 20	91 ± 18	1495

TEM images show layers of CNT, CO_x and the characteristic stacked bamboo-like tubules for CN_x are presented in Fig. 2.6. It should be noted the surface roughness found for CO_x.

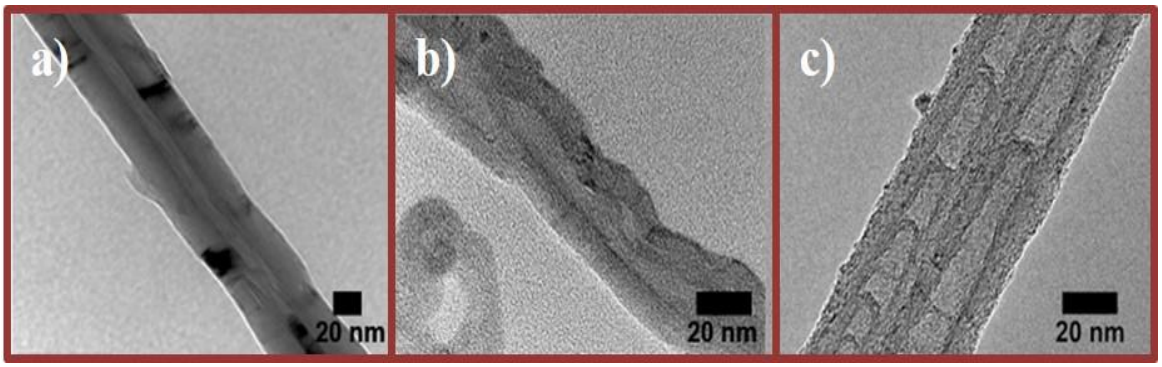

Fig. 2.6 TEM image of: a) CNT; b) CO_x; and c) CN_x

2.3.4 Thermogravimetric Analysis (TGA)

The thermal stability of synthesized nanotubes was checked by TGA in air and N_2 atmospheres (Fig. 2.7 and Table 2.3).

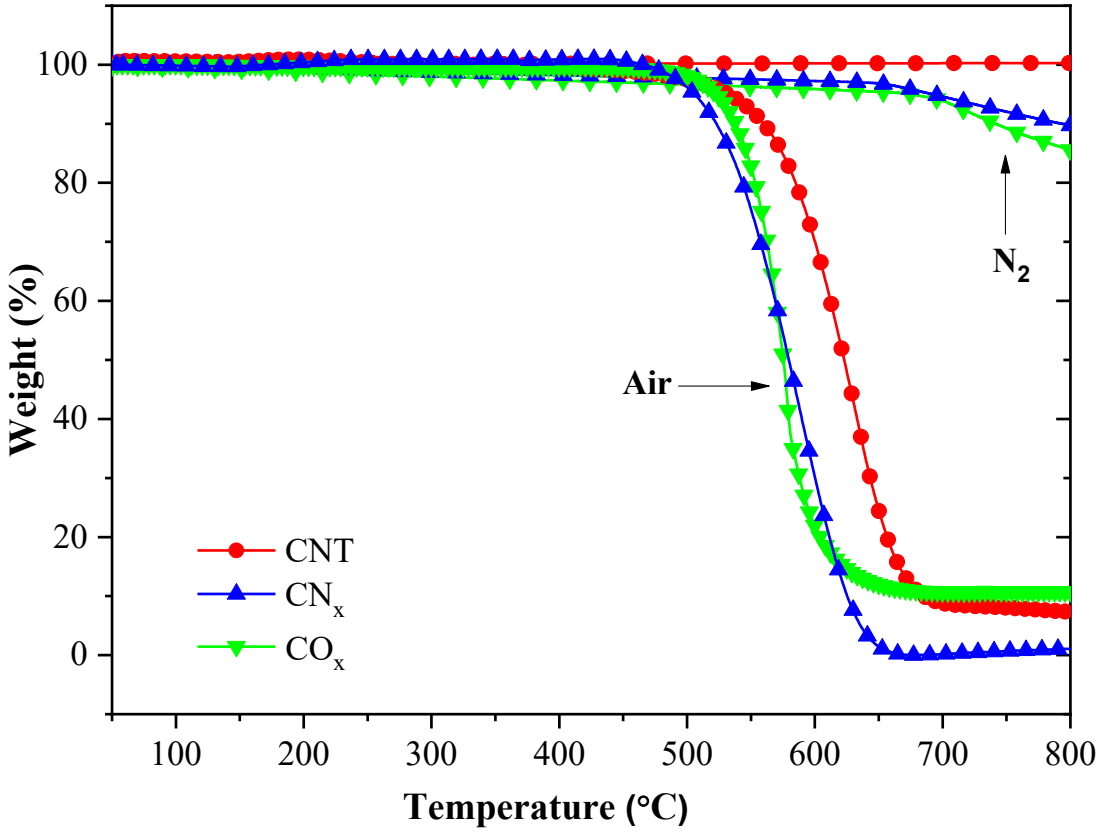

Fig. 2.7 Thermal stabilities of CNT, CO_x and CN_x in air and N_2 atmospheres

CNT presented the highest thermal stability and the lower values of the degradation temperature for CO_x and CN_x were attributed to the presence of defects induced by doping and considerably more edge plane sites [75] that facilitate high temperature oxidation.

Moreover, among the doped nanotubes, CO_x presents the highest weight reduction rate at the lowest temperature reflecting that this kind of nanotubes are much more reactive than CNT or CN_x; intuitively, the surface roughness and the surface functionalities of

these tubes may contribute to increase its reactivity.

Table 2.3 % residual mass at 700 ºC, temperature at maximum loss weight rate, temperature at 5% loss weight and maximum weight loss rate (air)

Sample	%Residual mass at 700 °C		T_{max} (°C)		$T_{5\%}$ (°C)		$(dm/dt)_{max}$ ($ºC^{-1}$)	
	N_2	Air	N_2	Air	N_2	Air	N_2	Air
CNTs	98.9	8.8	-	636	733	532	-	1.0
CO_x	95.4	10.7	-	578	675	523	-	2.6
CN_x	96.8	0.2	-	584	692	506	-	1.0

However, these doped nanotubes are more thermally stable than oxygen and nitrogen functionalized nanotubes obtained by chemical treatments of pristine CNT either in solution or in gas phase [88].

2.4 Conclusions of chapter 2

In this part of work, three different carbon nanotubes in combination were synthesized by CVD method through changing the initial precursor solution. The synthesized pristine carbon nanotube (CNT), oxygen doped carbon nanotubes (CO_x), and nitrogen doped carbon nanotubes (CN_x) were well defined by different characterization methods like XRD, XPS, TEM, SEM, Raman spectroscopy, and TGA. The most important difference between the synthesized nanotubes was their aspect ratio which was calculated to be 1500 and 3000 for CN_x and CO_x respectively Pristine CNT showed the lowest aspect ratio, about 2000.

Chapter 3

Microwave-assisted
Synthesis & Decoration
of Graphene Oxide (GO) by Copper
Hydroxy Nitrate $Cu_2(OH)_3NO_3$ (DS),
Cuprous Oxide (Cu_2O),
Copper Oxide (CuO),
and Metallic Copper

3.1 Introduction

The application of copper salts NP is limited by instability under atmospheric conditions. Hence, Cu NP located on a generally inert support could be a suitable alternative to increase their stability [89].

Up to now, a wide range of accessible oxidation states of copper (Cu^0, Cu^I in Cu_2O, Cu^{II} in CuO) decorated on graphene oxide via different methods, have been explored as a suitable heterogeneous catalyst in various chemical transformations [90].

Besides the aforementioned common copper compound, there is another copper salt with oxidation number of (+2) in copper hydroxy double salts with the common formula; $Cu_2(X)(OH)_3$ (X= inorganic anion, organic anion, …) that is interesting compound with limited applications as anion exchangers.

In this work we have studied copper hydroxy nitrate double salt ($Cu_2(OH)_3NO_3$), the most important member of this group. Therefore, it would be necessary to have some more information about this double salt.

3.2 What is copper hydroxy double salt (DS)?

In recent years, several articles report the structure of transition metal double salts with general composition $M_2(OH)_3X$ (M=Cu, Co; X= inorganic anion, organic anion, …) as consisting of a two-dimensional nanostructure of positively charged metal hydroxide and interlayered anions with tunable physical and chemical properties [91].

Copper hydroxy (or hydroxide/ hydroxyl) nitrate, $Cu_2(OH)_3NO_3$ (DS), one of the most important members of this group, exists in two structurally dimorph varieties: a conventional synthetic metastable monoclinic phase and a natural orthorhombic phase

occurring in the mineral Gerhardtite. There has been considerable research on the exact structure of these two dimorphs and the relationship between the two phases [92].

The structure of DS (Scheme 3.1) consists of $Cu_2(OH)_4$ layers where 25% of the OH^- ions are replaced by NO_3^- anions. One oxygen of the NO_3^- group occupies the position of one hydroxide ion of the layer. The nitrate anions are directly coordinated to copper (II) cations through one of its oxygen atoms whereas the two further oxygen ions lie between the hydroxide layers. These dangled NO_3^- groups contribute to the anion-exchange behavior of DS [93,94].

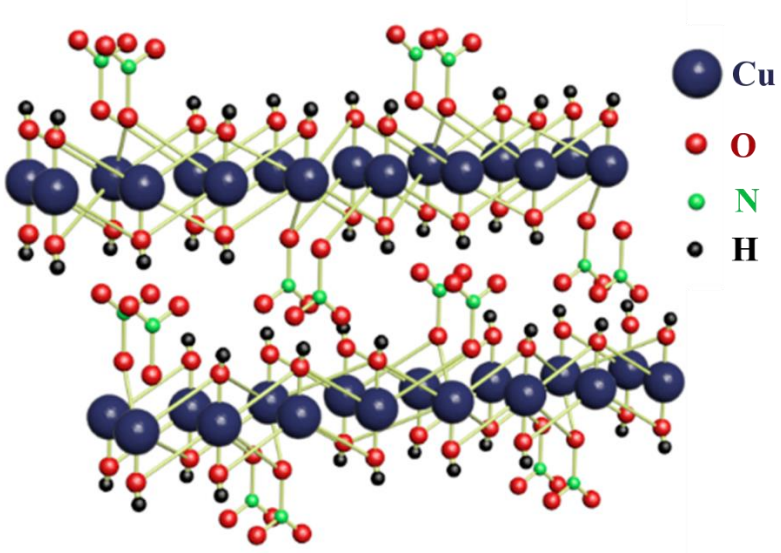

Scheme 3.1 Chemical structure of copper hydroxy nitrate (DS)

Over the past few decades, different methods have been proposed to synthesize this double salt. The most commonly used method consist of the direct mix of aqueous solutions of copper nitrate and sodium hydroxide [95]. Ammonium bicarbonate (NH_4HCO_3) and sodium carbonate (Na_2CO_3) were used by Wolf *et al.* [96] and Bushong *et al.* [97], respectively, as a base reservoirs to synthesized $Cu_2(OH)_3NO_3$. These methods demand strict control of experimental variables, especially pH,

temperature and concentration of the reactants to avoid the formation of by-products like $Cu(OH)_2$, CuO and other stoichiometric ratios with available ions ($Cu_2(OH)_3(NO_3)$, $Cu_3(OH)(NO_3)_5$, …).

Urea hydrolysis was utilized by Henrist *et al.* [98] and Cho *et al.* [99] as an OH generator instead of NaOH for the formation of copper hydroxy nitrate. Anandan *et al*. [100] improved this method by using high-intensity ultrasonic irradiation. The inevitable contamination of $Cu_2(OH)_3NO_3$ by CO_3 ions in urea hydrolysis is the main drawback of this method [101].

Wang *et al.* [102] has reported another method to obtain $Cu_2(OH)_3NO_3$ by adding copper powder into the copper nitrate solution and high-intensity ultra-sonication for several hours. Copper hydroxy nitrate can be prepared through the reaction of magnesium hydroxide ($Mg(OH)_2$) and copper nitrate aqueous solution [103].

$Cu_2(OH)_3NO_3$ was also obtained by dispersion of copper oxide (CuO) in copper nitrate solutions but the reaction time was quite long (e.g. 7 weeks) [104].

Heating aqueous copper nitrate up to 200°C for about 3 days [105], and interaction of solution of copper nitrate and propanol in the solvothermal condition [106] was an alternative method to synthesize copper hydroxy nitrate; however this method is long, consumes high amount of energy and requires severe control of the process.

DS has shown applications in vehicle airbags [107], ion exchangers [104], radiochemical applications [108], oxidation degradation [109], fire retardant of polymers [110], and recently as an effective protective material against organophosphate nerve agents [114]. The copper hydroxy nitrate was used as a raw material for other products. For example, it can be a good precursor for preparing

$Cu(OH)_2$ and CuO [111], Some other different copper hydroxy double salts can be synthesized easily by anion exchange of nitrate anions [112].

Due to the drawbacks of the previous methods, also the importance of this salt, we have decided to propose a new microwave treatment as an alternative convenient and cost effective way to synthesize DS alone and decorated on GO.

The experimental part of this chapter is divided by three parts; synthesis of different copper salts nanoparticles, decoration of copper salts on GO and then characterization of all synthesized products.

3.3 Experimental procedures

3.3.1 Materials

Graphite powder (with a purity >99.999%) was purchased from Alfa Aesar., H_2O_2 30% W/V (Panreac), $KMnO_4$ (Panreac), $NaNO_3$ (Sigma-Aldrich) and H_2SO_4 98% V/V (Panreac) were employed for graphite oxidation and used without any further purification. Copper (II) nitrate hemi (pentahydrate) $Cu(NO_3)_2$. 2.5 H_2O was purchased from Sigma-Aldrich was utilized for GO decoration.

3.3.2 Study on time & solvent effects

According to the previous work in our group, we had some experience about microwave copper decoration on carbon nanotubes [87]. Therefore, we decided to study more about the effect of time duration and changing the solvent on the proposed microwave assisted method.

The schematic illustration of the copper salts synthesize method is shown in Scheme

3.2. In a general procedure, a solution of $Cu(NO_3)_2.2.5\ H_2O$ was microwaved in an on-off system (10 seconds heating and 5 seconds calm) to avoid solvent evaporation. After cooling, the solution was filtered, and the obtained precipitate was washed with deionized water and hot ethanol, at least for five times and dried in a vacuum oven at 50 ºC overnight.

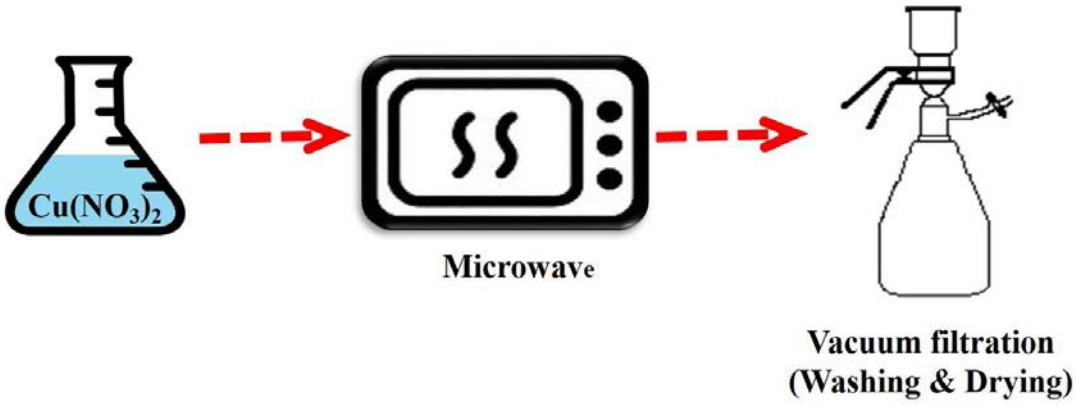

Scheme 3.2 General procedure for synthesis of copper salts

We have repeated the general procedure with some common solvent in our lab by starting from distilled water, ethanol, methanol, ethylene glycol, diethylene glycol and polyethylene glycol. According to the XRD patterns of the products, it was found that microwave irradiated of copper nitrate resulted in some products with well-characterized patterns only in the case of ethanol and ethylene glycol. Therefore, we decided to continue with these two solvents.

Checking the conversion % at different irradiation times in the case of ethanol as a solvent, it was found that 2 minutes MW resulted in the maximum yield (Table 3.1). Hence, 2 minutes microwave was chosen for all experiments.

Table 3.1 Effect of microwave irradiation time on the weight amount of product

Time	1 min	2 min	3 min	4 min	5 min
% Conversion	30%	75%	78%	75%	80%

In the case of ethanol, different volumetric percentage of ethanol/water solutions have been tested. According to the weight amount of solid product showed in Fig. 3.1, the 95% (V/V) ethanol/water solution (The first beaker on the right) was chosen for the rest of the experiments.

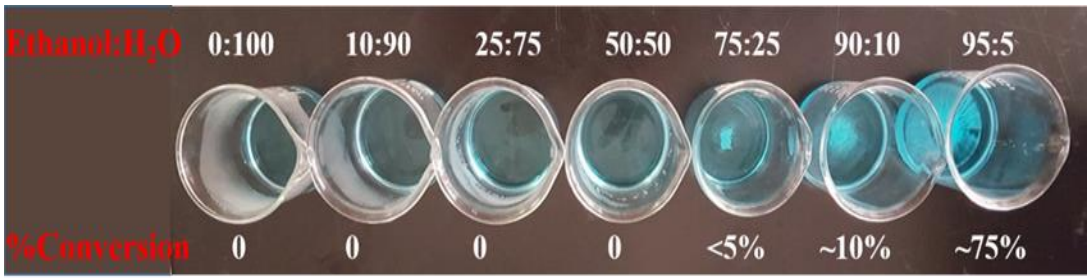

Fig 3.1 Effect of ethanol/water % (V/V) on the conversion % to the product

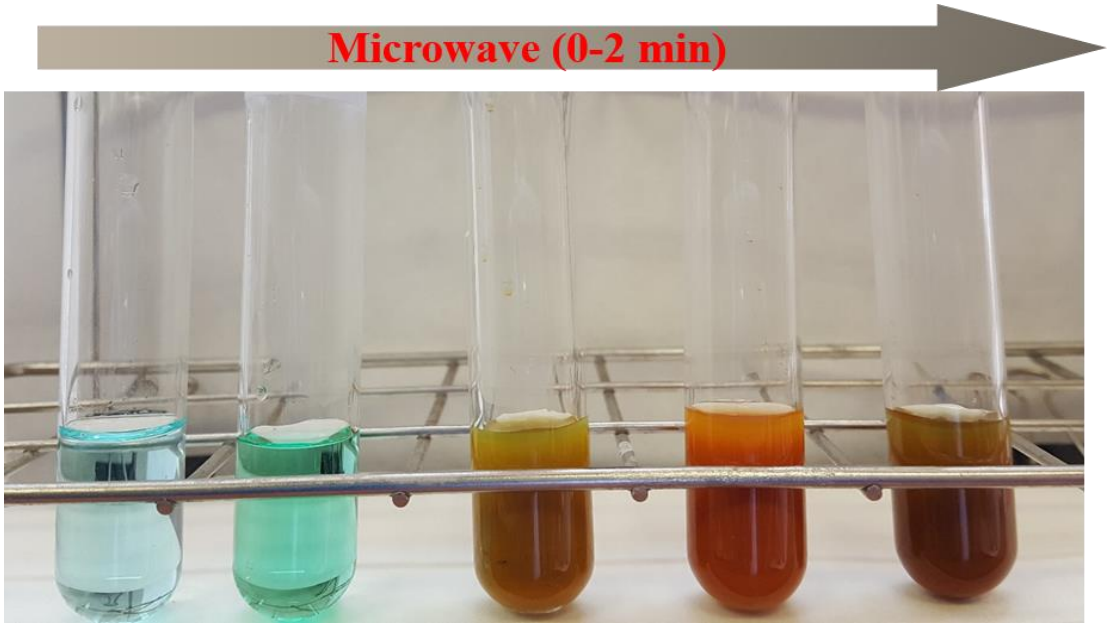

Fig. 3.2 Microwave irradiated copper nitrate/ethylene glycol solution at different times

Furthermore, we found that 2 minutes microwave irradiation was enough for copper nitrate/ ethylene glycol solution according to the XRD pattern of the products (Fig. 3.2) obtained at different times.

3.3.3 Synthesis of copper bare salts

I) Copper hydroxyl nitrate (DS)

Following the Scheme 3.1 by starting from copper nitrate in ethanol under 2 minutes MW and then filtration and washing leads us to DS.

II) Cuprous oxide (Cu_2O)

By changing the solvent to ethylene glycol and following the Scheme 3.1, cuprous oxide was obtained.

III) Copper oxide (CuO)

We could obtain black pristine copper oxide (CuO) by heating DS in 250 ℃ for 10 min in an oven.

We found that it is possible to obtain CuO by heating Cu_2O but it needs more time (~30 min).

IV) Metallic copper nanoparticles (Cu^0)

50 mL of a 1 M ascorbic acid solution was added into 50 mL 0.2 M solution of DS and stirred for 30 min. The color of the mixture changed from green blue to red brown, indicating the formation of metallic Cu particles. When the reaction was completed,

the final product was separated by filtration.

In the next step of our work these different copper compound have been synthesized and decorated on GO at the same time. At first it will be explained about preparation of graphene oxide, (GO) as a support.

3.3.4 Preparation of graphene oxide (GO)

Graphene Oxide was prepared from natural flake graphite powders using a modified Hummers' method because of the mentioned reasons (section 1.5.1). Briefly,

1. Concentrated H_2SO_4 (180 mL) was added to a mixture of graphite (4 g) and $NaNO_3$ (2 g),
2. The mixture was cooled down to 0 °C in an ice bath,
3. $KMnO_4$ (11 g) was added slowly in small doses to keep the reaction temperature below 20 °C,
3. The solution was heated to 35 °C and stirred for 2h,
4. 300 mL water was added to complete the oxidation reaction,
5. 30 mL H_2O_2 30% was slowly added for elimination of excess $KMnO_4$,
6. The reaction mixture was stirred for 30 minutes,
7. The mixture was centrifuged (3700 rpm for 30 min), after which the supernatant was decanted away,
8. The remaining solid material was washed with water and centrifuged again, this process being repeated until the pH was between 6 and 7,
9. The obtained brown-yellow graphene oxide was dispersed in water (quantified at 5 mg mL^{-1}) and poured into the plastic tube,

10. The tubes were frozen by liquid nitrogen and transferred into an ultra-low freeze dryer (-50°C, 15 Pa) for at least 72 h until flocculated powder was obtained,

11. Ultimately, prepared GO was kept in sealed container for the next experimental tests.

3.3.5 Decoration of copper salts on graphene oxide

In this method, microwave can prepare copper salts nanoparticle and decorate them on GO simultaneously that can be mentioned as one pot synthesis. In this part we have followed our previous microwave procedure for synthesize the bare salts and add the GO in different solvents (ethanol and ethylene glycol) (Scheme 3.3)

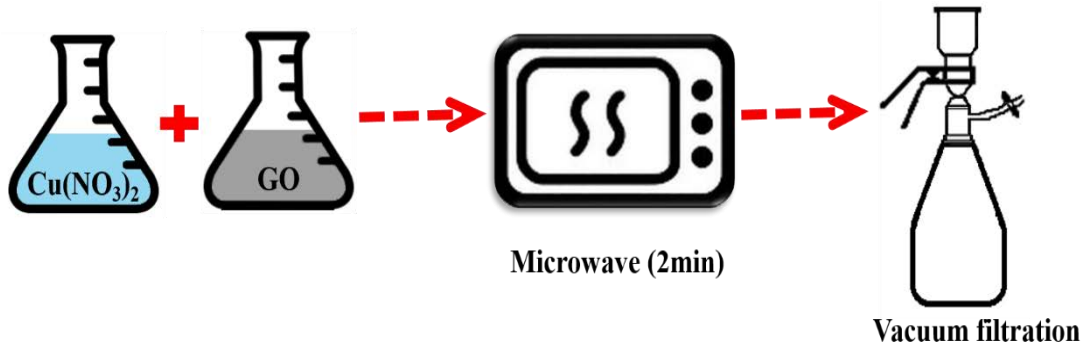

Scheme 3.3 Microwave assisted procedure to decorate copper compound on GO

I) Decoration of DS on GO

The schematic illustration of DS/GO nanohybrid shows in Scheme 3.2. A mixture of 100 mg GO mg in ethanol (dispersed under 5 min sonication) was added to 100 mL of $Cu(NO_3)_2$ 0.01 M, then the solution was microwaved for 2 minutes (on-off system). Subsequently, the mixture was filtered after cooling, and the obtained precipitate was washed with deionized water and hot ethanol, at least for five times and dried in a

vacuum oven at 60 mmHg/ 90 ºC overnight.

II) Decoration of Cu_2O on GO

A mixture of GO 100 mg in ethylene glycol (dispersed after 5 min sonication) was added to 100 mL of $Cu(NO_3)_2$ 0.01 M in ethylene glycol, then the solution was microwaved in an on-off system with 5-10 seconds heating and 10 seconds calm until totally 2 minutes heating. After cooling to room temperature, the mixture was filtered, and the obtained solid was washed with deionized water and hot ethanol, for at least 5 times, and finally dried in a vacuum oven at 60 mmHg/ 90 ºC overnight.

III) Decoration of CuO on GO

Copper oxide (CuO) decorated on GO was obtained by heating DS/GO at about 250°C for 10 min in an oven.

The same as bare CuO, it is possible to obtain CuO/GO by heating Cu2O/GO at 250°C for about 30 minutes.

IV) Decoration of Cu^0 on GO

50 mL of a 1 M ascorbic acid solution was added into 1gr of DS/GO and stirred for 30 min. The color of the mixture changed from green blue to red brown, indicating the formation of Cu/GO particles. When the reaction was completed, the final product was separated by filtration.

All collected products were well characterized with XRD, SEM, TEM, and TGA.

3.4 Characterization and discussion

3.4.1 XRD of GO

X-ray diffractgrams of GO, supported and non-supported copper nanoparticles are presented in Fig. 1. The diffraction peak of GO was observed at 2θ = 10.7º (Fig. 1) and corresponds to the (002) plane. The calculated interplanar distance layers according to the Bragg's law was 0.7 nm, similar to the value reported in the literature (~0.5-0.9 nm). This value depends on the number of oxygen containing functional groups on carbon sheets as well as to adsorbed H_2O molecules [113] (Fig. 3.3).

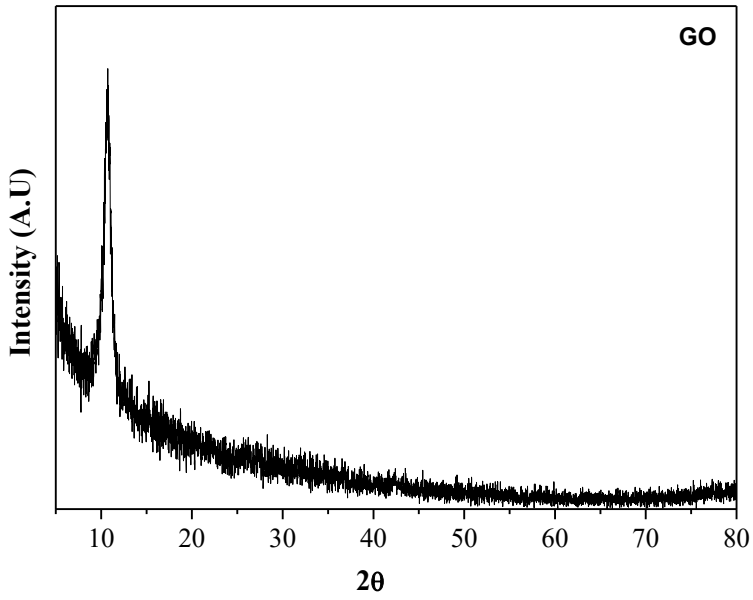

Fig. 3.3 X-ray diffraction patterns of graphene oxide

The distance between graphene oxide layers according to the Bragg's law was about 0.7 nm.

3.4.2 XRD of Cu/GO nanohybrides

The X-ray diffraction patterns of decorated GO with different solvent shows well-defined and sharp peaks.

The XRD pattern of synthesized copper hydroxyl nitrate double salt (DS) and decorated on GO (DS/GO) (Fig 3.4) show excellent accordance with the DS obtained by conventional methods [114]. The peak corresponding to the GO in the XRD pattern of nanohybrids cannot be observed because of the high quantity and high crystallinity of copper-based nanoparticles.

Changing the solvent to ethylene glycol in the same condition can synthesize and decorate cuprous oxide nanoparticles (Cu_2O) on GO with XRD pattern which is in a full agreement with the literature [115] (Fig. 3.5).

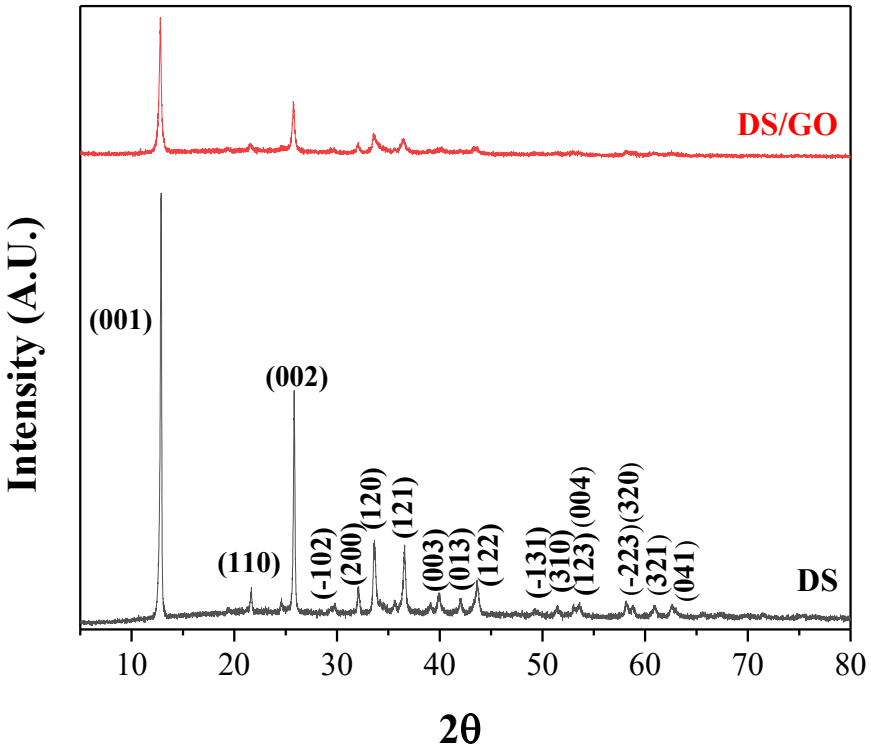

Fig. 3.4 X-ray diffraction patterns of DS and DS/GO nanohybrid

We have also checked the XRD of CuO and CuO/GO obtained from DS and DS/GO, respectively. Fig 3.6 shows the XRD pattern of these products which are in full agreement with the literature [116].

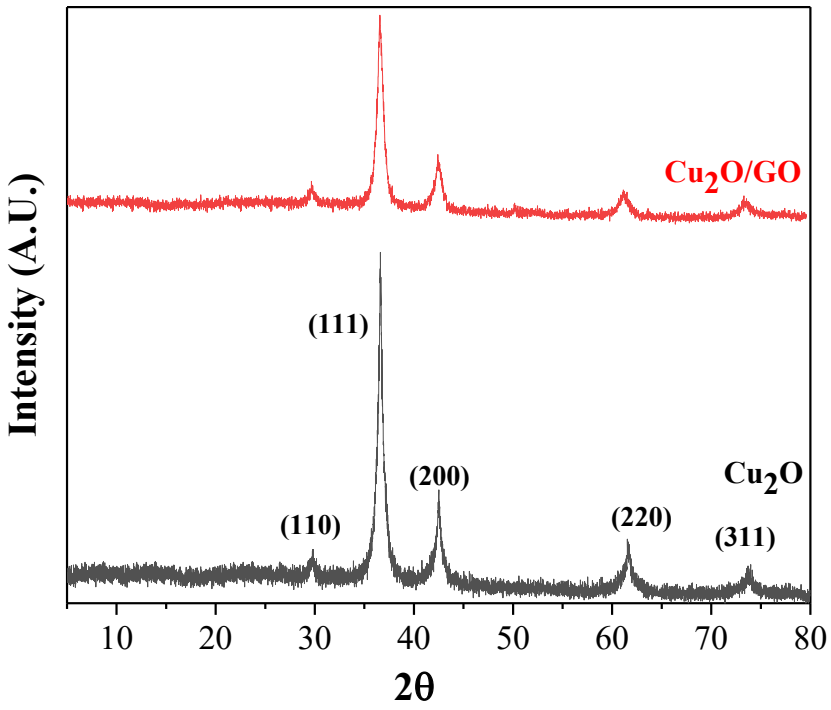

Fig. 3.5 X-ray diffraction patterns of Cu_2O and Cu_2O/GO nanohybrid

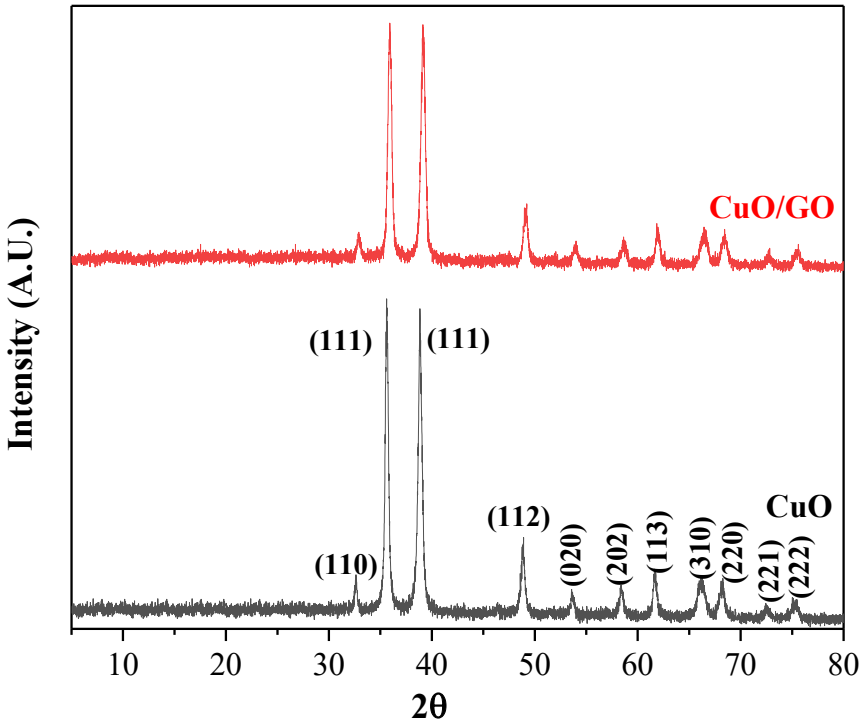

Fig. 3.6 X-ray diffraction patterns of CuO and CuO/GO nanohybrid

The last copper product was analyzed by XRD and it was found a good accordance between the results of metallic copper obtained from reduction of DS by ascorbic acid (Fig. 3.7).

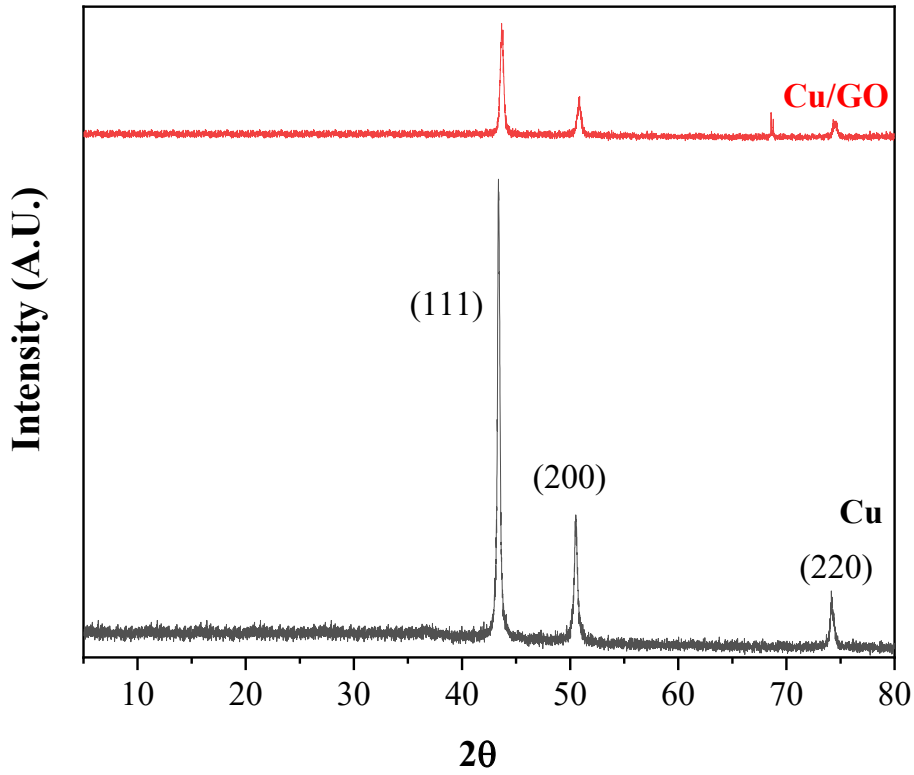

Fig. 3.7 X-ray diffraction patterns of Cu and Cu/GO nanohybrid

The crystallite size of Cu particles alone and decorated on GO have been estimated by using Debye-Scherer equation:

$$d = \frac{0.9\lambda}{\beta_{1/2}\cos\theta}$$

d is the average crystallite size (nm) of particles, λ is the wavelength of the X-ray used (0.15406 nm), $\beta_{1/2}$ is the width of the diffraction peak at half height in radians and θ is the angle at the position of the peak maximum.

Table 3.2 Calculated average crystallite size of DS, Cu and CuO nanoparticles alone and decorated on GO

Sample	Crystallite size (nm)	
	Supported on GO	Non-supported
Cu	21	32
Cu_2O	9	9
CuO	18	21
$Cu_2(OH)_3NO_3$	27	47

As shown in Table 3.2, the size of synthesized Cu, Cu_2O, CuO, and DS in bulk are slightly bigger than supported ones, especially for the DS sample, which show that graphene oxide as a support did not have a negative effect on crystalline degree. It seems that the simultaneously synthesize and decoration could be resulted in smaller copper salt particles.

Furthermore, we found that the salts decorated and non-decorated could be stored in air for at least six months without any changing in their XRD pattern.

3.4.3 FTIR & Raman spectroscopy

For more investigation, we have checked the synthesized DS by FTIR and Raman spectroscopy. Fig. 3.8 shows FTIR and Raman spectra of DS.

The IR peaks at 878, 785 and 673 cm^{-1} can be assigned to hydrogen bonding frequencies related to Cu-O-H [106]. The doublet of equal intensity peaks at 717 cm^{-1}, singlet peak at 811cm^{-1}, intense and fine peak at 1048 cm^{-1} and multiplet peaks at 1352,

1384 and 1421cm^{-1} are assigned to the nitrate ion embed in the crystal [98].

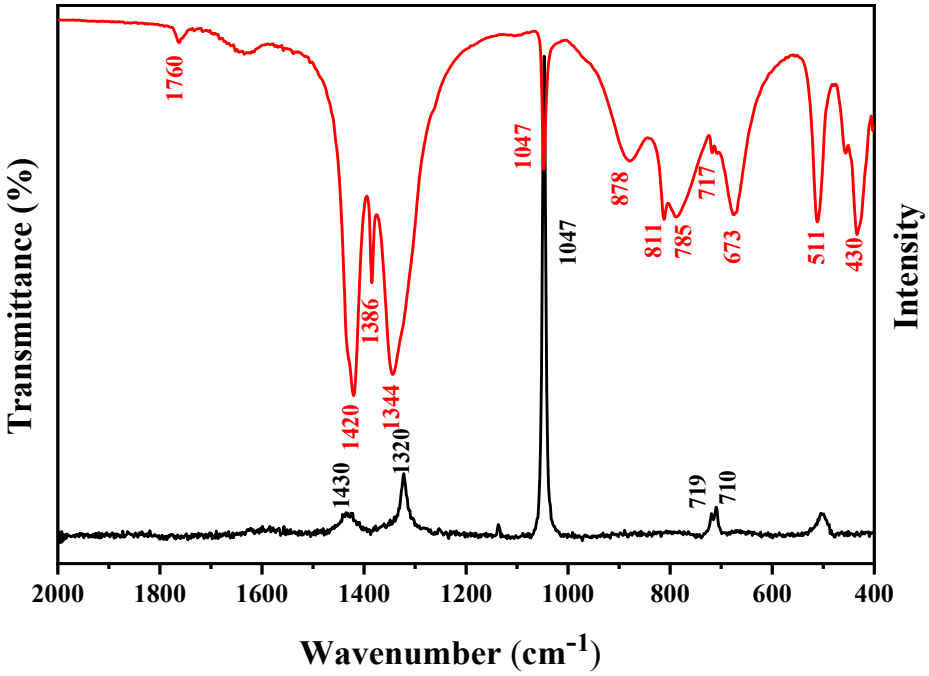

Fig. 3.8 FTIR (up) and Raman (down) spectra of DS

The peaks at 709, 717, 1045, 1320 and 1430 cm^{-1} in Raman spectrum are in good agreement with previously reported works [117].

3.4.4 Thermogravimetry analysis (TGA)

The thermal stability and the composition of GO and the copper salts/GO nanohybrides were further investigated by using TGA in air atmosphere (Fig. 3.9). Graphene oxide showed three degradation steps. The initial ~10% weight loss at near 100 ℃, was assigned to the loss of physisorbed water. The major loss of mass of GO consisted of two steps: first a sudden weight loss at ~200 ℃ followed by another steep step at 522℃, which were assigned to the pyrolysis of oxygen-containing functional groups (carboxylate, anhydride, or lactone groups) and GO combustion respectively [118].

Finally, the total residual weight of GO obtained at 800 °C was around 6.2 %.

DS/GO exhibited no weight loss up to 200 °C; however, in the temperature range of ~200°C–270 °C, showed a weight loss of ~30% due to the decomposition of DS in one step to produce CuO according to the chemical equation [117]:

$$4\ Cu_2(OH)_3NO_3 \rightarrow 8\ \mathbf{CuO}_{(s)} + 4\ NO_{2(g)}\uparrow + O_{2(g)}\uparrow + 6\ H_2O_{(g)}$$

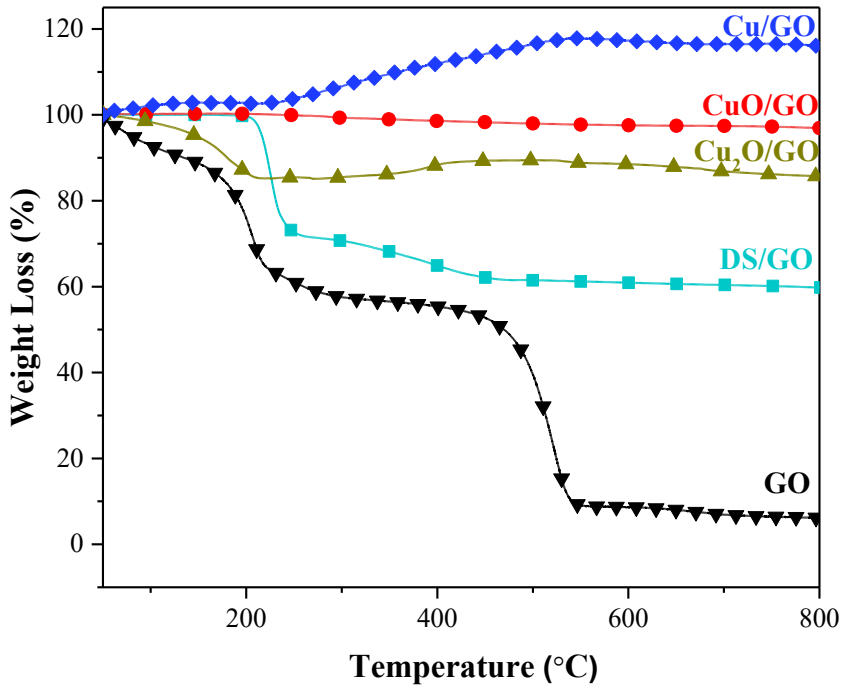

Fig. 3.9 TGA traces of GO and DS/GO, Cu_2O/GO, and Cu/GO nanohybrids

The TGA of Cu_2O/GO shows an initial loss of about 15% coincident with the loss of the graphene oxide support, that remains constant up to 300ºC were an increase of mass associated to the oxidation of Cu (I) can be observed. In the case of Cu/GO sample a steep mass increase starting at 260 ºC can be observed up to 550ºC. This was attributed to the oxidation of Cu^0 to Cu^{II}. No significant mass loss was detected for CuO on GO. TGA is an effective analytical technique to evaluate the ratio of copper salts/GO. The content of CuO and metallic copper in the nanohybrids were calculated by amount of

residue at 800 ºC. According to the amount of residue in each sample, the loading of Cu^0, its oxides and DS in the samples could be calculated. Results appear in Table 3.3.

Table 3.3. TGA data of Cu/GO, DS/GO, CuO/GO and Cu_2O/GO

Nanohybrid	(% w/w) Cu compound in nanohybrid
Cu/GO	92.4
DS/GO ($Cu_2(OH)_3NO_3$/GO)	88.6
CuO/GO	96.7
Cu_2O/GO	75.8

3.4.5 Transmission Electron Microscopy (TEM)

The morphology of synthesized samples was characterized using TEM measurements. As it can be seen in Fig. 3.10, nearly three kinds of morphology in copper products are obtained with copper nitrate as precursor: rods DS, spherical Cu_2O and cubic CuO.

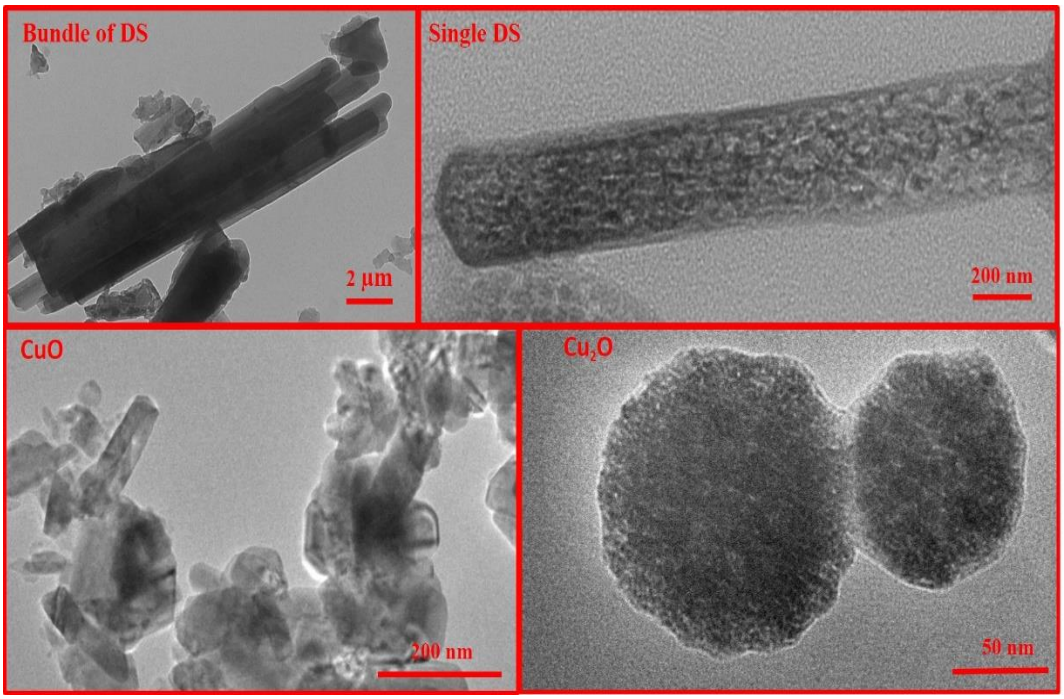

Fig 3.10 TEM images of bundle and a single DS, CuO and Cu_2O synthesized

The characteristics of copper nanoparticles deposited on the surface of graphene oxide

could be clearly seen in Fig. 3.11, two different morphologies in supported copper products were obtained: rods for DS and spheres for Cu and its oxides.

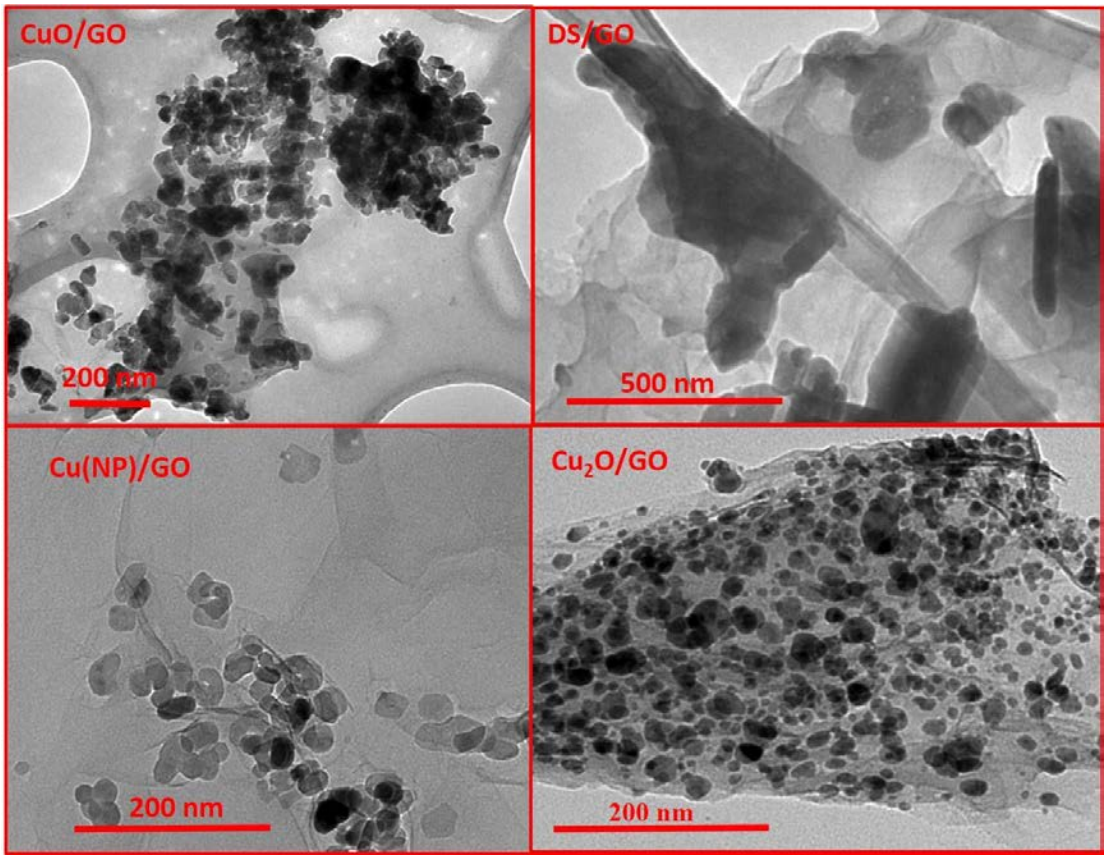

Fig. 3.11 TEM images of CuO, DS, Cu, and Cu_2O/graphene oxide

One can clearly see the aggregation and disposition of the nanoparticles deposited on the surface of graphene oxide and how it seems that the particles were well anchored and dispersed on GO nanosheets. The GO in nanohybrids exhibited plentiful wrinkles, which resulted from the graphitization of GO sheets in the exfoliation process. Apparently, GO nanosheets could effectively prevent the aggregation of Cu^0 and cuprous oxide particles, although this disaggregation effect is not evident in CuO or DS systems.

From TEM images and with the use of Image J software it was possible to measure the

size distribution for supported nanoparticles as depicted in Figure 3.12, where size histograms for populations of 500 particles are plotted along with the corresponding log-normal distributions.

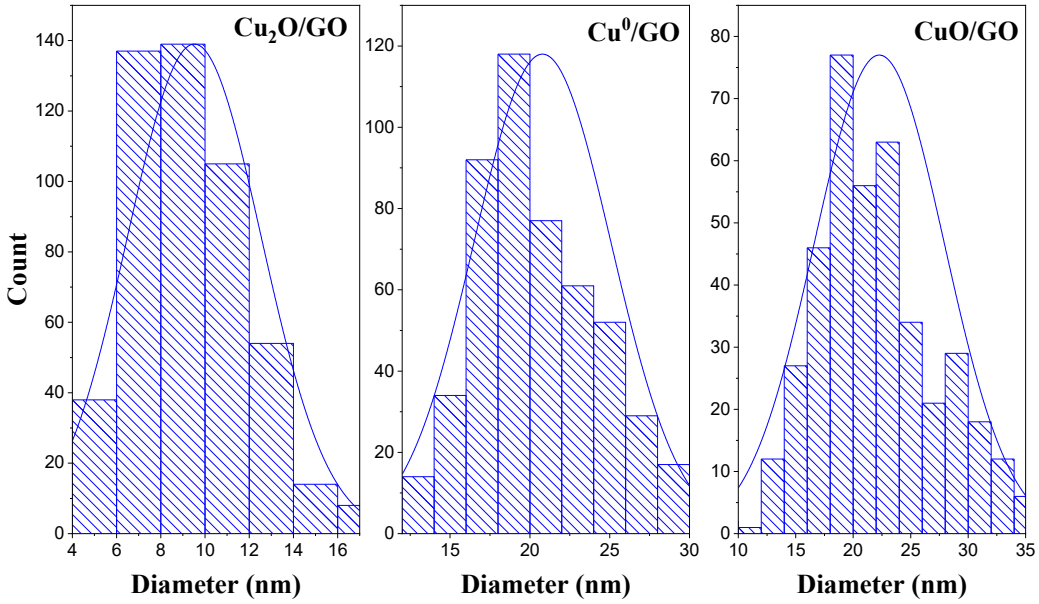

Fig. 3.12 Particle size distribution of supported Cu and its oxides from image analysis

Statistical analysis yield the following average sizes: 20 ± 4 nm for Cu^0/GO, 9 ± 3 nm for Cu_2O/GO, and 22 ± 5 nm for CuO/GO. These results are in fair accordance with sizes obtained from XRD (Table 3.2).

3.5 Conclusions of chapter 3

The addition of copper nitrate solution to GO under microwave condition can be resulted in decorated copper salts in different structure depending on the different solvents. In the case of using ethanol as a solvent copper hydroxy nitrate (DS) can be synthesized and supported on GO. Whereas utilizing ethylene glycol can lead to cuprous oxide/GO nanohybrids. Furthermore, we could easily obtain copper oxide

(CuO)/GO nanohybrid by heating DS/GO up to 350 °C for 10 minutes in the oven (Scheme 3.4).

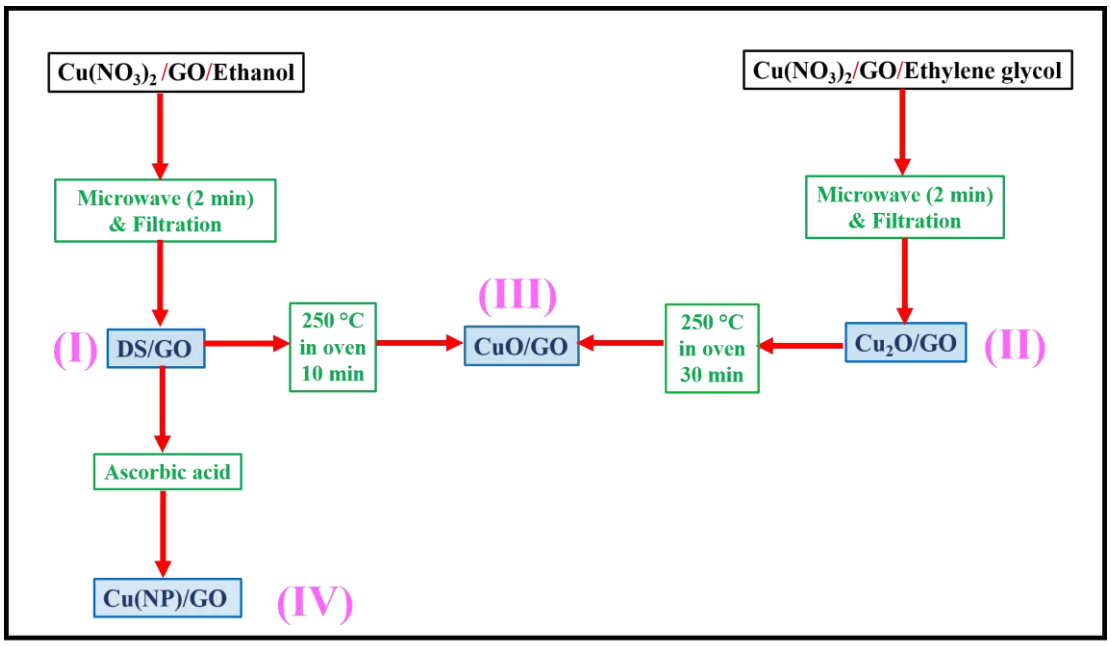

Scheme 3.4 Synthesis procedure of the four copper/GO nanohybrids

The copper salts/GO nanohybrids were well defined by different characterization methods such as XRD, TGA, and TEM. The significant advantage of the fast and reasonable microwave assisted method proposed in our work is carrying the simultaneous synthesize and decoration of copper salts nanoparticles on graphene oxide.

The purity and stability of the copper-decorated samples in air condition were further investigated. According to the XRD data, it was observed that, after 6 month, no changes have been occurred on the oxidation state of the salts.

Chapter 4

Comparative Study of the Effect of CNT, CN_x and CO_x on Flame Retardancy of Epoxy Nanocomposites

4.1 Introduction

Epoxy resin (EP) is one of the most important thermosetting polymers (EP) with low-molecular-weight containing more than one epoxide group, which are cured using a wide variety of curing agents (amines, anhydrides, etc.).

Due to the significant characteristics of EPs such as high tensile and impact strength, good fatigue resistance, micro cracking resistance, chemical and corrosion resistance, excellent electric insulation and low manufacturing cost, they are widely used as advanced matrix in different fields of electrical, electronic, aerospace industries and anticorrosion laminate coatings [119].

The very high flammability property of EP has greatly limited the development and application of epoxy based composites. Therefore improving the flame retardant (FR) properties of EPs has developed automatically and has become one of the most attractive subject between researchers in advanced applications. Halogenated compounds (also known as organohalogen FR) containing Cl or Br bonded to C, were traditional fillers to improve the FR properties of EP. Chemicals with Organohalogens are considered Persistent Organic Pollutants (POPs) and present significant risks to human health and environment. Nowadays, a wide variety of chemical compounds containing N, P, B and Si, have attracted more attention to replace traditional toxic halogenated FR to improve flame retardancy of polymer materials [120,121]. The high loadings needed of these new additives is the major problem, which cause degradation of the mechanical properties of the final composites.

The growing up of the nanocomposite technology has proposed nano-fillers in a very low loading (<10 wt.%) as a new replacement for flame retardant polymer materials.

Nano-materials such as clays, montmorillonite, double-layered hydroxides (LDH), etc. have been introduced into epoxy aiming to increase FR [122,123].

According to the amazing properties of carbon nanoparticles (CNTs, graphene, GO), they have attracted special attention by researchers to utilize as FR in nanocomposites. Kashiwagi et al. reported improving the flame retardancy by adding CNT for the first time [124,125].

The effects of CNTs will be affected by aggregation of the nano-fillers due to the strong Van der Waals forces. Therefore, high dispersion state of the CNTs constituted a key point for enhancement of the fire retardancy [126]. Up to now, different strategies have been reported to increase the dispersion degree of CNTs such as ultrasonication, pre-dispersed CNTs into polymer, chemical modification through functionalization, etc (section 1.8).

This chapter is related to the study about the effect of synthesized carbon nanotubes as filler on flame retardancy of Diglycidyl ether bisphenol-A (DGEBA) as a good example of thermosetting polymer. First, the method of preparing and characterization of CNT based epoxy nanocomposites will be explained. The structure of nanocomposites were characterized by TGA, SEM and TEM and Flame retardancy research was carried out through microscale combustion calorimetry (MCC), limiting oxygen index (LOI) determination and thermogravimetry analysis (TGA).

Mechanical properties of the nanocomposites were evaluated by DMTA and glass transition temperatures were measured by DSC. The obtained results of this chapter has been reported in our paper [127].

4.2 Preparation of epoxy nanocomposites

Three samples containing 2 wt.% nanotubes (CNT, CN_x or CO_x) were prepared mixing appropriate amounts of EP and using a three roll mill at 120 ºC to decrease epoxy viscosity (equivalent weight of DGEBA per epoxide group is 480 $g.mol^{-1}$) (Fig. 4.1) and disperse the nanoparticles. After milling, the mixture was gently stirred at the same temperature to partially eliminate trapped air from the mixture.

Fig. 4.1 Preparation of epoxy nanocomposites in the required size for LOI test

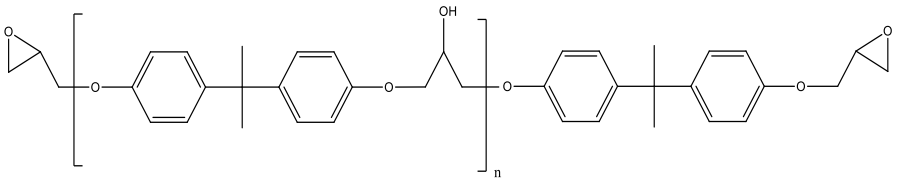

DGEBA

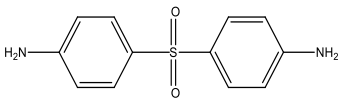

DDS

Fig. 4.2 Chemical structures of epoxy (DGEBA) and the hardener (DDS)

Stoichiometric amount of 4,4′- Diamino diphenyl sulfone (DDS) a curing agent (Fig. 4.2) was then added to the mixture and the temperature was then increased to 130 ºC to dissolve the curing agent for 20 minutes under vacuum to get a clear, homogeneous and degassed mixture.

The mixture was then poured into a preheated Teflon mold and cured in an oven at 140 °C for 5 h and then post cured for 3 h at 180 °C. Specimens for the entire tests were cut from this block. The sample without nanotubes was the reference.

4.3 Structure characterization of carbon nanocomposite

The existence of a CNT network was confirmed by a detailed microscopic examination of cryo-fractured specimens. Fig. 4.3 shows some representative examples of the different microstructural features of the nanocomposites.

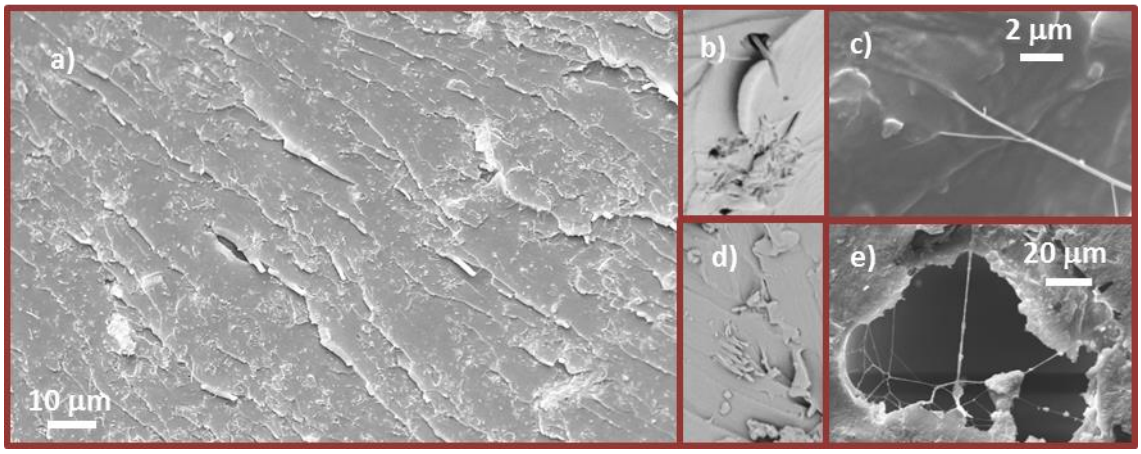

Fig. 4.3 FESEM images of cryo-fractured nanocomposites. a) Representative image of the surface of CNT, CN_x and CO_x nanocomposites. b) An example of a bad interfacial coupling in CNT. c) An example of a good interfacial contact in CN_x. d) Presence of an aggregate in CN_x. e) Nanotube network detected inside a defect in CN_x nanocomposite

A representative image of the dispersion degree is presented in Fig. 4.3. (a) where it can be observed an apparently homogeneous distribution of the nanofiller on the surface of CNT nanocomposites. The surfaces of CN_x and CO_x appear to be similar. Some aggregates, as depicted in Fig. 4.3. (b) and (d), were observed for CNT and CN_x nanocomposites while no aggregates could be observed for CO_x. Concerning the interfacial contact, we have observed a wide range of cases within the same samples. In some cases a complete decoupling of the nanotubes from the matrix was observed (Fig. 4.3. (b)) but inspection of other portions of the same sample revealed a good interaction of the tubes (Fig. 4.3. (c)). Therefore, we can conclude that there are no specific features of the microstructure of the nanocomposites that could be attributable to the effect of doping except for the case of oxygen doping. However, the most interesting finding appears in Fig. 4.3 (e), were inspection inside a defect free of polymer matrix revealed the presence of a network of interconnected nanotubes, confirming thus the existence of a percolative network.

4.4 Thermal stability and mechanical behavior of epoxy nano-composites

4.4.1 Thermogravimetry analysis (TGA)

The influence of the pristine and doped CNTs on the thermal stability of epoxy nanocomposites was investigated by TGA, as shown in Fig. 3.4 and Table 4.1.

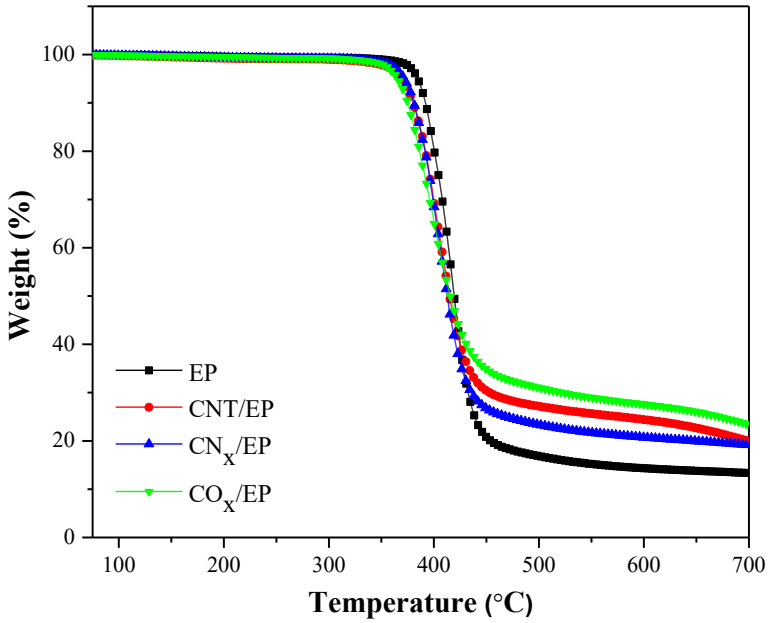

Fig. 4.4 TGA curve of epoxy and its nanocomposites in N_2

Table 4.1 The TGA data of EP and its nanocomposites

Sample	$T_{5\%}$ (°C)	T_{max} (°C)	$(dm/dt)_{max}$ ($°C^{-1}$)	wt.% residue yield at 700 °C	
				Experimental	Calculated
EP	384.6	418	1.9	13.3	--
CNT/EP	369.3	402	1.4	19.9	15.0
CN_x/EP	371.4	404	1.5	19.1	15.0
CO_x/EP	365.3	401	1.1	23.4	14.9

Pure epoxy shows a sharp mass loss in the temperature range of 400-450°C, and its residual mass percentage is 13.3% under N_2 atmosphere. The introduction of either pristine or doped CNT caused the earlier initial decomposition of the nanocomposites in about 16°C as reflected by $T_{5\%}$ and T_{max} data. This effect may be attributed to the high thermal conductivity of the nanofillers. However, as degradation starts under N_2

atmosphere, a char layer begins to be formed; this layer has a protective effect and it should be therefore expected a delay or reduction of gaseous products. This is just what was observed since the incorporation of the nanotubes led to an increase in the char yield at 700 °C in about 6–10% (Table 2.3) following the sequence CO_x/EP> CNT/EP>CN_x/EP. Notably, these experimental char residues were higher than the calculated ones assuming additivity of char residue (see Table 2.3 for the weight loss under N_2 at 700 ºC), suggesting the existence of synergism among the modifiers. Furthermore, it is interesting to note that the thermal oxidative resistance of the nanocomposites close correlates with the length to diameter ratio of the nanotubes (Table 2.2). It seems that the higher length to diameter ratio, the higher char yield is produced, and this suggests to be an effect of the percolative network formed by the nanotubes as already suggested by other authors [128].

However, analysis of char residue is concerned with the end of the degradation process and some effect of the percolative network should be expected at any other stage of the process. We have carefully examined the TGA thermograms of both the pure nanotubes and the nanocomposites, and we have found a significant difference in the maximum rate at which weight is lost, $(dm/dt)_{max}$ which can be considered as a measure of the degradation rate. Among the three tubes examined in this work, CO_x presents the maximum degradation rate (Table 2.3) in air but when it is incorporated into the epoxy, the resulting nanocomposite presents the lowest degradation rate (Table 4.1). The three nanotubes lower the degradation rate of pure epoxy but CO_x almost halves the value. Since CO_x alone degrades quickly in air, this effect may be also associated to its high aspect ratio.

4.4.2 DSC and DMTA

DSC was used to determine the glass transition temperature (Tg) of the nanocomposites using a Mettler Toledo DSC 822 with a liquid nitrogen reservoir. Samples of about 5 mg were scanned from 25 °C to 250 °C at 10 °C.min^{-1}. In order to minimize the effects of previous thermal history, data from a second scan were used for analysis.

Dynamic mechanical thermal properties were measured using a DMTA Q800 Dynamic Mechanical Analyzer (TA Instruments), with amplitude of 30 μm at 1 Hz. Nanocomposite specimens with nominal dimensions of 60×10×2 mm^3 were mechanically tested in single cantilever mode. The samples were heated from room temperature to 250 °C at a linear rate of 3 °C.min^{-1}.

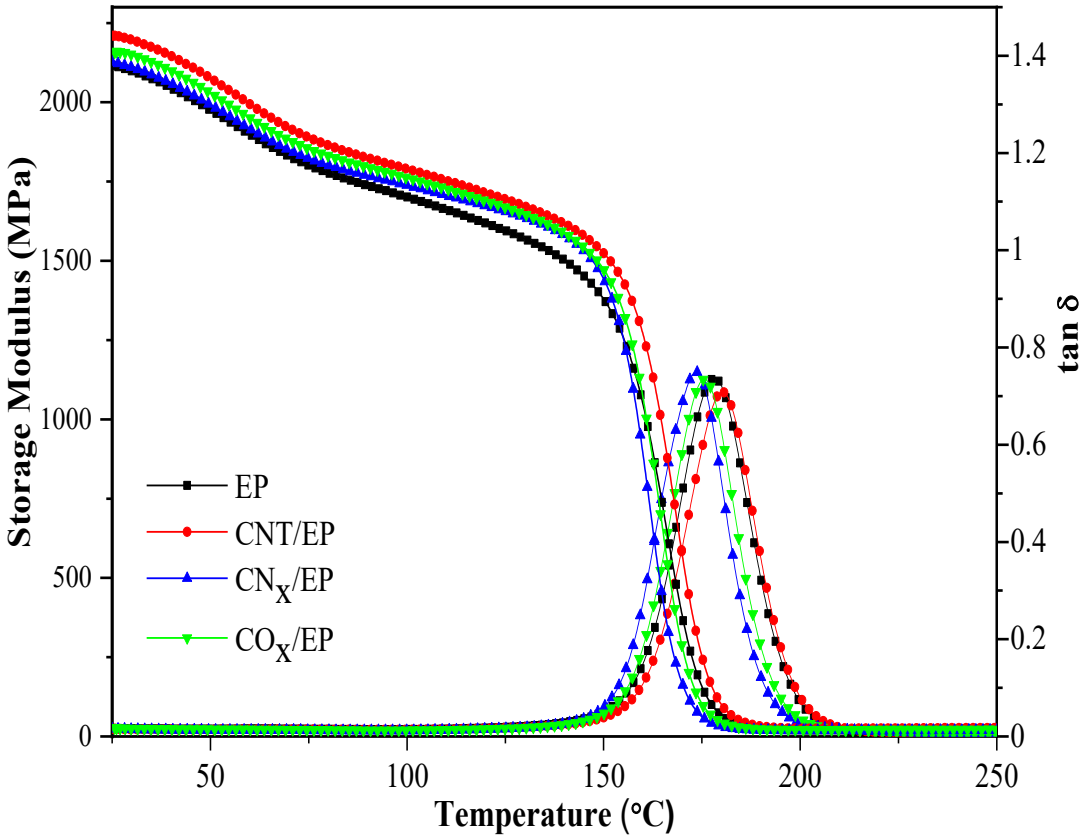

Fig. 4.5 Storage modulus and tan δ versus temperature plots of epoxy and its composites

The influence of addition of nanofillers on the relaxational and mechanical behavior of nanocomposites has been evaluated also by DSC and DMTA. Glass transition temperatures of all the composites were measured by DSC, and DMTA (maximum in tanδ, Fig. 4.5) and the results are summarized in Table 4.2.

Reported values of the Tg for epoxy resins cured with DDS are in the range 184 ºC [129] to 230 ºC [130]. Differences with our case are attributed to the high molecular weight of the prepolymer used in this work (480 g/mol instead of the usual 340 g/mol used by other authors).

Table 4.2 DSC and DMTA results for nanocomposites

Sample	**Tg (ºC) (DSC)**	**Tg (ºC) (DMTA)**	**E' (GPa)**	**FWHM***
EP	179	178	2.11	23
CNT/EP	178	180	2.21	22
CO_x/EP	177	175	2.13	21
CN_x/EP	174	178	2.11	23

* Full width at half maximum

Storage modulus (Fig. 4.5) shows an apparent drop at about 60ºC that is attributed to the tail of the β relaxation that typically appears at -59ºC, as reported by other authors on a similar system [131]. R.t. values are presented in Table 4.2. No significant variations were found in the Tg on adding 2% nanotubes. Neither in the storage modulus nor in the width of the loss tangent peak meaningful alterations were detected as well. Bad CNT-Epoxy interfacial interactions usually manifest as a decrease in both,

the storage modulus and Tg and it is usually justified as an increase in free volume. Our results indicate that addition of nanofillers do not negatively affect the relaxational and mechanical behavior of the nanocomposites.

4.5 Flammability

The flammability behavior of nanocomposites was investigated by LOI and MCC.

4.5.1 Limiting Oxygen Index (LOI)

The limiting oxygen index (LOI) is defined as the minimum oxygen concentration (in vol %) that is necessary to sustain a stable combustion of the specimen after ignition. "The higher the LOI of a polymer material the lower the flammability". Air consists of approximately 21% oxygen. Therefore, any material with an LOI <21 will probably support burning in an open-air situation.

The LOI value is a basic property of the plastic but tells us nothing about how the plastic will react to burning in an open atmosphere. Therefore, this test is simply used to compare the relative flammability and rank polymer and composite materials due to the simple and repeatable condition [132].

LOI tests are performed under standard conditions (as specified by Fire Testing Technology, UK) according to ASTM D 2863-97 with specimens of dimension 130×6.5×3.2 mm^3 [133].

A rod sample with special size is placed vertically at the center of a glass chimney and a slow stream of O_2/N_2 mix is fed from the bottom of the column. The O_2/N_2 ratio is changeable (Fig. 4.6 (a) and (b)).

The test starts by ignition the top edge of the test sample with a candle-like flame. The

O_2/N_2 ratio of the flow is decreased until the flame is no longer supported.

LOI percent is calculated from the minimum concentration of O_2 that will just support combustion. The experimental error in LOI estimation was ± 0.2%.

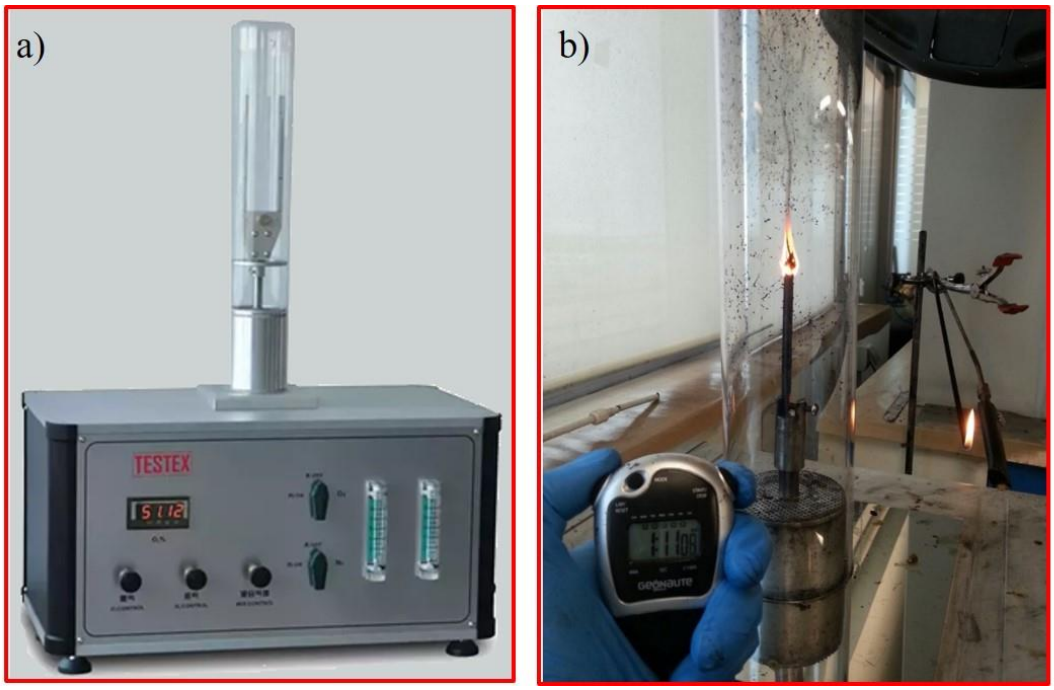

Fig. 4.6 (a) LOI test equipment; (b) Checking the flammability of a sample

The three different types of CNTs (CNT, CO_x and CN_x) have been incorporated into the epoxy matrix and their flammability was examined by measuring their limiting oxygen index (LOI); results are summarized in Fig. 4.6.

Pure epoxy exhibited a LOI value of 21.5%, indicating an easily ignited material. With the addition of 2 wt.% CNT, the LOI of the resultant epoxy composite increases to 33.5%. LOI values above 27 are normally indicative of materials that are self-extinguishing [134]. The incorporation of CO_x into epoxy results in a highest LOI value of 35%. In contrast, the addition of CN_x does not lead to a significant increment in LOI as CO_x, but still exhibiting a high LOI value of 31.5%. In terms of LOI increment: 12%

(CNT), 13.5% (CO_x) and 10% (CN_x).

Obviously, LOI values of the composites strongly depend on the LOI value of the polymer matrix and on the presence of other additives (Fig. 4.7).

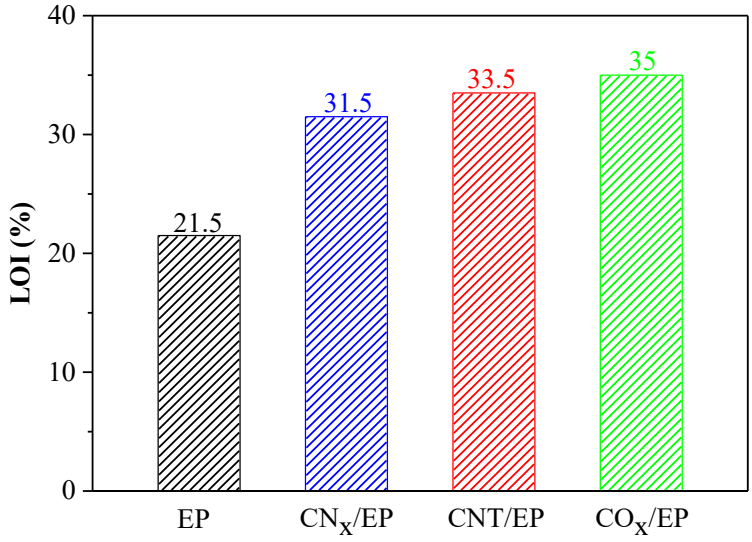

Fig. 4.7 LOI data of pure EP and its nanocomposites

Therefore, a more indicative parameter of the effect of carbon nanofillers may be the LOI increment with respect to the same material without carbon nanofillers. A literature search on the maximum LOI increments found for epoxy thermosets modified with carbon nanotubes yields the following data: 0.2% for epoxy loaded with double walled CNT [135], 3% for epoxy with CNT synthesized by the sol-gel method [136], 5% for epoxy with amino functionalized CNT [131]. Therefore, it seems that the LOI increments found in this paper represent the maximum values ever reported for epoxy thermosets.

Complimentary data to TGA and LOI experiments are supplied by micro-scale combustion calorimetry (MCC) experiments, a testing technique that provides a variety of information on the combustion behavior of polymeric materials [137].

4.5.2 Microscale combustion calorimetry (MCC)

Microscale combustion calorimetry (MCC) (Fire Testing Technology, UK) was used to investigate the combustion of nanocomposites according to ASTM D7309. About 5 mg of sample were heated up to 700 °C at 1°C.s^{-1} under nitrogen at 80 cm^3.min^{-1}. The volatile and anaerobic thermal degradation products in the nitrogen stream were mixed with a 20 cm^3.min^{-1} N_2/O_2 stream (20% O_2) prior entering the combustion furnace at 800 °C. Each sample was run in three replicates.

The relevant parameters obtained from the MCC include peak heat release rate (pHRR), total heat released (THR), temperature at pHRR (T_{max}) and char yield. Results are illustrated in Fig. 4.8 and Table 4.3.

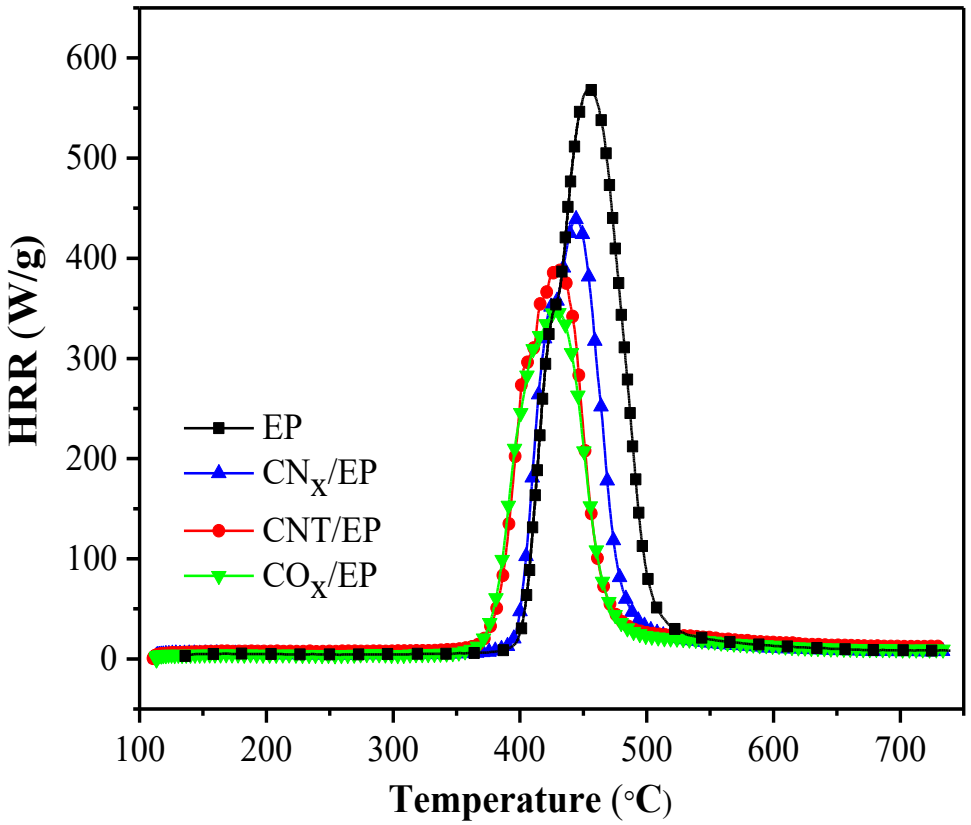

Fig. 4.8 The HRR curves of samples from MCC

Table 4.3 shows that pHRR and THR of neat epoxy (EP) are reduced by 22.7% and 25.3% respectively, by the addition of 2 wt.% of CN_x. A further minor reduction in pHRR and THR was achieved by the incorporation of CNTs in comparison with the sample containing CN_x. However, the highest reduction in pHRR (38.7%) and THR (32.8%) was achieved by incorporation of 2 wt.% of CO_x into the epoxy matrix.

These results are in accordance with previously reported experiments on poly-propylene/MWCNT at low loadings [128]. It can be also noted from Table 4.1 that the char residue increased on addition of nanotubes in accordance with TGA results presented previously, except for the CN_x case.

Table 4.3 Peak heat release rate (pHRR), total heat released (THR), temperature at pHRR and char residue as obtained from MCC measurements

Sample	**pHRR (W/g)**	**THR (KJ/g)**	**T_{max} (ºC)**	**Residue (%)**
EP	568±15	33.2±0.9	454±13	12.1±0.2
CN_x/EP	439±12	24.8±1.1	444±9	14.0±0.1
CNT/EP	384±16	23.0±0.3	433±8	16.4±0.3
CO_x/EP	348±14	22.3±1.2	429±4	18.9±0.3

Interestingly, char residue for CO_x composites is higher than the char residue of pure epoxy plus amount of nanotubes, indicating that the tubes may induce some additional charring (~5-7%) of the epoxy matrix.

4.6 Morphology of the char residue

The surface morphology of the samples after LOI test was checked by SEM and presented in Fig. 4.9. EP, CNT/EP and CN_x/EP (Fig. 4.9 a, b and c) nanocomposites showed a fluffy and cracked char layer full of open holes all along the surface; however CO_x/EP displayed a thick and homogeneous layer which may explain the significant reduction of heat and mass transfer associated to the enhanced flame retardancy presented by the nanocomposites made with this filler.

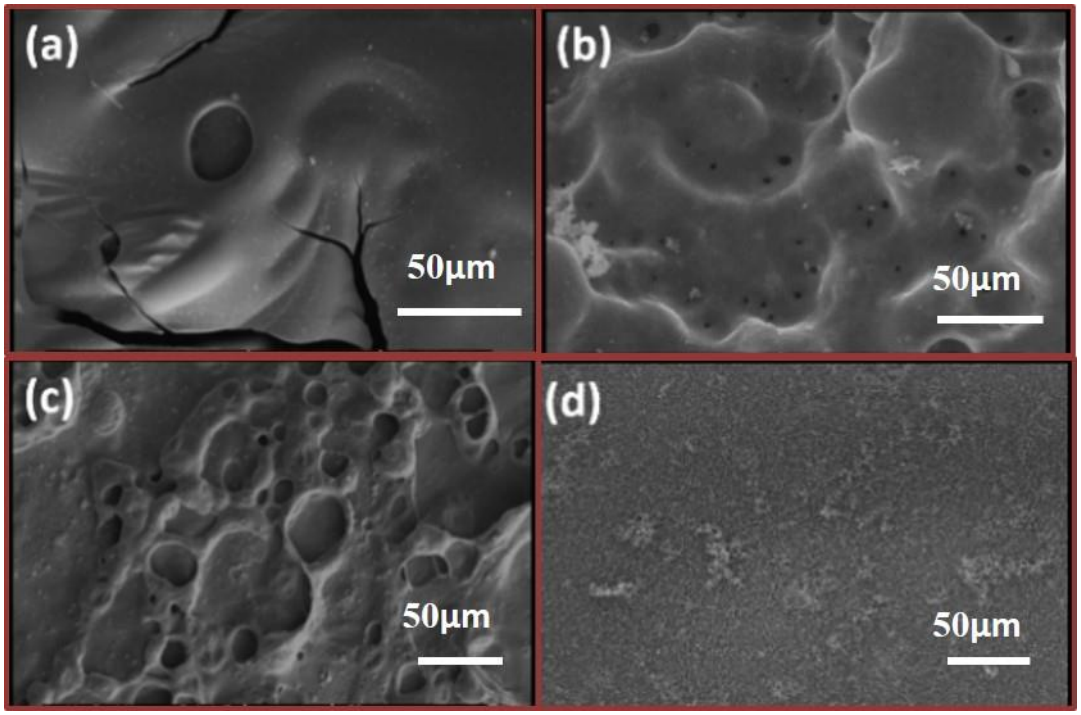

Fig. 4.9 SEM images of the surface of the residual chars of EP (a), CNTs/EP (b), CN_x/EP (c), and CO_x/EP (d) after the LOI test

4.7 Discussion

Based on the LOI and MCC results, the CO_x/EP system is illustrative of a condensed phase burning mechanism with a significantly lower mass loss and higher char yield

compared to the other samples. The higher char residue quenches the fire. Therefore, less epoxy converted into combustible fuel.

The early appearance of a network structure on the external surface of the sample (Scheme 4.1 b) right after the ignition, followed by formation of a thick char layer, served as a thermal barrier to separate burning materials from oxygen [138] also preventing feeding the flame zone from combustible gases, as shown in (Scheme 4.1 c).

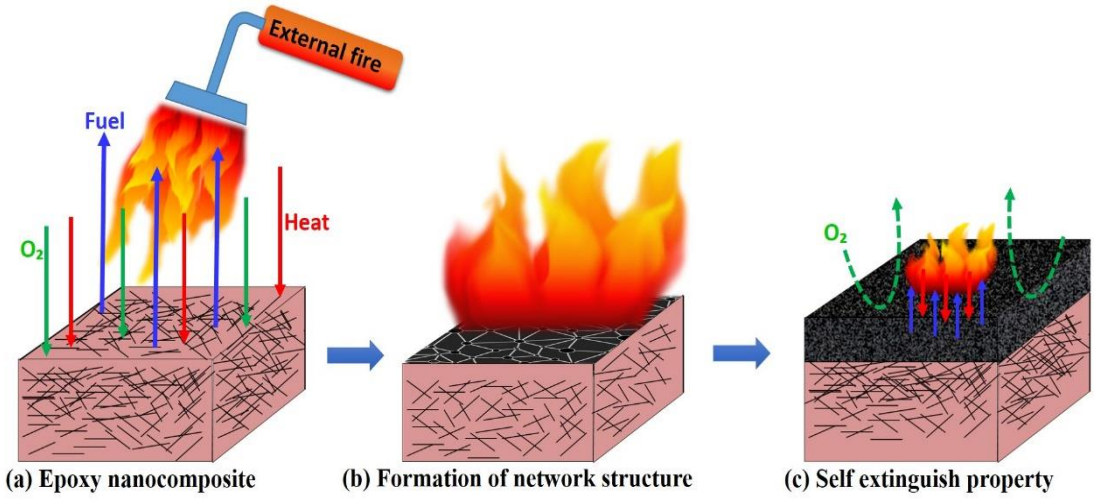

Scheme 4.1 Proposed flame retardant mechanism

4.8 Conclusions of chapter 4

Epoxy nanocomposites containing the three types of carbon nanotubes were prepared by three roll mill at a constant loading of 2% in an epoxy/DDS thermoset and curing them in two stages to ensure the maximum conversion degree. Morphological observations revealed that the CNTs were homogeneously dispersed in the epoxy matrix. Some aggregates and some regions in which nanotubes decoupled from the matrix were observed for CNT and CN_x systems. However, no such defects were

observed for CO_x nanocomposites (Fig. 4.3).

The influence of pristine and doped CNTs on the thermal stability of epoxy nanocomposites was investigated by TGA. The results showed that introduction of the nanofillers at 2 wt.% loading caused the earlier initial decomposition of the nanocomposites, an increased char yield, and a reduction of the degradation rate of in comparison with pure epoxy.

The influence of addition of nanofillers on the relaxational and mechanical behavior of nanocomposites was evaluated by DSC and DMTA. No significant variations in Tg, storage modulus or loss tangent width were detected, indicating that the addition of nanofillers does not negatively affect the relaxational and mechanical response of the nanocomposites.

The flammability behavior of nanocomposites was investigated by LOI and MCC. The LOI increments for CN_x, CNT and CO_x nanocomposites were observed 31.5, 33.5 and 35 respectively, being the latter the highest increment observed for epoxy doped with carbon nanotubes.

The MCC results showed a remarkable reduction in pHRR and THR of 38.7% and 32.8% respectively for CO_x system.

From the SEM images taken from the residual char layer formed by CO_x nanocomposite after burning, a uniform and continuous char layer was observed. However, the other studied systems presented a fluffy surface with plenty of open holes. In the absence of specific effects that could be associated to the surface chemical nature of the carbon nanotubes, our results suggest that the effective improvement in the flame retardant properties of the studied nanocomposites is due to a homogeneous dispersion

of CNTs in the epoxy matrix. In the case of ethanol synthesized carbon nanotubes, which presents notably enhanced flame retardancy, a more effective barrier was formed and this finding must be associated to the formation of a denser percolative network due to its very large aspect ratio. Hence, the key role of percolative networks suggests the need of exploring the flame retardancy properties of systems with the varying aspect ratio, which is the aim of our ongoing research.

Chapter 5

Comparative Study of the Photocatalytic Activity of Copper Salts /GO Nanohybrids

5.1 Photocatalytic degradation of dyes

Dyes in wastewater as one of the most important groups of pollutants are usually of recalcitrant nature and non-bio-degradable. Therefore, a large amount of different catalysts such as photocatalysts to accelerate the pollutant degradation has been recommended so far today [139].

Activated carbons with high surface area have been widely used for water purification [140]. Graphene which theoretically shows nearly twice the surface area of activated carbon can be a very good alternative for water purification [141] but normally does not have catalytic effect on dyes degradation.

Metal oxides have also been employed as photocatalysts for the degradation of various water pollutants and have shown promising results [142]. The use of metal oxides is not still competitive against the traditional water purification techniques such as reverse osmosis and filtration due to some drawbacks. Firstly, metal oxides are only active in UV region because of their wide bandgap. Secondly, due to the possibility of charge carrier recombination, the lifetime of the active species responsible for the degradation is short.

Metal oxide nanoparticles (MONPs) especially semiconductors (e.g. TiO_2, FeO, ZnO, Cu_2O, etc.) decorated on GO as heterogeneous photocatalysts is an effective and rapid strategy to remove dye pollutants [143]. The most important reasons of increasing the photocatalytic activity of metal oxide by the electron scavenging properties of GO are summarized below:

(i) The functional groups of GO (carbonyl, epoxy and hydroxyl groups) act as the nucleation sites for the growth of nanoparticles

(ii) MONPs prevent aggregation of GO layers improving the surface area of the support [144]

(iii) Positive effect of graphene nano-sheets on enhancing the dispersion of MONPs

(iv) Prevent of the MONPs' leaching into the treated solution and extend the lifetime of the adsorbent material [145]

(v) Reduce the bandgap energy of metal oxide by GO via energy-favored hybridization of 2p atomic orbitals of oxygen and carbon [146]

(vi) Limitation of the electron hole recombination by efficient separation of the photo-generated charge carriers due to the GO role

In our work, the catalytic application of the prepared samples was estimated from the decomposition of rhodamine B (RhB) (Fig. 5.1) in an aqueous solution under ambient dark conditions.

RhB was chosen as one of the famous dyes which is commonly used as a colorant in textiles industries due to its high stability. According to its toxic properties for humans and animals, different removal methods in recent studies in the literature have been introduced.

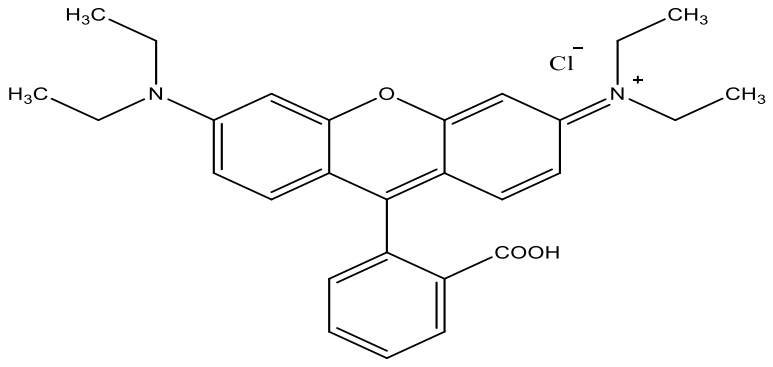

Fig. 5.1 Rhodamine B's chemical structure

Furthermore, we have selected RhB as model compound because of its high stability

in native light and relatively nondegradability in the absence of any photocatalyst [147]. It is well known that Cu_2O can be used as photocatalyst to remove organic pollutants via photodegradation [148]. So we will compare the performance of the three copper salts decorated GO hybrids (DS, CuO and Cu_2O/GO) prepared by the microwave assisted method as catalysts in photodegradation of rhodamine B.

As explained in chapter 4, copper oxide (CuO), cuprous oxide (Cu_2O) and copper hydroxy nitrate double salt (DS) have been synthesized and also decorated on GO according to our proposed method. According to the literature, DS has limited application in comparison to the other copper oxides. So synthesize and decoration of DS on GO is our significant achievement and we have decided to explore more about the properties, conventional synthesis methods and applications of DS in detail (see section 3.2).

5.2 Experimental

5.2.1 Calibration curve of Rhodamine B concentration

Photocatalytic behavior of samples was recorded on UV–vis spectrophotometer (Jasco V-650) over the range of 450-600 nm because the strongest photon absorption of RhB can be detected in this range (λ_{max} (RhB)= 554 nm)

An initial calibration of the UV-vis spectrophotometer was performed by measuring known concentrations of RhB. A calibration line (Fig. 5.2 (a)) was obtained from the absorbance analysis of the aqueous standard solutions of RhB at different concentrations (2, 4, 6, 8, and 10 ppm) (Fig. 5.2 (b)). The straight line shows that the absorbance (A) of a solution is directly proportional to the concentration (C) of the

absorbing species in the solution and the path length (l) according to the Beer-Lambert's law:

$$A = \varepsilon . C . l$$

ε is molar extinction coefficient and characteristic for each substance at a particular wavelength (λ).

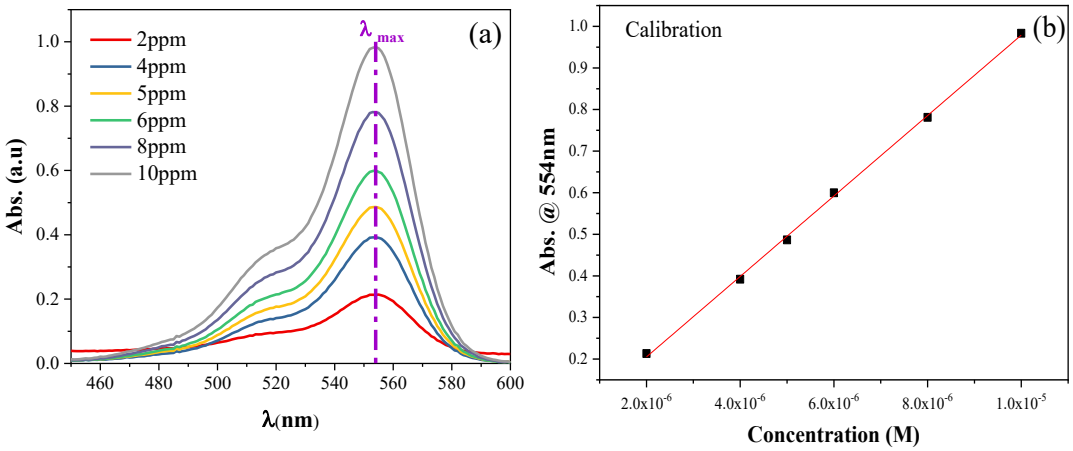

Fig. 5.2 (a) visible spectra of aqueous solution of the different concentrations of RhB and (b) a linear calibration plot for RhB at room temperature at 554 nm

5.2.2 Evaluation of photocatalytic activity of samples

The experimental setup that has been used to study the photodegradation of RhB in the presence of catalysts is schematically depicted in Scheme 5.1.

While conducting the tests, the reaction unit was isolated to prevent contact of the reaction mixture with light from the environment as well as the leakage of UV light, which is harmful to health.

The heat effect in the illumination was minimized by the water circulation. All experiments were done at room temperature.

At the bottom of the reactor, a magnetic stirrer assures homogenization during

photodegradation. The experiments were performed on samples of 500 mL aqueous solutions of dye prepared with distilled water.

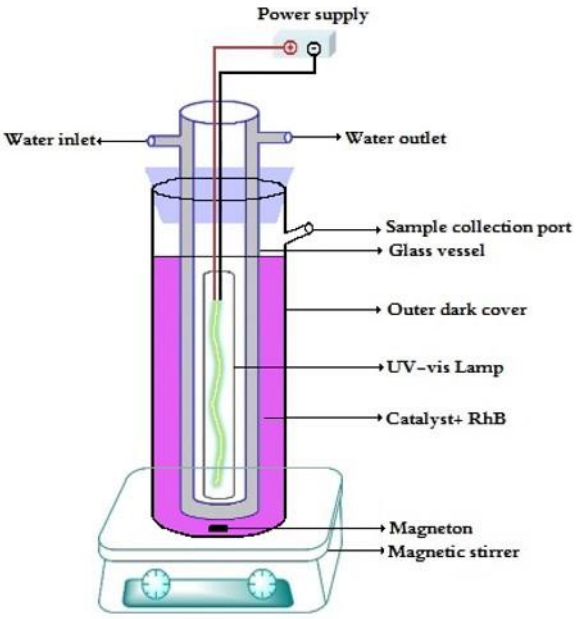

Scheme 5.1 Experimental set-up for checking the photodegradation of RhB

In a typical experiment 10 mg of catalyst (as-prepared products: GO and decorated versions) was dispersed in a 100 mL water by 5 min ultrasonic bath. The solution was added into 400 mL of RhB solution. Initial concentration of our solution should be around 10 ppm of RhB because in the range of 1 to 10 ppm the ratio between absorbance and concentration was linear (Fig. 5.2 (b)). Before starting irradiation, the suspension was stirred moderately in darkness for 30 minutes to ensure the adsorption/desorption equilibrium of the organic dye. Then illumination under UV-vis light from a TQ 150W lamp began.

During the illumination, approximately 2 mL suspension was withdrawn at fixed intervals (30 minutes) and analyzed by an UV–vis spectrophotometer over the specific mentioned range.

First test has been carried out in the absence of any catalyst to check the light effect.

Then we have done the experiment in the presence of GO, DS/GO, Cu_2O/GO, CuO/GO and also pristine DS, Cu_2O and CuO to compare the effect of GO as substrate. Furthermore, the effect of GO without illumination has been checked.

We have tested the performance of TiO_2 Degussa P-25 as a common photocatalyst reference.

Fig. 5.3 depicts the absorbance light vs time of remained RhB in the solutions in presence of bare and supported DS catalysts as an example. The main absorption peak of RhB at 554 nm, decreases with time as the degradation proceeds. The rate of degradation in copper salts/GO nanohybrids is higher than bare salts.

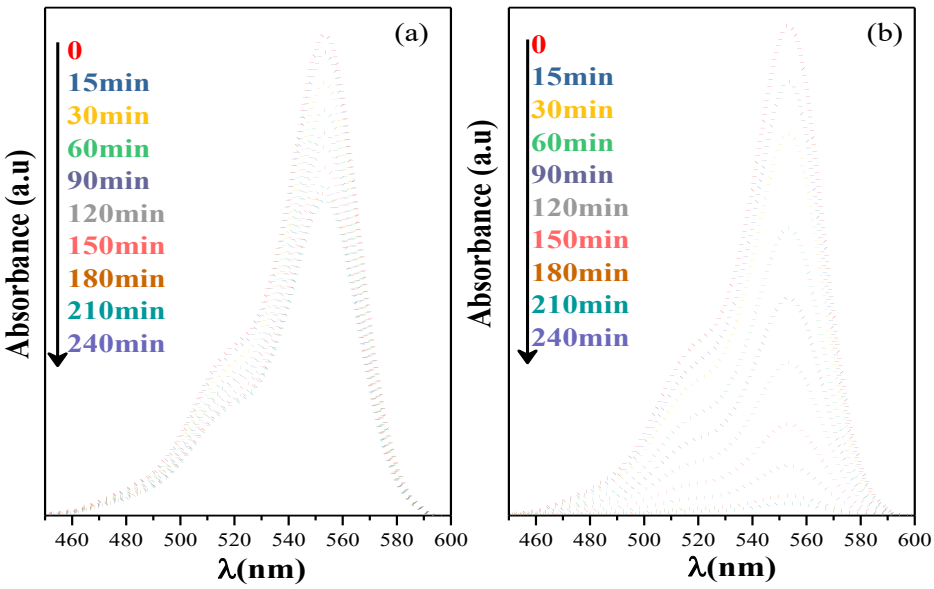

Fig. 5.3 Absorbed light spectra for RhB at different reaction time affected by (a) DS, and (b) DS/GO catalysts

Ultimately, after collecting the data from the experiments and checking the maximum absorbance at 554 nm for each sample in the specific time, a plot of degradation percentage versus irradiation time for the aforementioned samples was obtained.

$$\%\ \text{Conversion}\ \alpha = \frac{C_0 - C}{C_0} \times 100$$

The plot of degradation vs time illustrates that the decomposition of RhB under light without any catalyst (<5 % during 240 min exposure) is negligible (Fig. 5.4).

% Conevrsion in the presence of GO with and without illumination was 20% and 17% respectively. However, in the presence of Cu_2O/GO, DS/GO and CuO/GO nanohybrids, 97.7%, 97.5% and 93.7% of the dye is removed from the solution after 240 min, respectively.

RhB was decomposed in the presence of 10 mg of DS, Cu_2O and CuO salts around 34.4%, 51.4% and 41.1% respectively under the same condition. The reference, TiO_2 Degussa could be decomposed 62.8% of RhB in 4 hours.

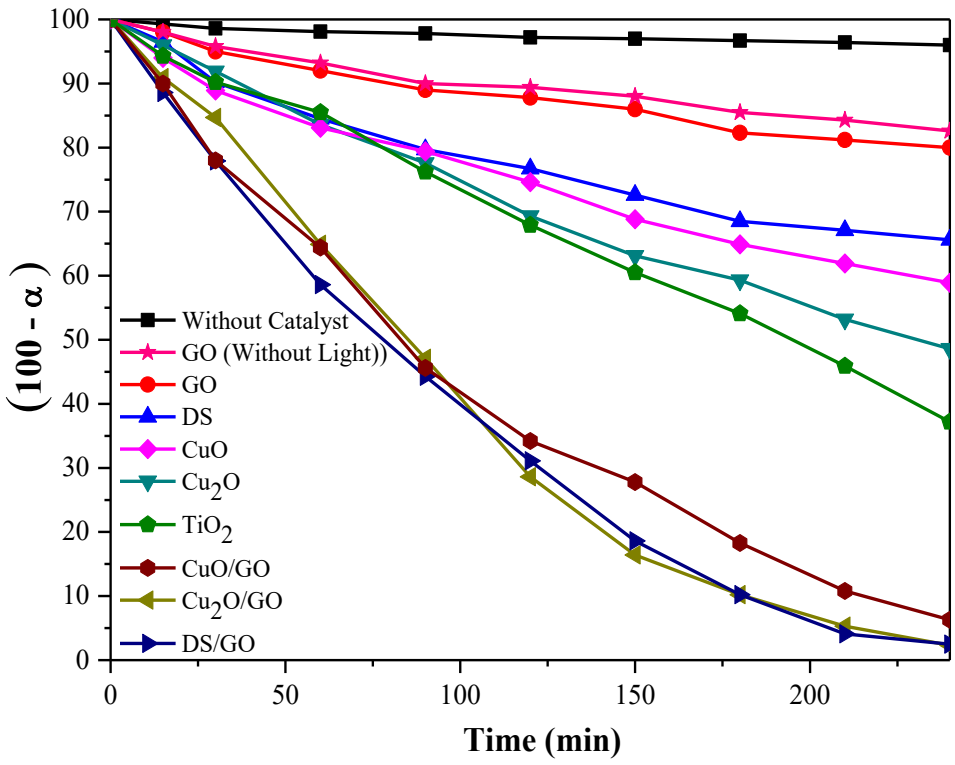

Fig. 5.4 % Degradation as measured by 1-α, vs illumination time of RhB in presence of different catalysts

It is fully demonstrated that GO decorated with copper salts decorated GO have much

higher photo-catalytic activity than the bare nanoparticles and even better than the well-known photocatalyst TiO_2. This trend might be attributed to the improvement of the collection of sunlight, excellent electron mobility and charge transfer in GO, and the higher specific surface area in nanohybrids to absorb a broad spectrum of radiation (see section 5.1). Whereas the decrease in bandgap and consequently promoting the charge efficiency is attributed to the enhanced photocatalytic activity [149], we decided to check bandgap energy of our catalysts.

5.3 Bandgap energy

The bandgap energy or forbidden energy zone (E_g) stands the minimum energy that is required to excite an electron up from a state in the valence band to the conduction band where it can participate in conduction [150].

One of the best method of determining E_g is based on Kubelka–Munk function evaluated from the diffuse reflectance data (DRS).

The reflectance data can be converted to absorption according to the K-M theory;

$$F(R_\infty) = (1 - R_\infty)^2/2R_\infty$$

where, R_∞ is reflectance, $F(R_\infty)$ is the K-M function.

The optical bandgaps of the catalysts can be estimated by using Tauc plot (Fig. 5.5)

$$(\alpha h\nu)^{1/n} = A\ (h\nu - E_g)$$

where α, hν, A, and E_g are the absorption coefficient, incident light frequency, proportionality constant and band gap, respectively. The absorption coefficient ($\alpha = F(R_\infty)$) is obtained from Kubelka–Munk function. The value of exponent 'n' determines the nature of electronic transition; for direct transition, $n = 1/2$ and for indirect

transition, n=2. The linear extrapolation of $(\alpha h\nu)^{1/n}$ to zero gives the band gap energy of the sample [151] (Fig. 5.5).

Diffuse reflectance spectra (DRS) were measured with Lambda 14P, Perkin-Elmer spectrophotometer, using a 60 mm integration sphere, in the diffuse reflectance mode $F(R_\infty)$ (absolute reflectance) and using $BaSO_4$ as pattern.

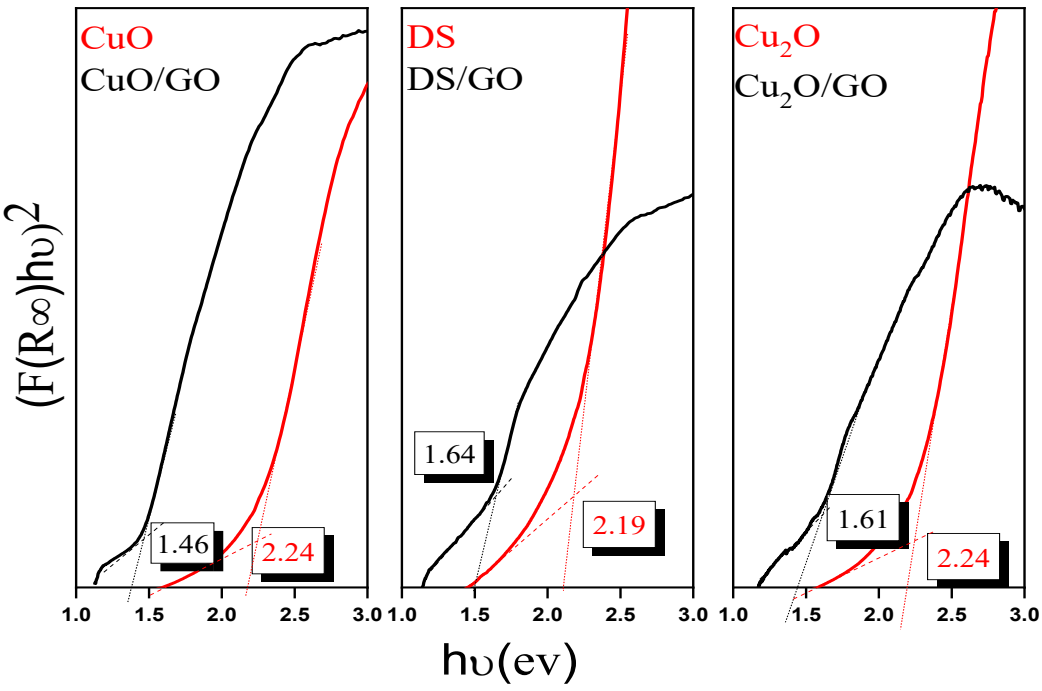

Fig. 5.5 Determination of the bandgap from the Kubelka-Munk transformed reflectance spectra for DS, Cu_2O and CuO

The large bandgap energy and rapid recombination of photogenerated charge carriers in the case of bare copper salts limited their performance. Incorporation of the copper salts in GO leads to a decrease in bandgap energy in about 25-35% (Table 5.1). Narrower bandgap reveals that the optical properties of nanohybrids haves been improved, thereby improving the utilization of light and photodegradation [152].

Table 5.1. Bandgap energy extracted of Fig. 5.5

Catalyst	Bandgap energy (ev)	
	Bare salt	Supported on GO
DS	2.19	1.64
Cu_2O	2.24	1.61
CuO	2.24	1.46

The bandgap red shifts can be attributed to the crystallite size/morphology and type of electronic transition due to the covalent link between copper salts and graphene oxide [153].

5.4 Kinetic analysis of photodegradation

The heterogeneous catalysis mechanism can be divided in three steps, dye adsorption (ads) over catalyst, dye degradation (deg) and product desorption (dsp) from catalyst as depicted in Scheme 5.2.

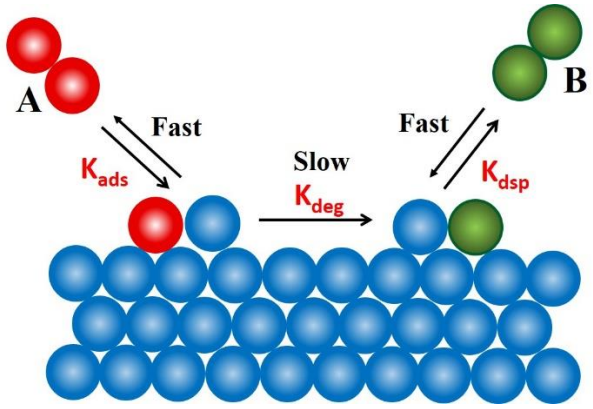

Scheme 5.2 Langmuir-Hinshelwood model for a heterogeneous catalytic unimolecular reaction

Heterogeneous photocatalytic processes of dyes are usually studied in terms of the Langmuir-Hinshelwood model, which is given by

$$r = -\frac{dC}{dt} = \frac{k_r K C}{1 + KC} \qquad (1)$$

Where r represents the rate of reaction that changes with time, C is the concentration of the dye at any reaction time during degradation, K is the equilibrium constant for adsorption of the substrate and k_r is the limiting rate constant of reaction at maximum coverage of the solid support. The product $k_r K$ is sometimes globally evaluated as an apparent rate constant (k_{app}; min^{-1}). The integrated form of equation (1) is [154]:

$$\frac{C}{C_0} = e^{K(C_0 - C)} e^{-k_r K t} \qquad (2)$$

Equation (2) can be expressed in a non exponential form and in terms of the conversion degree as follows:

$$K C_0 \alpha - \ln(1 - \alpha) = k_r K t \qquad (3)$$

The units of constants appearing in the above equation are: $[C_0] = mg/L$, $[K] = L/mg$ and $[k_r] = mg/L \cdot min$. For fitting purposes, equation (3) has been slightly modified in the form:

$$t = \alpha A - B \ln(1 - \alpha)$$

Where $A = \frac{C_0}{k_r}$ and $B = \frac{1}{k_r K}$ are fitting parameters. These parameters can be found using common non-linear fitting routines. In Fig. 5.6, we present experimental conversion vs time plots along with the fitted curves.

The three supported systems present very similar kinetic profiles: cuprous oxide and the double salt systems are essentially identical while cupric oxide appears to be slightly less efficient.

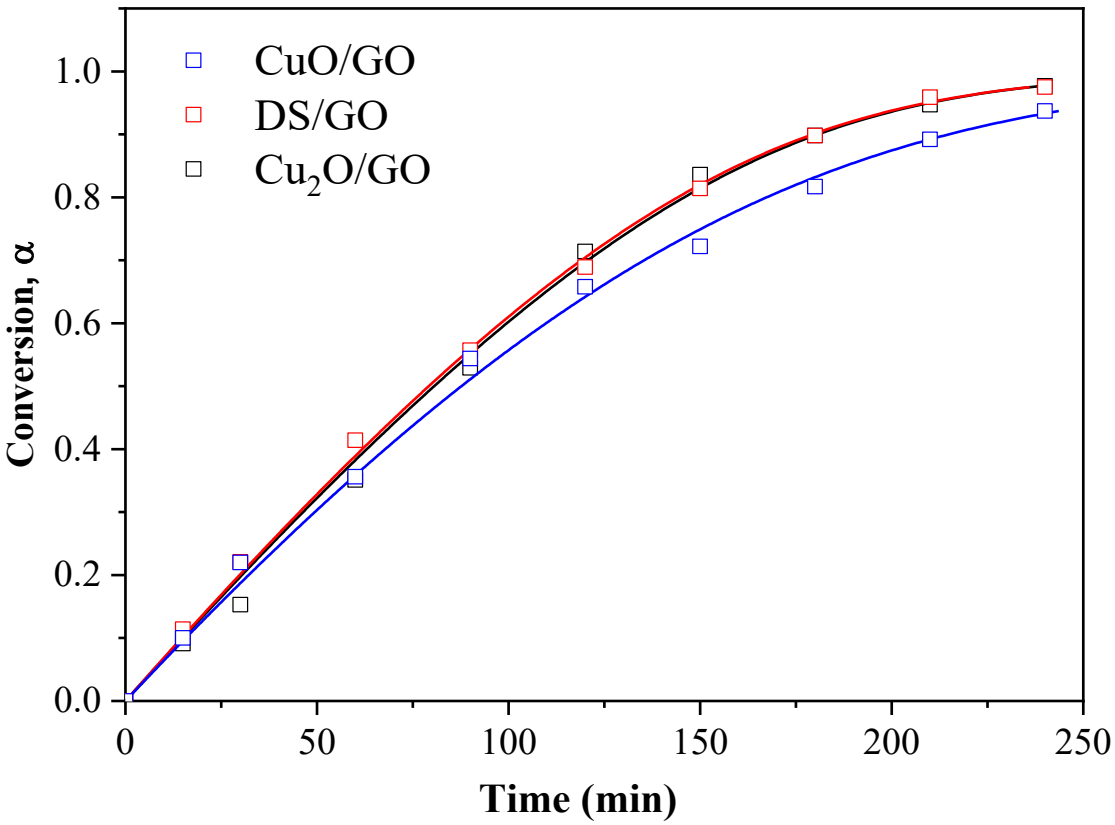

Fig. 5.6 Conversion vs time plots for three supported catalysts

Analysis of the fitting parameters allows a plausible explanation. Summary of the fitting parameters along with fitting goodness r^2 are presented in the Table 5.2.

Table 5.2 Fitting parameters of three supported catalysts

System	$A = \frac{C_0}{k_r}$	$B = \frac{1}{k_r K}$	r^2
Cu₂O/GO	114.2 ± 7.3	33.8 ± 2.6	0.997
DS/GO	109.9 ± 5.8	34.9 ± 2.1	0.998
CuO/GO	100.4 ± 10.9	54.1 ± 4.8	0.996

The values of the calculated rate constants are given in Table 5.3 along with the initial concentration of rhodamine B dye.

Table 5.3 Calculated rate constants in three supported catalyst system

System	C_0 (mg/L)	k_r $(mg/Lmin)$	K (L/mg)	k_{app} (min^{-1})	TOR$\times 10^7$ $(mol/gmin)$
Cu_2O/GO	4.034	$(3.54 \pm 0.22)\cdot 10^{-2}$	0.83 ± 0.12	$(2.94 \pm 0.62)\cdot 10^{-2}$	4.54
DS/GO	4.063	$(3.69 \pm 0.20)\cdot 10^{-2}$	0.77 ± 0.09	$(2.86 \pm 0.48)\cdot 10^{-2}$	5.25
CuO/GO	4.007	$(4.01 \pm 0.44)\cdot 10^{-2}$	0.46 ± 0.09	$(1.85 \pm 0.58)\cdot 10^{-2}$	4.91

The three rate constants k_r, for the three systems are equal within the experimental error. No variations are found. However, a significant difference is found in the adsorption/desorption equilibrium constant for the cupric oxide system reflecting that rhodadmine has less tendency to adsorb on graphene oxide when it is decorated with Cu(II) oxide. A possible explanation can be found in the surface properties of thin films of cupric and cuprous oxides from contact angle measurements [155]. According to these measurements, Cu(I) oxide has a lower dispersive component than Cu(II) oxide which may enhance adsorption of a polar dye such as Rhodamine B.

With respect to non-supported dyes, it was found that these systems followed pseudo first order kinetics in all cases, i.e.,

$$C = C_0 e^{-k_{app}t} \qquad (4)$$

Where $k_{app}$is the apparent first order reaction rate. For fitting purposes equation (4) was linearized in terms of the conversion and it was allowed free intercept

$$ln\frac{C_0}{C_t} = \ln(1-\alpha) = k_{app}t \qquad (5)$$

In the following figure (Fig. 5.7), we present the plot of $\ln(1-\alpha)$ versus time for all the unsupported systems.

Except for the case of cuprous oxide, which shows a very good correlation, the rest of the systems do not fit completely to a first order equation at least as well as the

supported systems do to the complex Langmuir-Hinshelwood model.

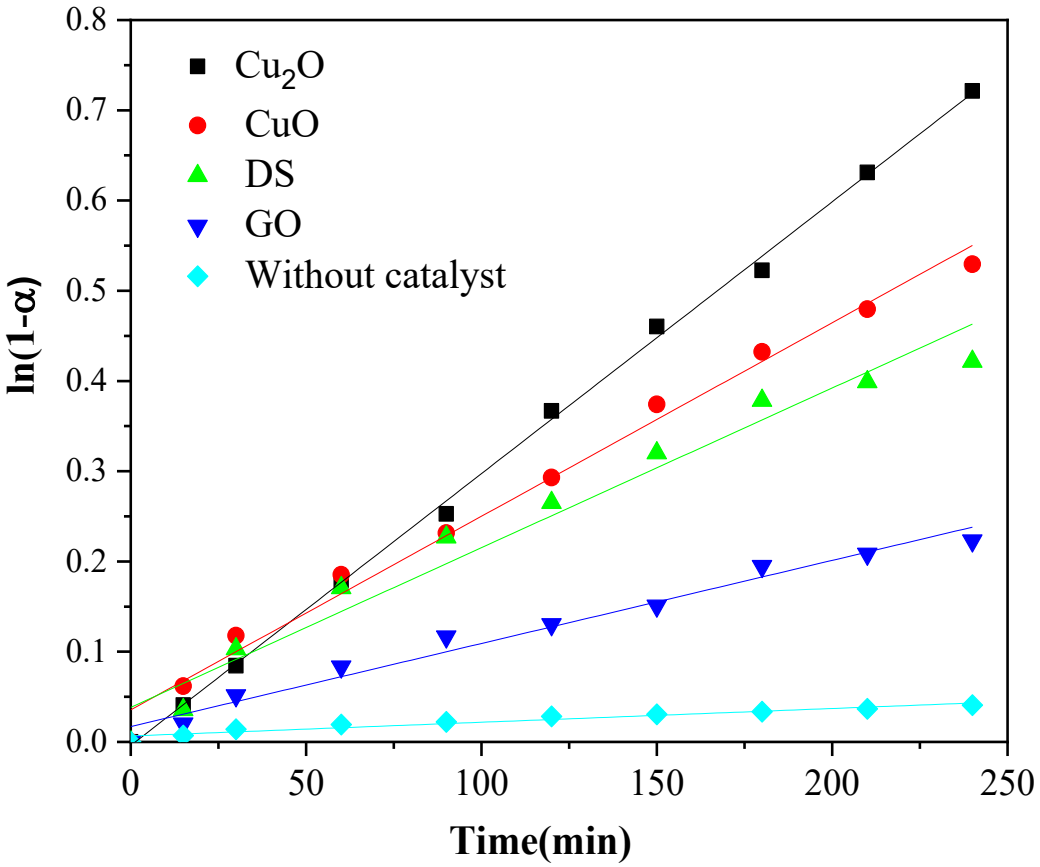

Fig. 5.7 $\ln(1-\alpha)$ vs time for unsupported catalysts, GO and without catalyst systems

Apparent rate constants and correlation coefficient are presented in Table 5.4. In this table it has been included the results for a non catalyzed system (WC) and for a system containing pure GO as catalyst.

Table 5.4 Calculated rate constants in the presence of unsupported catalysts, GO and without catalyst systems

System	k_{app}(min)	r^2	TOR× 10^7 $(mol/gmin)$
Cu₂O	$(3.01 \pm 0.04)\cdot 10^{-3}$	0.999	2.32
DS	$(1.77 \pm 0.11)\cdot 10^{-3}$	0.96	2.09
CuO	$(2.14 \pm 0.08)\cdot 10^{-3}$	0.988	2.48
GO	$(0.92 \pm 0.05)\cdot 10^{-3}$	0.97	1.34
WC	$(0.15 \pm 0.01)\cdot 10^{-3}$	0.93	-

Apparent rate constants are one order of magnitude lower for the unsupported catalysts than for the GO supported ones.

According to Wachs et.al. [156] one of the interesting parameter to compare heterogeneous photocatalysis activity is the Turnover Rate (TOR: moles converted or produced per gram of photocatalyst per unit of time):

$$\mathrm{T.O.R} = \frac{\text{amount of removed RhB (mol)}}{\text{amount of catalyst (gr)} \times \text{reaction time(min)}}$$

In the previous tables, TOR has been calculated for all the systems.

5.5 Conclusions of chapter 5

In this chapter, we have discussed about the performance of copper salts/GO nanohybrids as photocatalyst in degradation of one common dyes (Rhodamine B). According to the results, it was found that microwave assisted decoration of copper salts (CuO, Cu_2O, and DS) on graphene oxide can significantly improve their photocatalytic activities.

As we expected, incorporation of copper oxides (copper with different oxidation number) onto GO via our method resulted in enhancing the properties of initial metal oxides and it was comparable with the CuO and Cu_2O/GO hybrids produced of conventional methods [157, 158, 159].

Photocatalytic activity of DS alone and decorated on GO has been reported for the first time in this work.

A decrease in bandgap energy (E_g) of decorated copper salts on GO leads to an increase of light absorption especially in low energy region, being this mechanism the most probable reason of the enhanced catalytic activity.

In relation to the study of photocatalytic degradation kinetics, GO decorated with copper oxides follow the Langmuir-Hinshelwood model. Non-linear fitting of results to that model allows to obtain the apparent rate constants as well as the adsorption/desorption equilibrium constant. Cu_2O/GO and DS/GO systems present very similar kinetics while CuO/GO appears to be slower probably because adsorption of rhodamine B is less favoured.

Bare copper oxides follow pseudo first order kinetics although fittings are not good. The apparent rate constant are one order of magnitude lower than for decorated GO catalysts.

Chapter 6
Comparative Study of Organic Chemistry Catalysis Activity of Copper Salts /GO

6.1 Introduction

Copper is a natural essential element which is the third most abundant element found in the human body, after iron and zinc. Currently, copper compounds are particularly attractive for the scientific community because they can be good replacement for palladium compounds in some catalytic reactions and improve the efficiency for several reasons: copper is cheaper than palladium, copper has a higher natural abundance and is less toxic than palladium, especially in large-scale reactions. Furthermore, copper chemistry is richer than palladium's, copper can easily access to different oxidation states (Cu^0, Cu^I, Cu^{II}, and Cu^{III}) allowing it to react through one or two-electron processes and palladium chemistry is usually restricted to Pd^0 and Pd^{II} species. Finally, it is well known from recent investigations that, copper can take part in coupling and cross-coupling catalytic reactions in a way significantly similar to palladium but with a unique chemoselectivity and reactivity [90].

In the catalytic context, copper salts as catalysts have been known for more than one century since the findings of the Ullmann reaction [160] showing very interesting results in different coupling reactions (C–C, C–N, C–O, C–S, etc.) [161]. In recent years, copper has also received increasing attention because of its catalytic activity in oxidation and reduction reactions, and other wide range of catalytic reactions such as cycloaddition, hydrogenation, etc. [67]. All the catalytic studies have demonstrated that, generally, copper nanoparticles (Cu NPs) with small sizes and different shapes present more interesting catalytic results than copper complexes or copper-based bulk materials because of their highly accessible surface areas and higher reactivity [162].

However, one of the main current challenges in the development of catalyst copper-

based materials is the design of novel nanosystems with higher activity, selectivity, stability, and lower production prices. Thus, some of the most widely used strategies for these purposes are the support of copper complexes onto different nanostructured scaffolds, or the support of Cu NPs in different materials for increasing dispersibility, avoiding serious aggregation to improve the catalytic efficiency [163].

In this sense, some studies have reported on the support of copper pro-catalysts in different materials in order to help the recovery and reuse of copper catalytic centers reducing the final product contamination [164]. In addition, copper-based composites, have also been synthesized using zeolite, mesoporous silicas [165], polymers [166], metal oxides [167] and carbon-based nanomaterials, such as carbon nanotubes, graphene oxide (GO) or reduced graphene oxide (rGO) as solid supports [89].

The catalytic activity of (DS/GO, Cu^0/GO, CuO/GO or Cu_2O/GO) nanohybrids were tested in different reactions of interest in organic chemistry such as oxidation of alcohols, C-C, C-N or C-S coupling. The results reported here show that the copper-based nanomaterials have very good catalytic efficiency in a wide number of reactions showing a high versatility. Indeed, these novel systems show comparable catalytic performance with conventional activated carbon based composites or other reported catalysts [163].

Although there are some reports about the study of catalytic application of copper or copper oxides (I, II) /GO nanohybrids synthesized via microwave assisted method, to the best of our knowledge, the present work is, one of the first studies on the catalytic performance of DS/GO nanohybrid microwave assisted synthesized [168,169].

Thus, in this part, the catalytic activity GO decorated with copper-based materials by

our microwave assisted method: DS/GO, Cu/GO, CuO/GO and Cu_2O/GO were studied in different catalytic reactions of interest in organic chemistry such as oxidation of alcohols and coupling reactions (C-C, C-N and C-S). All the catalytic tests were carried out at the Department of Biology and Geology, Physics and Inorganic Chemistry (ESCET), Rey Juan Carlos University.

The attractive results found for these tests encourages a future more exhaustive study of the potential application of these systems in sophisticated organic reactions of both academic and industrial interest.

6.2 Experimental

6.2.1 Materials & general remarks for the catalytic studies

All reactions were performed using standard Schlenk tube techniques in an atmosphere of dry nitrogen (Fig. 6.1 (a)). Solvents were distilled from the appropriate drying agents, and degassed before use. The reagents of the catalytic reactions, namely, benzyl alcohol (Fluorochem), iodobenzene (Sigma-Aldrich), phenyl boronic acid (Sigma-Aldrich), 3,5-dimethylthiophenol (Fluorochem), benzylamine (Fluorochem) and methylamine (30% in water, Sigma-Aldrich) and H_2O_2 (Sigma-Aldrich) were used directly without further purification.

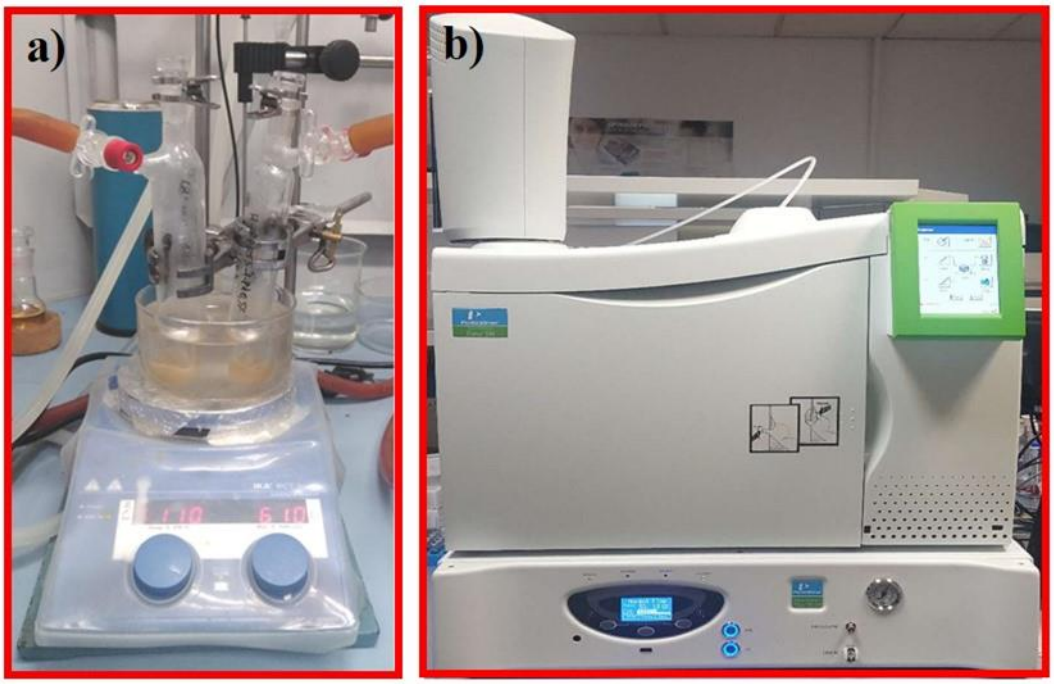

Fig. 6.1 (a) Experimental set-up to study the catalytic activity of the synthesized samples in Schlenk tube technique (b) GC equipment

6.2.2 Quantification of the conversion rate

The technique employed to quantitatively analyze the conversion of the reactions and to identify the reaction product was gas chromatography (GC) with FID detector (Perkin-Elmer GC Clarus 580) with a Velocity® column (poly(dimethylsiloxane), 30 m, 0.25 mm, 1.00 µm) (Fig. 6.1 (b)).

The kinetics or the conversion of the reactions were determined by following the variation of the concentration of iodobenzene in DMF for all tests except for oxidation reaction. The concentration of benzyl alcohol has been measured in this reaction test. The changes of the iodobenzene concentration was checked by using standard calibration curve of iodobenzen/DMF in the range of 0-0.15 M (Fig 6.2) with compare to the areas relating to the signals of iodobenzene in chromatogram.

The temperature conditions were; injector temperature: 240 °C, detector temperature: 250 °C, oven temperature program 130 °C (10 min); from 130 °C to 210 °C (with a ramp of 20 °C/min) and 210 °C (10 min). Operating under these conditions the retention times of the chemical species in solution were, DMF: 3.5 min.

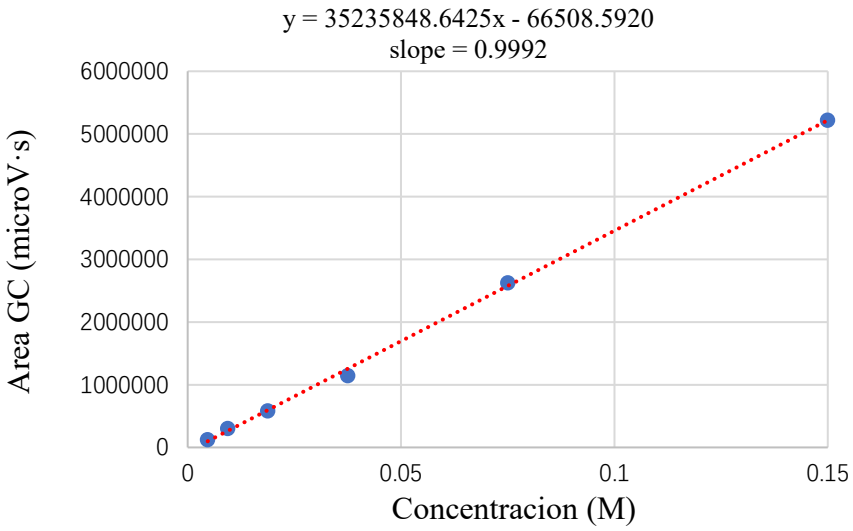

Fig. 6.2 Typical calibration curve of iodobenzene in DMF

6.3 Study of the catalytic performance of copper/GO nanohybrides

6.3.1 Catalytic oxidation of benzyl alcohol (BzOH)

DS/GO, Cu/GO, CuO/GO and Cu_2O/GO were tested as heterogeneous catalysts for benzyl alcohol oxidation to determine their catalytic activity and selectivity towards the formation of benzaldehyde. In a typical catalytic experiment, 108 mg (1.0 mmol) of benzyl alcohol dissolved in DMF (5 mL), 0.15 mL (4.4 mmol) of hydrogen peroxide solution 30 % (w/w) in H_2O and 25 mg of copper-containing material were added under nitrogen atmosphere to a Schlenk tube (Scheme 6.1).

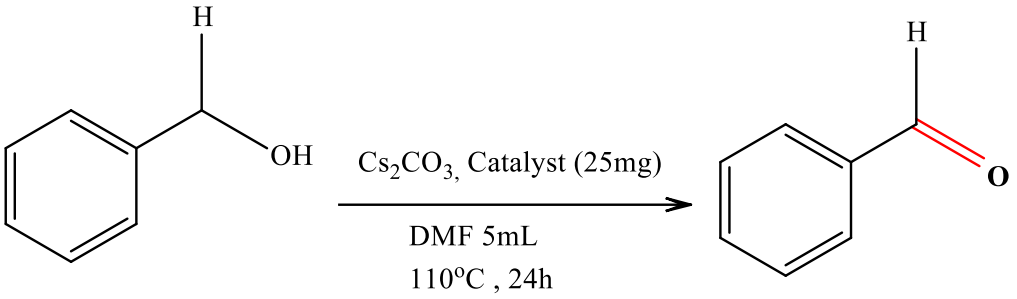

Scheme 6.1 Oxidation reactions of Benzyl alcohol catalyzed by Cu/GO nanohybrides

The mixture was stirred at 110 °C during 24 hours. Subsequently, the reaction mixture was filtered through a nylon filter (0.45 µm) and the filtrate was analyzed by GC-FID (Perkin-Elmer GC Clarus 580) with a Velocity® column (dimethylpolysiloxane, 30 m, 0.25 mm, 1.00 µm) to quantify the conversion to benzaldehyde. The temperature program for the column for the detection and quantification was 90 ºC (5 minutes), heating for 3 minutes (ramp 20 ºC/min) to 150 ºC (5 minutes), heating for 4 minutes (ramp 25 ºC/min) to 250 ºC (6 minutes) and heating for 2 minutes (ramp 20 ºC/min) to 290 ºC. The GC had an injection temperature of 240 °C and the detector temperature was of 300 °C.

The collected results are shown in Table 6.1. Turnover numbers have been calculated according to the following formula:

$$\text{Turnover number} = \frac{\text{Conversion\%}}{\text{Amount of active site of catalyst (mmol)}}$$

The amount of copper active site for each nanohybrid was estimated of the copper compound extracted of TGA data (Table 6.1).

The catalytic study shows a much higher oxidation conversion of benzyl alcohol to benzaldehyde for DS/GO nanohybrid. The conversions of ca. 85% compared with the other catalysts which range from 47 to 69% indicating that the oxidation capacity of

the supported DS is very high bearing in mind that this material shows a Turnover number (TON) value of 4.72 which is much higher than all the others of between 1.46 and 2.27 (Table 6.2).

Table 6.1 Calculated amount of copper active sites in 25 mg of each catalyst

Catalyst	(% w/w) Cu compound in nanohybrid*	(mg) Cu compound in 25 mg catalyst	(mmol) Cu compound in 25 mg catalyst	(mmol) Cu Active-sites in 25 mg of catalyst
Cu/GO	92.4	23.1	0.361	0.361
DS/GO	88.6	22.15	0.092	0.184
CuO/GO	96.7	24.2	0.303	0.303
Cu_2O/GO	75.8	18.9	0.132	0.264

* Values from Table 3.3

Table 6.2 Results of the catalytic oxidation reactions of copper compound/GO nanohybrides at 24 hours

Reaction	Catalyst	Conversion (%mol)[a]	TON
Oxidation BzOH	Cu^0/GO	53.0 [>99]	1.46
	DS/GO	86.9 [>98]	4.72
	Cu_2O/GO	47.5 [>99]	1.8
	CuO/GO	68.9 [>98]	2.27

[a] Data in brackets refer to the selectivity towards benzaldehyde

In all cases, the systems are quite selective as the quantity of obtained benzaldehyde is higher than 98% and only traces of benzoic acid and benzyl benzoate were obtained. The conversion % benzyl alcohol to benzaldehyde in the case of DS/GO is the highest. These materials present similar if not somewhat higher TON values than other supported systems based on Pd nanoparticles [170].

6.3.2 Catalytic Suzuki C-C coupling reactions

The studied reaction was the coupling of iodobenzene (Ph-I) with phenylboronic acid (Ph-Bor) at 110 °C during 24 h. The coupling reaction was carried out in 5 mL of a mixture 95:5 DMF:water. Iodobenzene was used as limiting reagent and with a molar ratio between the halide and the boronic acid of 1:1.2. In addition, the molar ratio between the halide and the base (Cs_2CO_3) was 1:1 and the amount of catalyst was in all cases 25 mg. All the reactions were carried out using degassed solvents and under a nitrogen atmosphere. A solution of 153 mg (0.75 mmol) of iodobenzene was prepared in 5.0 mL of a mixture of degassed solvents (DMF:H_2O 95:5) was carried out under nitrogen in a Schlenk tube. Subsequently, a Schlenk flask was filled with phenylboronic acid (110 mg, 0.90 mmol), and Cs_2CO_3 (244 mg, 1.50 mmol) and copper-based materials as catalyst (25 mg) (Scheme 6.2). Three vacuum/N_2 cycles (10 min/1 min) were carried out to eliminate oxygen from the reaction atmosphere and reduce the quantity of hypothetical adsorbed water from the solids. After the vacuum/N_2 cycles the solution of 1-iodobenzene was transferred under N_2 to the Schlenk flask containing the solid mixture and the resulting suspension was then heated to 110 °C and stirred for 24 hours.

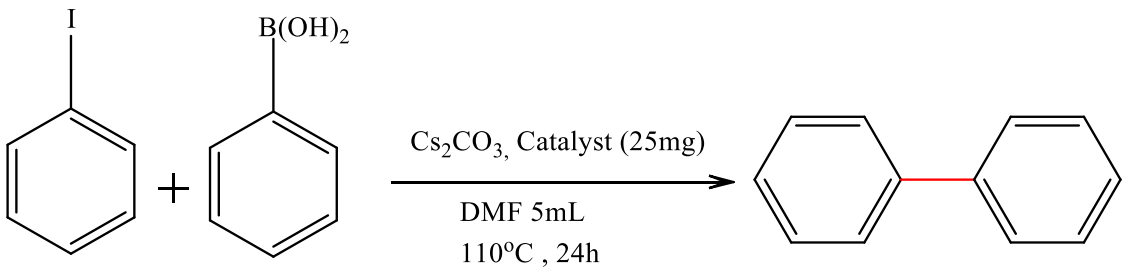

Scheme 6.2 C-C coupling reaction catalyzed by Cu/GO nanohybrides

After this time, the solution was cooled to room temperature and filtered over a nylon filter (0.4 μm). The filtrated reaction mixture was then characterized by injecting in GC in the same condition as described in 6.3.1.

The studied materials show a moderate catalytic activity with very similar conversion values of around 40% with no significant differences of conversion between the different studied materials. However, again as it happened in the oxidation reactions the higher TON values are observed for the system DS/GO which point towards a higher catalytic activity than their Cu, CuO or Cu_2O analogues.

Table 6.3 Results of the catalytic C-C coupling reaction of copper compound/GO nanohybrides at 24 hours

Reaction	Catalyst	Conversion (%mol)[a]	TON
Ph-I + Ph-Bor	Cu^0/GO	45.5	0.95
	DS/GO	41.1	1.67
	Cu_2O/GO	34.3	0.97
	CuO/GO	36.5	0.90

In general, the obtained conversions are lower than those obtained in hybrid systems based on palladium nanoparticles supported onto other supports such as graphene oxide, alumina or silica [171,172], however, the conversions show that these systems may also serve as C-C coupling agents confirming their catalytic versatility.

6.3.3 Catalytic C-S coupling reactions

The studied reaction was the coupling of iodobenzene and 3,5-dimethylthiophenol (Me_2PhSH) at 110 °C during 24 h. The reaction was carried out using DMSO (5 mL) as solvent and Cs_2CO_3 as base. Iodobenzene, 3,5-dimethylthiophenol and Cs_2CO_3 were

in a molar ratio of 1:1.2:2 and the amount of catalyst was in all cases 25 mg. All the reactions were carried out using degassed solvents and under a nitrogen atmosphere. To prepare the iodobenzene solution 153 mg (0.75 mmol) of iodobenzene were dissolved in 5.0 mL of degassed DMSO under nitrogen in a Schlenk tube. Subsequently, a Schlenk flask was filled with 3,5-dimethylthiophenol (124 mg, 0.9 mmol), and Cs_2CO_3 (488 mg, 1.50 mmol) and copper-based materials as catalyst (25 mg) and three vacuum/N_2 cycles (10 min/1 min) were carried out to eliminate oxygen from the reaction atmosphere and reduce the quantity of hypothetical adsorbed water from the solids. Afterwards 1-iodobenzene solution was transferred under N_2 to the Schlenk flask containing the solid mixture and the resulting suspension was then heated to 110 °C and stirred for 24 hours (Scheme 6.3).

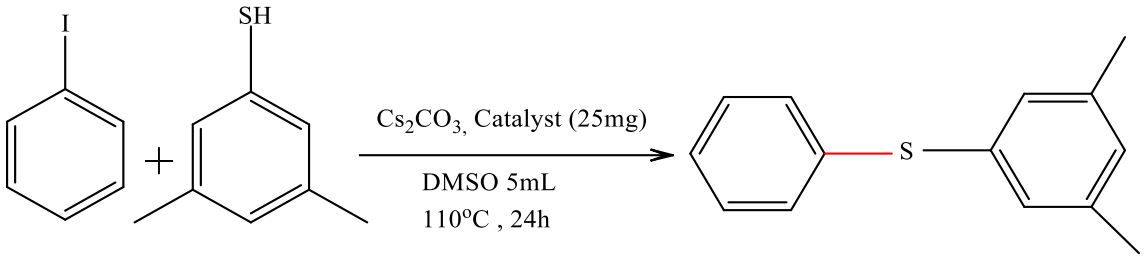

Scheme 6.3 C-S coupling reaction catalyzed by Cu/GO nanohybrides

After this time, the solution was cooled down to room temperature and filtered over a nylon filter (0.4 μm). The filtrated reaction mixture was then injected in a GC-FID apparatus (Perkin-Elmer GC Clarus 580) with the same column, temperature program, injection temperature and detector temperature than those described in the section (Section 6.3.1).

In this Ulmann-Goldberg type reaction for all the catalysts, with very high conversions

close to 100% for Cu/GO and Cu_2O/GO and close to 90% for DS/GO and CuO/GO indicating that all the studied materials present a very good catalytic activity (Table 6.4).

Table 6.4 Results of the catalytic C-S coupling reaction of copper compound/GO nanohybrides at 24 hours

Reaction	Catalyst	Conversion (%mol)[a]	TON
Ph-I + Me_2PhSH	Cu^0/GO	98.1	2.03
	DS/GO	88.4	3.6
	Cu_2O/GO	82.2	2.33
	CuO/GO	98.5	2.43

When the TON values were analysed, it could be observed, as in the case of the oxidation and C-C coupling reactions, that the most effective catalyst was DS/GO with a TON value of ca. 2.03. Again the catalytic versatility of these Cu-based systems was demonstrated and the slightly higher catalytic activity of the DS-supported system was confirmed [173]

6.3.4 Catalytic C-N coupling reactions

I) Reaction of iodobenzene with methylamine ($MeNH_2$)

The studied reaction was the coupling of iodobenzene and methylamine ($MeNH_2$) at 110 °C during 24 h. The reaction was carried out using a mixture DMF/water as solvent (using a final volume of 5 mL) and Cs_2CO_3 as base. Iodobenzene, methylamine and Cs_2CO_3 were in a molar ratio of 1:1.2:2 and the amount of catalyst was 25 mg. The reaction was carried out using degassed DMF/water and under a nitrogen atmosphere. To prepare the iodobenzene solution 153 mg (0.75 mmol) of iodobenzene were

dissolved in 5.0 mL of degassed DMF under nitrogen in a Schlenk tube. Subsequently a Schlenk flask was filled with 65.2 µL (0.90 mmol) of methylamine (40 % water solution), Cs_2CO_3 (488 mg, 1.50 mmol) and copper-based materials as catalyst (25 mg), and three vacuum/N_2 cycles were carried out to eliminate oxygen from the reaction atmosphere. Afterwards the solution of 1-iodobenzene was transferred under N_2 to the Schlenk flask containing the solid mixture and the resulting suspension was then heated to 110 °C and stirred for 24 hours. After this time, the solution was cooled down to room temperature and filtered over a nylon filter (0.4 µm). The filtrated reaction mixture was then injected in a GC-FID apparatus (Perkin-Elmer GC Clarus 580) with the same column, temperature program, injection temperature and detector temperature than those described in the section 6.3.1.

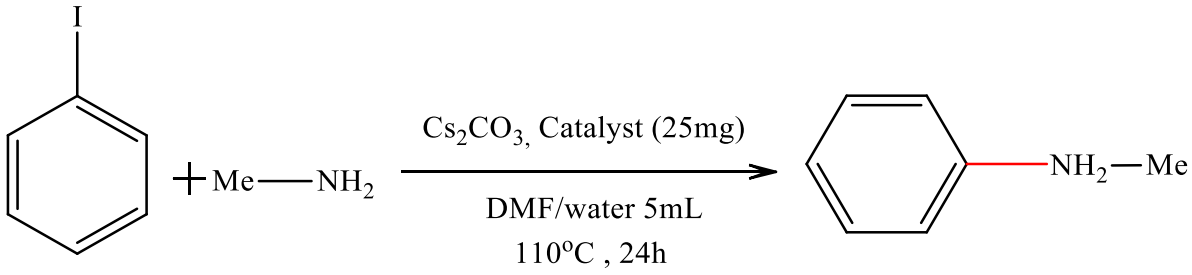

Scheme 6.4 C-N coupling reaction catalyzed by Cu/GO nanohybrides

II) Reaction of iodobenzene with benzylamine ($BzNH_2$)

The studied reaction was the coupling of iodobenzene and benzylamine ($BzNH_2$) at 110 °C during 24 h. The reaction was carried out using DMF (5 mL) as solvent and Cs_2CO_3 as base. Iodobenzene, benzylamine and Cs_2CO_3 were in a molar ratio of 1:1.2:2 and the amount of catalyst was in all cases 25 mg. The reaction was carried out using degassed DMSO under a nitrogen atmosphere. To prepare the iodobenzene solution,

153 mg (0.75 mmol) of iodobenzene were dissolved in 5.0 mL of degassed DMSO under nitrogen in a Schlenk tube. Subsequently, a Schlenk flask was filled with benzylamine (5.35 mg, 0.050 mmol), Cs_2CO_3 (16.3 mg, 0.050 mmol) and copper-based materials as catalyst (25 mg) and three vacuum/N_2 cycles were carried out to eliminate oxygen from the reaction atmosphere. Afterwards, the solution of 1-iodobenzene was transferred under N_2 to the Schlenk flask containing the solid mixture and the resulting suspension was then heated to 110 °C and stirred for 24 hours.

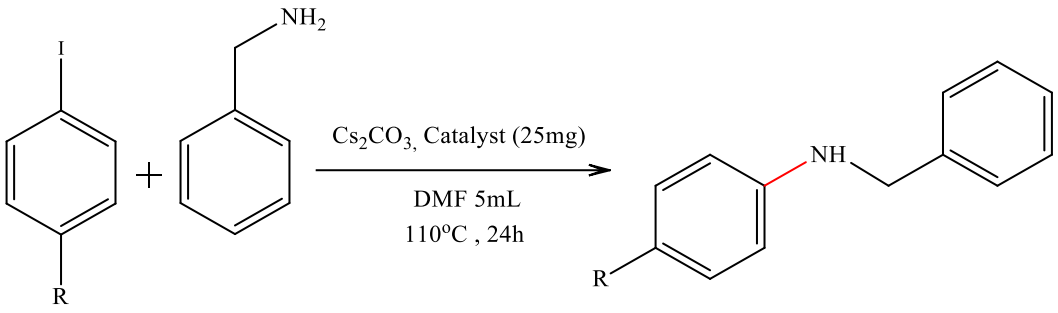

R= H, OMe

Scheme 6.5 C-N coupling reaction catalyzed by Cu/GO nanohybrides

After this time, the solution was cooled down to room temperature and filtered over a nylon filter (0.4 µm). The filtrated reaction mixture was then injected in a GC-FID apparatus (Perkin-Elmer GC Clarus 580) with the same column, temperature program, injection temperature and detector temperature than those described in the section 6.3.1.

III) Reaction of 4-iodoanisole with benzylamine

The studied reaction was the coupling of 4-iodoanisole (Ani-I) and benzylamine at 110 °C during 24 h. The reaction was carried out using identical procedure and molar quantities than those described in the section 6.3.1 for the reaction of iodobenzene with

benzylamine (Scheme 6.5).

In the case of coupling between iodobenzene and methylamine, the conversions are close to 90% or higher indicating a good catalytic activity of these systems for this reaction. Again, the DS/GO system presents the highest TON value of 4.01.

The copper-based nanostructured systems in similar C-N coupling reactions but replacing methylamine by benzylamine (Scheme 6.5 show a slight decrease of the conversion, to values of between 80-90%. The decrease in the activity is maybe due to the lower reactivity of benzylamine in comparison with methylamine due to both steric and electronic effects of the amine. In addition, the diffusion of the benzylamine in a heterogeneous system is more difficult and this may also decrease catalytic activity.

The copper-based nanostructured systems were also tested in similar C-N coupling reactions but replacing methylamine by benzylamine (Scheme 6.4). The catalytic results show a slight decrease of the conversion, to values of between 80-90%. The decrease in the activity is maybe due to the lower reactivity of benzylamine in comparison with methylamine due to both steric and electronic effects of the amine. In addition, the diffusion of the benzylamine in a heterogeneous system is more difficult and this may also decrease catalytic activity.

In the last reaction of benzylamine with 4-iodoanisole, it can be observed that the conversion of the iodophenyl derivative decreases to values between 60-70% (Table 6.5). In this case, this decrease of the catalytic activity is due to steric effects when comparing iodobenzene with 4-iodoanisole.

Again, in all cases the highest TON value is observed for the system based on the DS/GO hybrid material as it happened for all the other studied reactions.

Table 6.5 Results of the catalytic C-N coupling reaction of copper compound/GO nanohybrides at 24 hours

Reaction	Catalyst	Conversion (%mol)[a]	TON
Ph-I + $MeNH_2$	Cu^0/GO	99.1	2.05
	DS/GO	98.6	4.01
	Cu_2O/GO	89.9	2.55
	CuO/GO	90.6	2.24
Ph-I + $BzNH_2$	Cu^0/GO	92.2	1.91
	DS/GO	88.1	3.59
	Cu_2O/GO	79.8	2.26
	CuO/GO	80.5	1.99
Ani-I + $BzNH_2$	Cu^0/GO	68.5	1.42
	DS/GO	68.8	2.80
	Cu_2O/GO	60.2	1.71
	CuO/GO	63.5	1.57

6.5 Conclusions of Chapter 6

In this paper we have reported the facile and rapid preparation of GO decorated with different Cu nanostructured systems such as Cu/GO, DS/GO, CuO/GO and Cu_2O/GO The studied materials have been tested as catalysts observing that they present a high versatility in different catalytic reactions. Specifically, among the studied systems we have found that the most active material is DS/GO in all the studied reactions, improving the results obtained for copper nanoparticles Cu/GO.

These results open up the possibility of a more thorough study of the catalytic possibilities of the supported copper double salt in other conditions which may be applied in the future for different catalytic and consecutive processes of organic synthesis.

Our studies will be focused on the optimization of the synthetic methods and the extension of the catalytic use of DS/GO in other reactions trying to improve the current reported results in attractive catalytic heterogeneous reactions of interest.

References

[1] S. Iijima, Helical microtubules of graphitic carbon, *Nature* 354 (1991) 56-58

[2] M. Kumar, Y. Ando, Chemical vapor deposition of carbon nanotubes: A review on growth mechanism and mass production, *J. Nanosci. & Nanotechnol*. 10 (2010) 3739-3758

[3] T. A. Saleh, In: Syntheses and applications of carbon nanotubes and their composites, ed. S. Suzuki, InTech, 2013. Chapter 21, p. 779-493

[4] A. Kausar, I. Rafique, B. Muhammad, A review on applications of polymer/carbon nanotube and epoxy/CNT composites, *Polym.-Plast. Technol. Eng*. 55 (2016) 1167-1191

[5] D. S. Bethune, C. H. Kiang, M. S. De Vries, G. Gorman, R. Savoy, J. Vazquez and R. Beyers, Cobalt-catalyzed growth of carbon nanotubes with single-atomic-layer walls, *Nature* 363 (1993) 605-607

[6] M. Dresselhaus, G. Dresselhaus, R. Saito, Physics of carbon nanotubes, *Carbon* 33 (1995) 883-91

[7] X. Y. Tao, X. B. Zhang, F. Y. Sun, J. P. Cheng, F. Liu, Z. Q. Luo, Large-scale CVD synthesis of nitrogen-doped multi-walled carbon nanotubes with controllable nitrogen content on a $CO_xMg_{1-x}MoO_4$ catalyst, *Mater*. 16 (2007) 425-430

[8] M. J. Yacaman, M. M. Yoshida, L. Rendon, J. G. Santiesteban, Catalytic Growth of Carbon Microtubules with Fullerene Structure, *Appl. Phys. Lett*. 62 (1993) 202-204

[9] S. V. Morozov, K. S. Novoselov, M. I. Katsnelson, F. Schedin, D. C. Elias, J. A. Jaszczak, A. K. Geim, Giant intrinsic carrier mobilities in graphene and its bilayer,

Phys. Rev. Lett. 100 (2008) 016602, DoI:10.1103/PhysRevLett.100.016602

[10] C. Lee, X. D. Wei, J. W. Kysar, Measurement of the elastic properties and intrinsic strength of monolayer graphene, J. Hone, *Science* 321 (2008) 385-388

[11] A. A. Balandin, S. Ghosh, W. Z. Bao, I. Calizo, D. Teweldebrhan, F. Miao, C. N. Lau, Superior thermal conductivity of single layer graphene, *Nano. Lett*. 8 (2008) 902-907

[12] J. Moser, A. Barreiro, A. Bachtold, Current-induced cleaning of graphene, *Appl. Phys. Lett*. 91 (2007) 163513, DOI:10.1063/1.2789673

[13] W. Choi, I. Lahiri, R. Seelaboyina, Y. S. Kang, Synthesis of graphene and its applications: A review, *Solid State Mater. Sci*. 35 (2010) 52-71

[14] W. Choi, J. W. Lee, Graphene: Synthesis and Applications, CRC Press, Taylor and Francis Group; Boca Raton London New York, Chapter 2, 27-57

[15] B. C. Brodie, On the atomic weight of graphite, Phil. Trans. R. Soc. London 149 (1859) 249-259

[16] W. S. Hummers, R. E. Offeman, Preparation of graphitic oxide, *J. Am. Chem. Soc*. 80 (1958) 1339-1339

[17] R. Kumar Singh, R. Kumar, D. Pratap Singh, Graphene oxide: strategies for synthesis, reduction and frontier applications, *RSC Adv*. 6 (2016) 64993-65011

[18] D. Chen, H. Feng, J. Li, Graphene Oxide: Preparation, Functionalization, and Electrochemical Applications, *Chem. Rev*. 112 (2012) 6027-6053

[19] S. F. Pei, H. M. Cheng, The reduction of graphene oxide, *Carbon* 50 (2012) 3210-3228

[20] Md. S. Alam Bhuyan, Md. Nizam Uddin, Md. M. Islam, F. Alam Bipasha, S. Shafayat Hossain, Synthesis of graphene, *Int. Nano. Lett*. 6 (2016) 65-83

[21] Graphene-based UV-curable nanocomposite coatings. Available from: https://www.researchgate.net/publication [accessed May 02 2018]

[22] M. P. Ghatule, U. A. Devare, Study and Analysis on Synthesis of Graphene and its Applications in Solar Cells, *Inter. J. Innovative Res. Adv. Engine*. (IJIRAE) 2 (2015) 2349-2163

[23] Y. B. Zhang, J. P. Small, W. V. Pontius, P. Kim, Fabrication and electric-field dependent transport measurements of mesoscopic graphite devices, *Appl. Phys. Lett*. 86 (2005) 073104, DOI:10.1063/1.1862334

[24] K. S. Novoselov, A. K. Geim, S. K. Morozov, D. Jiang, Y. Zhang, S. V. Dubonos, I. V. Grigorieva, A. A. Firsov, Electric field effect in atomically thin carbon films, *Science* 306 (2004) 666-669

[25] W. W. Liu, J. N. Wang, Direct exfoliation of graphene in organic solvents with addition of NaOH, *Chem. Commun*. 47 (2011) 6888-6890

[26] U. Khan, O. Arnel, M. Lotya, D. Sukanta, J. N. Coleman, High-Concentration Solvent Exfoliation of Graphene, *Smll*. 6 (2010) 864-871

[27] Y. Hernandez, V. Nicolosi, M. Lotya, F. M. Blighe, Z. Y. Sun, S. De, I. T. McGovern, B. Holland, M. Byrne, Y. K. Gun'ko, J. J. Boland, P. Niraj, G. Duesberg, S. Krishnamurthy, R. Goodhue, J. Hutchison, V. Scardaci, A. C. Ferrari and J. N. Coleman, Nat. *Nanotechnol*. 3 (2008) 563-568

[28] S. Vadukumpully, J. Paul, S. Valiyaveettil, Cationic surfactant mediated exfoliation of graphite into graphene flakes, *Carbon* 47 (2009) 3288-3294

[29] R. B. Rao, N. Patnaik, Scandinavian, Preparation of high pure graphite by alkali digestion method, *J. Metall*. 33 (2004) 257-260

[30] Y. H. Wu, T. Yu, Z. X. Shen, Two-dimensional carbon nanostructures: fundamental properties, synthesis, characterization, and potential applications, *J. Appl. Phys.* 108 (2010) 071301, DOI: 10.1063/1.3460809

[31] C. E. Hamilton, J. R. Lomeda, Z. Z. Sun, J. M. Tour and A. R. Barron, High-Yield Organic Dispersions of Unfunctionalized Graphene, *Nano Lett*. 9 (2009) 3460-3462

[32] K. Jasuja, J. Linn, S. Melton, V. Berry, Microwave-reduced uncapped metal nanoparticles on graphene: Tuning catalytic, electrical, and raman properties, *J. Phys. Chem. Lett*. 1 (2010) 1853-1860

[33] K. Vinodgopal, B. Neppolian, I. V. Lightcap, F. Grieser, M. Ashokkumar, P. V. Kamat, Sonolytic design of graphene-Au nanocomposites. Simultaneous and sequential reduction of graphene oxide and Au (III), *J. Phys. Chem. Lett*. 1 (2010) 1987-1993

[34] S. F. Pei, H. M. Cheng, The reduction of graphene oxide, *Carbon*, 50 (2012) 3210-3228

[35] D. W. Boukhvalov, M. I. Katsnelson, Modeling of Graphite Oxide, *J. Am. Chem. Soc*. 130 (2008) 10697-10701

[36] N. Cao, Y. Zhang, Study of Reduced Graphene Oxide Preparation by Hummers' Method and Related Characterization, *J. Nanomat*. 2015 (2014) 168125, DOI: 10.1155/2015/168125

[37] C. Botas, P. Alvarez, P. Blanco, M. Granda, C. Blanco, R. Santamaría, L. J.

Romasanta, R. Verdejo, M. A. López-Manchado, R. Menéndez, Graphene materials with different structures prepared from the same graphite by the Hummers and Brodie methods, *Carbon* 65 (2013) 156-164

[38] N. Luhyna, F. Inam, 2nd International Conference on Advanced Composite Materials and Technologies for Aerospace Applications, June 11-13, 2012, Wrexham, Carbon nanotubes for epoxy nanocomposites: a review on recent developments

[39] P. J. F. Harris, Carbon nanotube composites, Int. Mater. Rev. 49 (2004) 31-43

[40] Y. Hu, O. A. Shenderova, Z. Hu, C. W Padgett, D. W Brenner, Carbon nanostructures for advanced composites, *Rep. Prog. Phys*. 69 (2006) 1847-1895

[41] Y. Wang, J. Wu, F. Wei, A treatment method to give separated multi-walled carbon nanotubes with high purity, high crystallization and a large aspect ratio, *Carbon* 41 (2003) 2939-2948

[42] H. Sadegh; R. Shahryari-ghoshekandi, Functionalization of carbon nanotubes and its application in nanomedicine: A review, *Nanomed. J*. 2(2015) 231-248

[43] J. Chen, H. Y. Liu, W. A. Weimer, M. D. Halls, D. H. Waldeck, G. C. Walker, Noncovalent Engineering of Carbon Nanotube Surfaces by Rigid, Functional Conjugated Polymers, *J. Am. Chem. Soc*. 124 (2002) 9034-9035

[44] R. Itzhak, D. Raichman, Z. Shahar, G. L. Frey, J. Frey, R. Yerushalmi-Rozen, Tailoring triblock copolymers for dispersion of individual, pristine, single-walled carbon nanotubes in organic solvents, *J. Phys. Chem*. C 114 (2010) 3748-53

[45] J. Bartelmess, C. Ehli, J-J. Cid, M. Garcia-Iglesias, P. Vázquez, T. Torres, D. M. Guldi, Tuning and optimizing the intrinsic interactions between phthalocyanine-

based PPV oligomers and single-wall carbon nanotubes toward n-type/p-type, *Chem. Sci*. 2 (2011) 652-660

[46] A. D. Crescenzo, V. Ettorre, A. Fontana, Non-covalent and reversible functionalization of carbon nanotubes, *Beilstein J. Nanotechnol*. 5 (2014) 1675-1690

[47] A. Hirsch, Functionalization of Single-Walled Carbon Nanotubes, *Angew, Chem, Int. Ed*. 41 (2002) 1853-1859

[48] J. Liu, A. G. Rinzler, H. Dai, J.H. Hafner, R. K. Bradley, P. J. Boul, A. Lu, T. Iverson, K. Shelimov, C. B. Huffman, F. Rodriguez-Macias, Y. S. Shon, T. R. Lee, D. T. Colbert, R. E. Smalley, Fullerene pipes, *Science* 280 (1998) 1253-1256

[49] V. J. Gonzalez, S. M. Vega-Díaz, A. Morelos-Gómez, K. Fujisawa, M. Endo, O. Martin Cadiz, J. Baselga Llido, M. Terrones, H_2O_2/UV layer-by-layer oxidation of multiwall carbon nanotubes: The “onion effect” and the control of the degree of surface crystallinity and diameter, *Carbon* 139 (2018) 1027-1034

[50] Y. Peng, H. Liu, Effects of oxidation by hydrogen peroxide on the structures of multiwalled carbon nanotubes, *Ind. Eng. Chem. Res*. 45 (2006) 6483-6488

[51] F. Aviles, J.V. Caauich-Rodriguez, L. Moo-Tah, A. May-Pat, R. Vargas-Coronado, Evaluation of mild acid oxidation treatments for MWCNT functionalization, Carbon 47 (2009) 2970-2975

[52] O. Martín, H. R. Gutierrez, A. Maroto-Valiente, M. Terrones, T. Blanco, J. Baselga, An efficient method for the carboxylation of few-wall carbon nanotubes with little damage to their sidewalls, *Mater. Chem. Phys*. 140 (2013) 499-507

[53] U. N. Maiti, W. J. Lee, J. M. Lee, Y. Oh, J. Y. Kim, J. E. Kim, J. Shim, T. H. Han,

S. O. Kim, Chemically modified/ doped carbon nanotubes & graphene for optimized nanostructures & nanodevices, *Adv. Mater*. 26 (2014) 40-67

[54] M. Terrones, A. G. S. Filho, A. M. Rao, (2007) Doped Carbon Nanotubes: Synthesis, Characterization and Applications. In: A. Jorio, G. Dresselhaus, M. S. Dresselhaus (eds) Carbon Nanotubes. Topics in Applied Physics, vol. 111. Springer, Berlin, Heidelberg

[55] K. Xia, H. Zhan, Y. Gu, Graphene and carbon nanotube hybrid structure: A review, Procedia *IUTAM*, 21 (2017) 94-101

[56] O. Zhou, R. M. Fleming, D. W. Murphy, C. H. Chen, R. C. Haddon, A. P. Ramirez, S. H. Glarum, Defects in carbon nanostructures, *Science* 263 (1994) 1744-1747

[57] E. Yu. Melnikova, V. N. Glushko, V. S. Ivanov and M. Yu. Zhila, Orient. Production Methods Of Iodine-doped Carbon Nano Tubes (A Review), *J. Chem*. 33 (2017) 2707-2712

[58] R. Sen, B. C. Satishkumar, S. Govindaraj, K. R. Harikumar, M. K. Renganathan, C. N. R. Rao, Nitrogen-containing carbon nanotubes, *J. Mater. Chem*. 7 (1997) 2335-2337

[59] G. Zhou, W. Duan, Field Emission in Doped Nanotubes, *J. Nanosci. Nanotechnol*. 5 (2005) 1421-1434

[60] V. J. Gonzalez, E. Gracia-Espinob, A. Morelos-Gómez, F. López-Uríase, H. Terrones, M. Terrones, Biotin molecules on nitrogen-doped carbon nanotubes enhance the uniform anchoring and formation of Ag nanoparticles, *Carbon* 88 (2015) 51-59

[61] Y. Cao, H. Yu, J. Tan, F. Peng, H. Wang, J. Li, W. Zheng, N. B. Wong, Nitrogen,

phosphorous- and boron-doped carbon nanotubes as catalysts for the aerobic oxidation of cyclohexane, *Carbon* 57 (2013) 433-442

[62] G. Zhong, H. Wang, H. Yu, F. Peng, Nitrogen doped carbon nanotubes with encapsulated ferric carbide as excellent electrocatalyst for oxygen reduction reaction in acid and alkaline media, *J. Power Sources* 286 (2015) 495-503

[63] X. Lin, X. Lu, T. Huang, Z. Liu, A. Yu, Xiujing Lin, Xu Lu, Tao Huang, Zhaolin Liu, Aishui Yu, Binder-free nitrogen-doped carbon nanotubes electrodes for lithium-oxygen batteries, *J. Power Sources* 242 (2013) 855-859

[64] A. Botello-Mendez, J. Campos-Delgado, A. Morelos-Gomez, J. M. Romo-Herrera, A. G. Rodriguez, H. Navarro, M. A. Vidal, H. Terrones, M. Terrones, Controlling the dimensions, reactivity and crystallinity of multiwalled carbon nanotubes using low ethanol concentrations, *Chem. Phys. Lett*. 453 (2008) 55-61

[65] V. J. González, C. Martín-Alberca, G. Montalvo, C. García-Ruiz, J. Baselga, M. Terrones, O. Martin, Carbon nanotube-Cu hybrids enhanced catalytic activity in aqueous media, *Carbon* 78 (2014) 10-18

[66] V. Dhand, K. Y. Rhee, H. J. Kim, D. H. Jung, A Comprehensive Review of Graphene Nanocomposites: Research Status and Trends, *J. Nanomater*. 2013, Article ID 763953, 14 pages

[67] M. B. Gawande, A. Goswami, F. X. Felpin, T. Asefa, X. Huang, R. Silva, X. Zou, R. Zboril, R. S. Varma, Cu and Cu-based nanoparticles: synthesis and applications in catalysis, *Chem. Rev*. 116 (2016) 3722-3811

[68] F. Ruffino, F. Giannazzo, A review on metal nanoparticles nucleation and growth on/in graphene, *Crystals* 7 (2017) 219-258

[69] R. Zhou, Y. Zheng, D. Hulicova-Jurcakova, S. Z. Qiao, Enhanced electrochemical catalytic activity by copper oxide grown on nitrogen-doped reduced graphene oxide, *J. Mater. Chem. A* 1 (2013) 13179-13185

[70] R. Gusain, P. Kumar, O.P. Sharma, S.L. Jain, O.P. Khatri, Reduced graphene oxide–CuO nanocomposites for photocatalytic conversion of CO_2 into methanol under visible light irradiation, *App. Catal. B Environ*. 181 (2016) 352-362

[71] M. Nasrollahzadeh, Z. Issaabadi, M. M. Tohidi, S. Sajadi, Recent progress in application of graphene supported metal nanoparticles in C-C and C-X coupling reactions, *Chem. Rec*. 18 (2018) 165-229

[72] C. Hu, T. Lu, F. Chen, R. Zhang, A brief review of graphene–metal oxide composites synthesis and applications in photocatalysis, *J. Chinese Adv. Mater. Soc*. 1 (2013) 21-23

[73] S. Zouai, A. Harabi, N. Karboua, E. Harabi, S. Chehlatt, S. Barama, S. Zaiou, F. Bouzerara, F. Guerfa, A new and economic approach to synthesize and fabricate bioactive diopside ceramics using a modified domestic microwave oven. Part 2: effect of P_2O_5 additions on diopside bioactivity and mechanical properties, *Materials Science and Engineering C* 61 (2016) 553-563

[74] H. P. Boehm, A. Clauss, G. Fischer, U. Hofmann, (1962). "Surface Properties of Extremely Thin Graphite Lamellae". Proceedings of the Fifth Conference on Carbon (PDF). Pergamon Press.

[75] K. Safarova, A. Dvorak, R. Kubinek, M.Vujtek, A. Rek, Usage of AFM, SEM and TEM for the research of carbon nanotubes, Modern Research and Educational Topics in Microscopy. A. Méndez-Vilas and J. Díaz (Eds.)

[76] G. Binning, C. Quate, Atomic Force Microscope, *Phys. Rev. Lett*. 56 (1986) 930-934

[77] T. Susi, T. Pichler, P. Ayala, Beilstein, X-ray photoelectron spectroscopy of graphitic carbon nanomaterials doped with heteroatoms, *J. Nanotechnol*. 6 (2015) 177-92

[78] T. Belin, F. Epron, Characterization methods of carbon nanotubes: A review, *Mater. Sci. Eng*. B 119 (2005) 105-118

[79] M. Dresselhaus, G. Dresselhaus, A. Jorio, Raman Spectroscopy of Carbon *Nanotubes, J. Phys. Chem. C*. 111 (2007) 17887-17893

[80] S. Arepalli, P. Nikolaev, O. Gorelik, V. Hadjiev,W. Holmes, B. Files, L. Yowell, Protocol for the characterization of single-wall carbon nanotube material quality, *Carbon* 42 (2004) 1783-1791

[81] A. A. Mamedov, N.A. Kotov, M. Prato, D.M. Guldi, J.P.Wicksted, A. Hirsch, Molecular design of strong single-wall carbon nanotube/polyelectrolyte multilayer composites, *Nat. Mater*. 1 (2002) 190-194

[82] M. Dresselhaus, A. Jorio, and R. Saito, Characterizing Graphene, Graphite, and Carbon Nanotubes by Raman Spectroscopy, Annu. Rev. Condens. *Matter. Phys*. 1 (2010) 89-108

[83] A. C. Ferrari, J. C. Meyer, V. Scardaci, C. Casiraghi, M. Lazzeri, F. Mauri, S. Piscanec, D. Jiang, K. S. Novoselov, S. Roth, A. K. Geim, Raman spectrum of graphene and graphene layers, *Phys. Rev. Lett*. 97(2006), 187401, DOI: 10.1103/PhysRevLett.97.187401

[84] A. C. Ferrari, J. Robertson, Interpretation of Raman spectra of disordered and amorphous carbon, *Phys. Rev. B* 61 (2000) 14095, DOI: 10.1103/PhysRevB. 61.14095

[85] C. E. Corcione, M. Frigione, Characterization of nanocomposites by thermal analysis, *Materials* 5 (2012) 2960-2980

[86] G. Bussu, A. Lazzeri, On the use of dynamic mechanical thermal analysis (DMTA) for measuring glass transition temperature of polymer matrix fiber reinforced composites, *J. Mater. Sci*. 41 (2006) 6072-6076

[87] V. H. Gonzales, Nanomateriales de Carbono, síntesis, funcionalización y aplicaciones (2015), Carlos III University, Madrid

[88] M. Khazaee, W. Xia, G. Lackner, R. G. Mendes, M. Rümmeli, M. Muhler, D. C. Lupascu, Dispersibility of vapor phase oxygen and nitrogen functionalized multi-walled carbon nanotubes in various organic solvents, *Sci. Rep*. 6 (2016) 26208, DOI: 10.1038/srep26208

[89] P. Munnik, P. E. de Jongh, K. P. de Jong, Recent developments in the synthesis of supported catalysts, *Chem. Rev*. 115 (2015) 6687-6718

[90] N. K. Ojha, G. V. Zyryanov, A. Majee, V. N. Charushin, O. N. Chupakhin, S. Santra, Copper nanoparticles as inexpensive and efficient catalyst: A valuable contribution in organic synthesis, *Coordination Chem. Rev*. 353 (2017) 1-57

[91] E. Kandare, J. M. Hossenlopp, Thermal degradation of Acetate-intercalated hydroxy double and layered hydroxy salts, *Inorg. Chem*. 45 (2006) 3766-3773

[92] N. Guillou, M. Louer, D. Louer, An X-ray and neutron powder diffraction study of a new polymorphic phase of copper hydroxide nitrate, *J. solid state Chem*. 109

(1994) 307-314

[93] Q. Yu, H. Huang, R. Chen, P. Wang, H. Yang, M. Gao, X. Peng, Z. Ye, Synthesis of CuO nanowalnuts and nanoribbons from aqueous solution and their catalytic and electrochemical properties, *Nanoscale* 4 (2012) 2613-2620

[94] S. Nakagaki, K. M. Mantovani, G. S. Machado, K. A. D Castro, F. Wypych, Recent advances in solid catalysts obtained by metalloporphyrins immobilization on layered anionic exchangers: A short review and some new catalytic results, Open Access *Molecules* 2016, 21(3), DOI: 10.3390/molecules21030291

[95] Seung-Ho Lee, Yie-Shein Her, Egon Matijevic, Preparation and growth mechanism of uniform colloidal copper oxide by the controlled double-jet precipitation, *J. Colloid Interface Sci*. 186 (1997) 193-202

[96] S. Wolf, C. Feldmann, $Cu_2X(OH)_3$ (X = Cl^-, NO_3^-): synthesis of nanoparticles and its application for room temperature deposition/printing of conductive copper thin-films, *J. Mater. Chem*. 20 (2010) 7694-7699

[97] E.J. Bushong, C.H. Yoder, The synthesis and characterization of rouartite, a copper hydroxy nitrate, An Integrated First-Year Laboratory Project, *J. Chem. Edu*. 86 (2009) 80-81

[98] C. Henrist, K. Traina, C. Hubert, G. Toussaint, A. Rulmont, R. Cloots, Study of the morphology of copper hydroxynitrate nanoplatelets obtained by controlled double jet precipitation and urea hydrolysis, *J. Cryst. Growth* 254 (2003) 176-187

[99] W. J. Cho, A. Jung, S. Han, S. Lee, T. Kang, K. Lee, K. C. Cho, J. K. Kim, Plasmonic Colloidal Nanoparticles with Open Eccentric Cavity via Acid-induced Chemical Transformation, *NPG Asia Materials* 7 e167 (2015), DOI:

10.1038/am.2015.15

[100] S. Anandan, J. J. Wu, M. Ashokkumar, Sonochemical synthesis of layered copper hydroxy nitrate nanosheets, *Chem. Phys. Chem*. 16 (2015) 3389-91

[101] S. Kratohvil, E. Matijevié, Preparation of copper compounds of different compositions and particle morphologies, *J. Mater. Res*. 6 (1991) 766-777

[102] S. Wang, X. Zhang, L. Pan, F. Zhao, J. Zou, T. Zhang, L. Wang, Controllable sonochemical synthesis of $Cu_2O/Cu_2(OH)_3NO_3$ composites toward synergy of adsorption and photocatalysis, *Appl. Catal. B: Environ*. 164 (2015) 234-240

[103] J. M. Aguirre, A. Gutiérrez, O. Giraldo, Simple route for the synthesis of copper hydroxy salts, *J. Braz. Chem. Soc*. 22 (2011) 546-551

[104] M. Meyn, K. Beneke, C. Lagaly, Anion-exchange reactions of hydroxy double salts, *Inorg. Chem*. 32 (1993) 1209-1215

[105] H. Niu, Q. Yang, K. Tang, A new route to copper nitrate hydroxide microcrystals, *Mater. Sci. Engin. B* 135 (2006) 172-175

[106] A. Srikhaowa, S. M. Smith, Preparation of $Cu_2(OH)_3NO_3$/ZnO, a novel catalyst for methyl orange oxidation under ambient conditions, *Appl. Catal. B: Environmental* 130-131 (2013) 84-92

[107] H. Schmid, N. Eisenreich, Propellants, Explosives, Investigation of a Two-Stage Airbag Module with Azide-Free Gas Generators, *Pyrotechnics* 25 (2000) 230-235

[108] B. Liu, One-dimensional copper hydroxide nitrate nanorods and nanobelts for radiochemical applications, *Nanoscale* 4 (2012) 7194-7198

[109] Y. Zhana, X. Zhoua, B. Fua, Y. Chen, Catalytic wet peroxide oxidation of azo dye (Direct Blue 15) using solvothermally synthesized copper hydroxide nitrate as

catalyst, *J. Hazard. Mater*. 187 (2011) 348-354

[110] E. Kandare, G. Chigwada, D. Wang, C. Wilkie, J. Hossenlopp, Nanostructured Layered Copper Hydroxy Dodecyl Sulfate: A Potential Fire Retardant for Poly (vinyl Ester) (PVE), *Poly. Degrad. Stab*. 91 (2006) 1781-1790

[111] S. Park, H. J. Kim, Unidirectionally aligned copper hydroxide crystalline nanorods from two-dimensional copper hydroxide nitrate, *J. Am. Chem. Soc*. 126 (2004) 14368-69

[112] C. S. Bruschini, M. J. Hudson, Structure and reversible anion exchange in Copper hydroxy double salts, In: T. J. Pinnavaia, M. F. Thorpe (eds) Access in Nanoporous Materials. Fundamental Materials Research. Springer, Boston, MA

[113] L. Stobinski, B. Lesiak, A. Malolepszy, M. Mazurkiewicz, B. Mierzwa, J. Zemek, P. Jiricek, I. Bieloshapka, Graphene oxide and reduced graphene oxide studied by the XRD, TEM and electron spectroscopy methods. *J. Electron Spectros. Relat. Phenomena*. 195 (2014)145-154

[114] J. A. Arcibar-Orozco, D. A. Giannakoudakis, T. J. Bandosz, Copper hydroxyl nitrate/graphite oxide composite as superoxidant for the decomposition/ mineralization of organophosphate-based chemical warfare agent surrogate, *Adv. Mater. Interfaces* 2 (2015) 1500215, DOI: 10.1002/admi.201500215

[115] P. Kabra, S. Meghana, S. Chakraborty, N. Padmavathy, Understanding the pathway of antibacterial activity of copper oxide nanoparticles, *RSC Adv*. 5 (2015) 12293-99

[116] S. B. Maddinedi, B. K. Mandal, Peroxidase like activity of quinic acid stabilized copper oxide nanosheets, *Austin J. Anal. Pharm. Chem*. 1(2014) 1008, DOI:

10.1039/c2an35072f

[117] D. C. Pereira, D. L. A. de Faria, V. R. L. Constantino, Cu II Hydroxy Salts: Characterization of Layered Compounds by Vibrational Spectroscopy, *J. Braz. Chem. Soc*. 17 (2006) 1651-1657

[118] B. Y. S. Chang, N. M. Huang, M. N. An'amt, A. Marlinda, Y. Norazriena, M. R. Muhamad, I. Harrison, H. N. Lim, C. H. Chia, Facile hydrothermal preparation of titanium dioxide decorated reduced graphene oxide nanocomposite, *Int. J. Nanomed*. 7 (2012) 3379-87

[119] Fan-Long Jin, X. Li, Soo-Jin Park, Synthesis and application of epoxy resins: A review, *J. Ind. Eng. Chem*. 29 (2015) 1-11

[120] W. Jiang, Fan-Long Jin, Soo-Jin Park, Synthesis of a novel phosphorus-nitrogen-containing intumescent flame retardant and its application to fabrics, *J. Ind. Eng. Chem*. 27 (2015) 40-43

[121] S. Song, J. Ma, K. Cao, G. Chang, Y. Huang, J. Yang, Synthesis of a novel dicyclic silicon-/phosphorus hybrid and its performance on flame retardancy of epoxy resin, *Polym. Degrad. Stab*. 99 (2014) 43-45

[122] P. Kiliaris, C.D. Papaspyrides, Polymer/layered silicate (clay) nanocomposites: An overview of flame retardancy, *Prog. Polym. Sci*. 35 (2010) 902-958

[123] E. N. Kalali, X. Wang, De-Yi Wang, Functionalized layered double hydroxide-based epoxy nanocomposites with improved flame retardancy and mechanical properties*, J. Mater. Chem. A* 3 (2015) 6819-6826

[124] T. Kashiwagi, E. Grulke, J. Hilding, R. Harris, W. Awad, J. Douglas, Thermal degradation and flammability properties of poly(propylene)/carbon nanotube

composites, *Macromol. Rapid Commun*. 23 (2002) 761-765

[125] X. Wang, E. Naderi kalali and D.-Y. Wang, Two-Dimensional Inorganic Nanomaterials: A Solution to Flame Retardant Polymers, *Nano Adv*. 1 (2016) 1-16

[126] B. Dittrich, K. A. Warting, D. Hofmann, R. Mulhaupt, B. Schartel, Flame retardancy through carbon nanomaterials: Carbon black, multiwall nanotubes, expanded graphite, multi-layer graphene and graphene in polypropylene, *Polym. Degrad. Stab*. 98 (2013) 1495-1505

[127] M. E. Shabestari, E. N. Kalali, V. J. Gonzalez, D. Y. Wang, J. P. Fernandez-Blazquez, O. Martin, J. Baselga, Effect of nitrogen and oxygen doped carbon nanotubes on flammability of epoxy nanocomposites, *Carbon* 121 (2017) 193-200

[128] T. Kashiwagi, E. Grulke, J. Hilding, K. Groth, R. Harris, K. Butlera, J. Shields, S. Kharchenko, J. Douglas, Thermal and flammability properties of polypropylene/carbon nanotube nanocomposites, *Polymer* 45 (2004) 4227-39

[129] J. K. Lee, K. D. Pae, Mechanical and Thermal properties of a Diglycidyl Ether of Bisphenol-A(DGEBA)-4,4'-Diaminodiphenyl Sulfone (DDS) System Cured under Hydrostatic Pressure, *Polymer J*. 26 (1994) 1093-1099

[130] S.G. Prolongo, M.R. Gude, A. Ureaa, Improving the flexural and thermomechanical properties of amino-functionalized carbon nanotube/epoxy composites by using a pre-curing treatment, *Compos. Sci. Technol*. 71 (2011) 765-771

[131] M. Hesami, R. Bagheri, M. Masoomi Combination effects of carbon nanotubes, MMT and phosphorus flame retardant on fire and thermal resistance of fiber-reinforced epoxy composites, *Iran Polym J.* 23 (2014) 469-476

[132] K. Benzarti, X. *Colin*, Understanding the durability of advanced fibre-reinforced polymer (FRP) composites for structural applications, *Adv. Fibre-Reinforced Polym. Compos. Struct. Appl*. (2013) 361-439

[133] Standard Test Method for Measuring the Minimum Oxygen Concentration to Support Candle-like Combustion of Plastics (Oxygen Index), The American Society for Testing and Materials,Philadelphia, USA (1970) 2863-2897

[134] H. G. Elias, Macromolecules: synthesis, materials, and technology, Vol. 2 Plenum Press, New York, 1984, p 1137

[135] C. Katsoulis, E. Kandare, B. K. Kandola, The effect of nanoparticles on structural morphology, thermal and flammability properties of two epoxy resins with different functionalities, *Polym. Degrad. Stab*. 96 (2011) 529-540

[136] C. Kuan, W. Chen, Y. Li, C. Chen, H. Kuan, C. Chiang, Flame retardance and thermal stability of carbon nanotube epoxy composite prepared from sol–gel method, *J. Phys. Chem. Solids* 71 (2010) 539-43

[137] R. E. Lyon, R. Walters, A Microscale Combustion Calorimeter, report DOT/FAA/AR-01/117, U.S. Department of Transportation, Office of Aviation Research, Washington DC, 2002

[138] Y. Hu, P. Xu, H. Gui, X. Wang, Y. Ding, Effect of r phosphate and multiwalled carbon nanotubes on thermal stability and flame retardancy of polylactide, *Composites Part A*, 2015, 77, 147-153

[139] S. Gaikwad, N. Jadhav, S. Mahadik, A. G. Thoka, M. B Mandake, Review: photocatalytic degradation of textile azo dyes, *Int. J. Ad. Eng. Res. Dev*. 4 (2017) 88-91

[140] M. Razvigorova, T. Budinova, N. Petrov and V. Minkova, Purification of water by activated carbons from apricot stones, Lignites and Anthracite, *Water Res*. 32 (1998) 2135-2139

[141] M. J. McAllister, J.-L. Li, D. H. Adamson, H. C. Schniepp, A. A. Abdala, J. Liu, M. Herrera-Alonso, D. L. Milius, R. Car, R. K. Prud'homme, Single Sheet Functionalized Graphene by Oxidation and Thermal Expansion of Graphite, *Chem. Mater.* 19 (2007) 4396-4404

[142] D. Chatterjee, S. Dasgupta, Visible light induced photocatalytic degradation of organic pollutants, *J. Photoch. Photobio. C: Photoch. Rev*. 6 (2005) 186-205

[143] A. K. Arora, V. S. Jaswal, K. Singh, R. Singh, Applications of metal/mixed metal oxides as photocatalyst: A review, *J. Chem*. 32 (2016) 2035-2042

[144] L. Hao, H. Song, L. Zhang, X. Wan, Y. Tang, Y. Lv, SiO_2/graphene composite for highly selective adsorption of Pb(II) ion *J. Colloid Interface Sci*. 369 (2012) 381-387

[145] R. K. Upadhyay, N. Soin, S. Sinha Roy, Role of graphene/metal oxide composites as photocatalysts, adsorbents and disinfectants in water treatment: a review, *RSC Adv*. 4 (2014) 3823-2851

[146] K. Li, T. Chen, L. Yan, Y. Dai, Z. Huang, J. Xiong, D. Song, Y. Lv and Z. Zeng, Design of graphene and silica co-doped titania composites with ordered mesostructure and their simulated sunlight photocatalytic performance towards atrazine degradation, *Colloids Surf. A*, 422 (2013) 90-99

[147] T. Kornprobst, J. Plank, Photodegradation of Rhodamine B in presence of CaO and NiO-CaO catalysts, *Int. J. Photoenergy*, 2012, 398230, DOI:

10.1155/2012/398230

[148] Z. Zhang, S. Zhai, M. Wang, H. Ji, L. He, C. Ye, C. Wang, S. Fang, H. Zhang, Photocatalytic degradation of rhodamine B by using a nanocomposite of cuprous oxide, three-dimensional reduced graphene oxide, and nanochitosan prepared via one-pot synthesis, *J. Alloys and Comp*. 659 (2016) 101-111

[149] S. Fatima, S. Irfan Ali, M. Z. Iqbal, S. Rizwan, The high photocatalytic activity and reduced band gap energy of La and Mn co-doped $BiFeO_3$/graphene nanoplatelet (GNP) nanohybrids, *RSC Adv*. 7 (2017) 35928-37

[150] https://energyeducation.ca/encyclopedia/Band_gap

[151] L. Muaoz-Fernandez, Sierra-Fernandez, G. Flores-Carrasco, O. Miloševic, M.E. Rabanal, Solvothermal synthesis of Ag/ZnO micro/nanostructures with different precursors for advanced photocatalytic applications, *Adv. Powder Technol*. 28 (2017) 83-92

[152] A. Kumar, G. Pandey, A review on the factors affecting the photocatalytic degradation of hazardous materials, *Material Sci. & Eng. Int. J*. 1 (2017) 00018, DOI: 10.15406/mseij.2017.01.00018

[153] H. Li, J. Liao, T. Zeng, A facile synthesis of CuO nanowires and nanorods, and their catalytic activity in the oxidative degradation of Rhodamine B with hydrogen peroxide, *Catalysis Commun*. 46 (2014) 169-73

[154] N. G. Asenjo, R. Santamaría, C. Blanco, M. Granda, P. Álvarez, R. Menéndez, "Correct use of the Langmuir–Hinshelwood equation for proving the absence of a synergy effect in the photocatalytic degradation of phenol on a suspended mixture of titania and activated carbon" *Carbon* 55 (2013) 62-69; DOI:

10.1016/j.carbon.2012.12.010

[155] A.A. Ogwu, E. Bouquerel, O. Ademosu, S. Moh, E. Crossan, F. Placido, "An investigation of the surface energy and optical transmittance of copper oxide thin films prepared by reactive magnetron sputtering" *Acta Materialia* 53 (2005) 5151–5159; DOI: 10.1016/j.actamat.2005.07.035

[156] I. E. Wachs, S. P. Phivilay, C. A. Roberts, Reporting of reactivity for heterogeneous photocatalysis, *ACS Catal*. 3 (2013) 2606-2611

[157] N. Zhigang, Reduced graphene oxide-cuprous oxide hybrid nanopowders: Hydrothermal synthesis and enhanced photocatalytic performance under visible light irradiation, *Materials Science in Semiconductor Processing* 23 (2014) 78-8

[158] L. Cheng, Y. Wang, D. Huang, T. Nguyen, Y. Jiang, H. Yu, N. Ding, G. Ding, Z. Jiao, Facile synthesis of size-tunable CuO/graphene composites and their high photocatalytic performance, *Materials Res. Bulletin* 61 (2015) 409-414

[159] N. Hassan, N. J. Roslani, A. A. Jalil, S. Triwahyono, N. F. Salleh, N. F. Jaafar, Copper oxide supported on graphene for phodegradation of Rhodamine B, Malaysian J. Fundament. *Appl. Sci*. 11(2015) 148-151

[160] C. Sambiagio, S. P. Marsden, A. J. Blacker, P. C. McGowan, Copper catalysed Ullmann type chemistry: from mechanistic aspects to modern development ulman, *Chem. Soc. Rev*. 43 (2014) 3525-50

[161] P. Rani, P. F. Siril, R. Srivastava, Cu nanoparticles decorated Cu organic framework based efficient and reusable heterogeneous catalyst for coupling reactions, *Mol. Catal*. 433 (2017) 100-110

[162] A. Fedorov, H. Liu, H. Lo and C. Copéret, Silica-Supported Cu Nanoparticle

catalysts for Alkyne semihydrogenation: Effect of ligands on rates and selectivity, *J. Am. Chem. Soc*. 138 (2016) 16502-507

[163] K. Wang, L. Yang, W. Zhao, L. Cao, Z. Sun, F. Zhang, A facile synthesis of copper nanoparticles supported on an ordered mesoporous polymer as an efficient and stable catalyst for solvent-free Sonogashira coupling Reactions, *Green Chem*. 19 (2017) 1949-1957

[164] A. Biffis, E. Scattolin, N. Ravasio, F. Zaccheria, Preoxidated polyacrylonitrile fiber mats supported copper catalyst for Mizoroki–Heck cross-coupling reactions, *Tetrahedron Lett*. 48 (2007) 8761-8764

[165] S. K. Das, S. Mukherjee, L. M. F. Lopes, Laura M. Ilharco, A. M. Ferraria, A. M. Botelho do Rego, A. J. L. Pombeiro, characterization and heterogeneous catalytic application of copper integrated mesoporous matrices, *Dalton Trans*. 43 (2014) 3215-26, Synthesis

[166] Y. He, C. Cai, Terminal alkyne homocoupling reactions catalyzed by an efficient and recyclable polymer-supported copper catalyst at room temperature under solvent-free conditions, *Catal. Sci. Technol*. 2 (2012) 1126-29

[167] J. Albadi, A. Mansournezhad, Z. Derakhshandeh, CuO-CeO_2 Nanocomposite: A highly efficient recyclable catalyst for the multicomponent synthesis of 4H-Benzo[β]Pyran derivatives, *Chin. Chem. Lett*. 24 (2013) 821-824

[168] Q. Zhu, Y. Zhang, J. Wang, F. Zhou, P. K. Chu, Microwave synthesis of cuprous oxide micro-/nanocrystals with different morphologies and photocatalytic activities, *J. Mater. Sci. Technol*. 27 (2011) 289-295

[169] M. Darvishi, G. Mohseni-Asgerani, J. Seyed-Yazdi, Simple microwave

irradiation procedure for the synthesis of CuO/Graphene hybrid composite with significant photocatalytic enhancement, *Surfaces and Interfaces* 7 (2017) 69-73

[170] A. Didi, L. M. Gómez-Calcerrada, A. Benhamou, S. Gómez-Ruiz, Versatility in the catalytic and photocatalytic reactions of composites based on Zr- and Zr-Pd-doped titania nanoparticles, *Ceramics In*. 44 (2018) 17266-76

[171] A. Balbín, F. Gaballo, J. Ceballos-Torres, S. Prashar, M. Fajardo, G.N. Kaluđerović, S. Gómez-Ruiz, Dual application of Pd nanoparticles supported on mesoporous silica SBA-15 and MSU-2: supported catalysts for C–C coupling reactions and cytotoxic agents against human cancer cell lines, *RSC Adv*. 4 (2014) 54775-87

[172] A. M. S. Hossain, A. Balbín, R.S. Erami, S. Prashar, M. Fajardo, S. Gómez-Ruiz, Synthesis and study of the catalytic applications in C–C coupling reactions of hybrid nanosystems based on alumina and palladium nanoparticles, *Inorganica Chimica Acta*. 455 (2017) 645-652

[173] A. Sujatha, A. M. Thomas, A. P Thankachan, G. Anilkumar, Recent advances in copper-catalyzed C-S cross-coupling reactions, *Reviews and Accounts* (2015) 1-28, ID: 15-8779LR